UNIVERSITY OF
BIRMINGHAM

University of Birmingham Research Archive

e-theses repository

This unpublished thesis/dissertation is copyright of the author and/or third parties. The intellectual property rights of the author or third parties in respect of this work are as defined by The Copyright Designs and Patents Act 1988 or as modified by any successor legislation.

Any use made of information contained in this thesis/dissertation must be in accordance with that legislation and must be properly acknowledged. Further distribution or reproduction in any format is prohibited without the permission of the copyright holder.

4th of 5 files

Chapter 6

EFFECT OF STRESS ON INITIATION AND PROPAGATION OF LOCALIZED CORROSION IN ALUMINIUM ALLOYS

By

SUKANTA GHOSH

A thesis submitted to
University of Birmingham
for the degree of
DOCTOR OF PHILOSOPHY
Metallurgy and Materials
School of Engineering
University of Birmingham

November 2007

6 EFFECT OF STRESS ON LOCALIZED CORROSION INITIATION IN ALUMINIUM ALLOYS

Application of stress is thought to induce changes in the local microstructural features which can act as preferential sites for localized corrosion initiation as modified features often show higher electrochemical activity. In this current chapter the effect of applied elastic and plastic stress in initiating localized corrosion in aluminium alloys will be investigated. The main focus of this chapter will be to compare the corrosion performance of unstressed samples with stressed samples and identify the key features responsible for changing the corrosion behaviour under stressing condition where applicable. Change in the electrochemical behaviour as a function of the degree of applied stress will also be discussed in detail.

Aluminium alloys are characterized by the presence of intermetallic particles and ambiguities still remain about the behaviour of these intermetallic particles under stress and their subsequent contribution towards changing the corrosion performance of the alloy. Therefore this chapter will focus on identifying the role of those intermetallic particles in enhancing localized corrosion activities under stress.

Figure 6.1 shows typical stress-strain curves of AA2024-T351. Two repeats experiments were performed. The yield strength (i.e., 0.2% proof strength) of this alloy is 375 ± 9 MPa and ultimate tensile strength (UTS) is 466 ± 10 MPa. From the standard deviation (9 MPa for YS and 10 MPa for UTS) it is clear that slight variations of the values are possible depending on the sample. However, throughout this current study, the yield strength of AA2024-T351 is taken as 375 MPa, i.e., any stress below and above this value is referred as elastic stress and plastic stress, respectively.

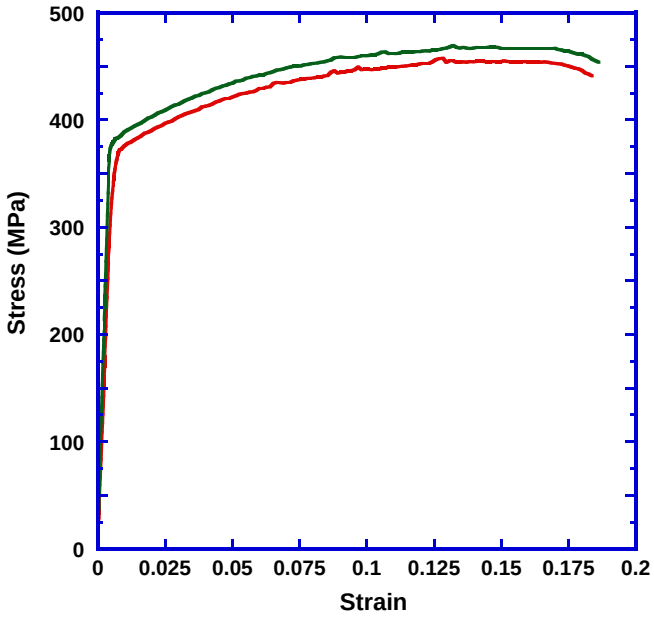


Figure 6.1 Typical stress-strain curves of AA2024-T351. Load is applied parallel to the rolling direction at a strain rate of 0.000417s^{-1}. Two repeat experiments have been performed. Yield Stress (at 0.2% offset) ~ 375 ± 9 MPa and Ultimate Tensile Strength ~ 466 ± 10 MPa.

In situ (i.e., stress application performed within an SEM) experiments using a four-point bend tensile stage inside a FEG-SEM were performed to document out the effect of applied stress on the intermetallic particle as well as the alloy matrix morphology. In a few specimens stress was applied parallel to the rolling direction whereas in other specimens applied stress was perpendicular to the rolling direction.[20] Details of the experimental method had already been discussed in Chapter 3. As the proof strength in bending may not be necessarily equal to the yield strength in tension, samples were calibrated utilizing a strain gauge in the four-point bend stage prior to the test. Strain was measured during the experiment and from the calibration curve the load value was referred whenever required. For example, when using the four-point bending stage

[20] In the earlier work by Connolly [36] it was observed that the delamination between the intermetallic particles and matrix occurred when the applied load was parallel and perpendicular to the rolling direction.

geometry, the load required to reach the 90% of the yield strength (~375 MPa) for the AA2024-T351 sample showed in Figure 6.1 was calculated to be approximately 1233 N. Moreover, the calibration curve showed the strain value at this load as 4308e-06. Similarly at 110% YS (1507 N) and at 120% YS (1644 N) the required strain was 5240e-06 and 6325e-06, respectively.

In situ FEG-SEM analysis revealed that delamination occurs at constituent intermetallic particle/matrix interfaces when the 2024-T351 samples are subjected to remote load greater than 90% of YS. It was observed that delamination occurs in very few of the particles even at very high applied load (i.e., ~140% YS, strain 9348e-06) in the plastic domain. Delamination at the edge of only one particle was found among the eighty particles analyzed on four different samples (approximately 2 mm ×2 mm area was examined for each sample) using FEG-SEM in this current study. These findings are in agreement with Connolly [36] who found more delaminations as more particles were examined over a greater area and number of specimens. Figure 6.2 shows delamination of one such particle as a function of applied stress. It can be clearly seen that once the remote load crossed 90% YS, delamination started and at 120% YS clear delamination between the particle and the matrix has been observed. These delaminations could play an important role in initiating localized corrosion at the particle/matrix interface by creating very tight micro/nano crevices [36]. Aggressive ions like chlorides could accumulate in these crevices making the condition more favourable for the initiation of localized corrosion.

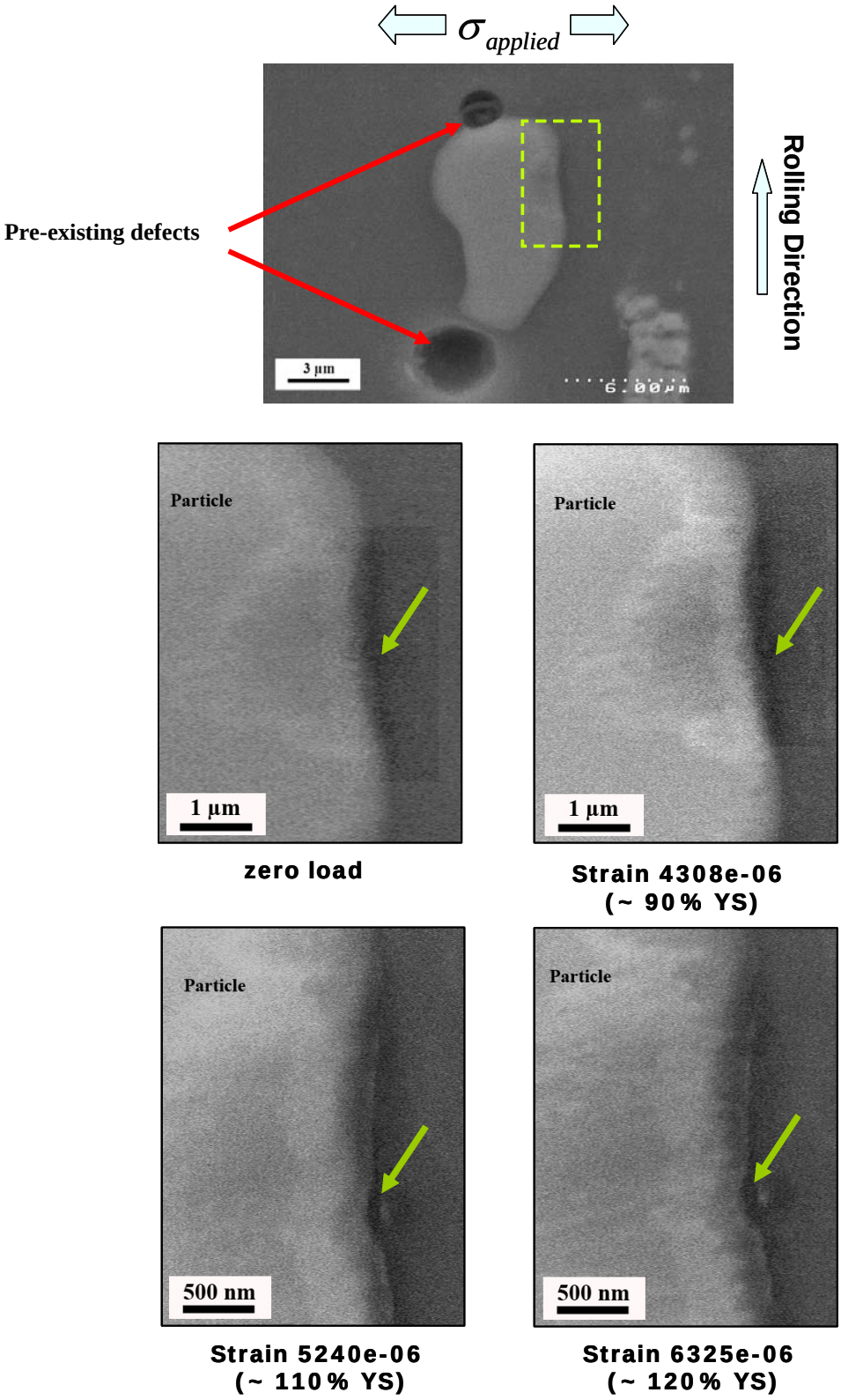


Figure 6.2 In situ study of particle delamination as a function of applied stress using 4-point bend stressing stage. Pre-existing defects can be seen adjacent to the particles. Delamination at the particle-matrix interface become prominent once applied stress goes beyond the yield strength of AA2024-T351.

Figure 6.3 shows the AFM images of a pre-existing defect at the edge of the intermetallic particle in an unstressed condition. Few intermetallic particles (especially Fe-Mn particles) show these types of pre-existing defects at the particle/matrix interface. These pre-existing flaws at the particle/matrix interface could act as initiation sites during the subsequent stressing and create micro/nano-crevices/cracks. Local electrochemical properties in terms of localized corrosion initiation could well be determined by the probability of exposure of such defects.

It should be noted that only one flaw is needed to provide the necessary weak point for initiating localized corrosion in the exposed area. With the presence of a large number of intermetallic particles in the AA2024-T351, the likelihood of exposing such a flaw is high even with very small (even with approximately 1 mm^2) exposure area. Chen *et al.* [8] found that the average density of particles with a projected surface area > 1 μm^2 is approximately ~ 323,000 particles per cm^2.

Buchheit *et al.* [9] performed detailed analysis on the type and distribution of different types of intermetallic particles in AA2024-T351 and found that different intermetallic particles covered about 4.2% of the total alloy surface. So, from these findings it would be logical to assume that statistics will play a governing role in whether corrosion initiation at the micro/nano crevices formed due to delamination at the particle/matrix interfaces occurs, especially when smaller exposure area (1 mm^2 area or an area under a 40 micron diameter capillary) are used in experimentation. As described earlier, one delamination between the particle/matrix is found in about eighty particles analysed during the current study. However, a small area of one mm diameter could possible contain more than 3500 particles, and hence it is possible that quite a few of would be delaminated after application of stress depending on the morphology of the particle.

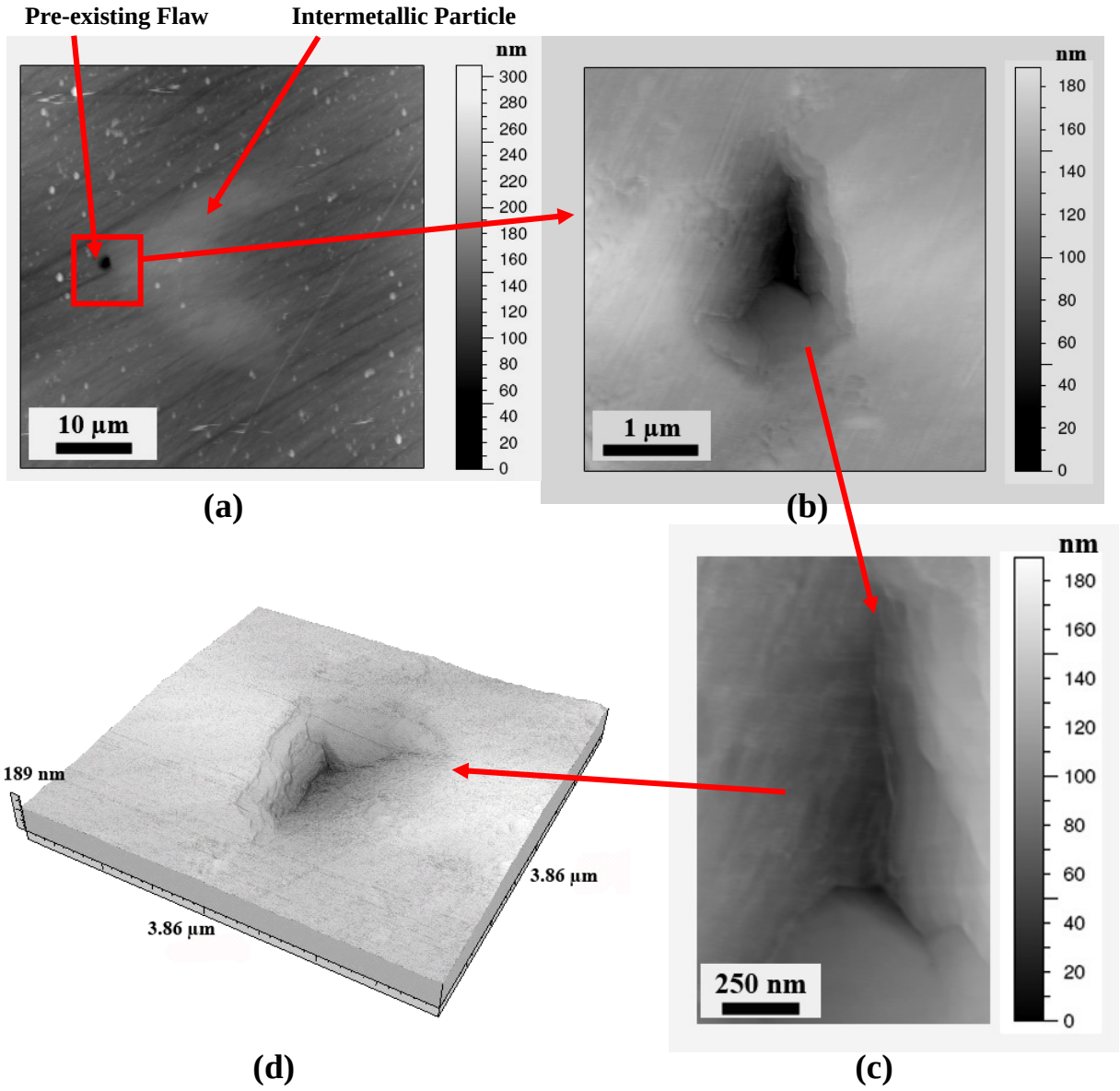


Figure 6.3 (a)-(c) AFM images of a pre-existing flaw at the edge of an intermetallic particle in unstressed condition. With the application of stress these pre-existing flaws can get extended/stretched and create micro or nano crevices which can act as potential sites for corrosion initiation. (d) Shows the 3D view of the pre-existing flaw.

6.1 Capillary Cell Electrochemical Studies Under Plastic Stress

6.1.1 Capillary Cell Electrochemical Studies of AA2024-T351

Electrochemical studies using one mm diameter capillary cell have been performed with and without application of plastic stress. All potentiodynamic polarizations were performed with a scan rate of 1mV/s in naturally aerated 10 mM NaCl (except one occasion where 0.1 M NaCl solution was used to compare the effect stress at different chloride concentration). Samples were stressed parallel to the rolling direction beyond their yield strength in bending using a 3-point bend stressing rig to produce plastic deformation on the exposed surface. Strain gauges (details of this method are already described in Chapter 3) were used to measure the strain level. Strain gauges failed after the deflection at the midspan of the sample in 3-point bend set up reached 1.3 mm with an associated strain value of ~ 48000e-06 (i.e., 4.8% strain). So, to maintain the equivalent stress level for all tests, samples were subjected to midspan deflection of 1.6 mm (i.e., strain > 5%). It should be noted that, the strain level for the capillary cell electrochemical tests using 3-point bend set up was much higher than the in situ FEG-SEM tests for particle delamination using the 4-point bend set up. The maximum strain in 4-point bend tests was 0.9% where as in 3-point bend tests strain level was always > 5% (close to ultimate tensile strength of AA2024-T351). So, the higher strain level in the plastic domain for 3-point bend set up might have resulted in higher possibilities of delamination at the particle/matrix interfaces.

The effect of plastic stress on the corrosion properties of AA2024-T351 is shown in Figure 6.4 with an exposed area of one mm diameter in naturally aerated 10 mM with a scan rate of 1 mV/s.

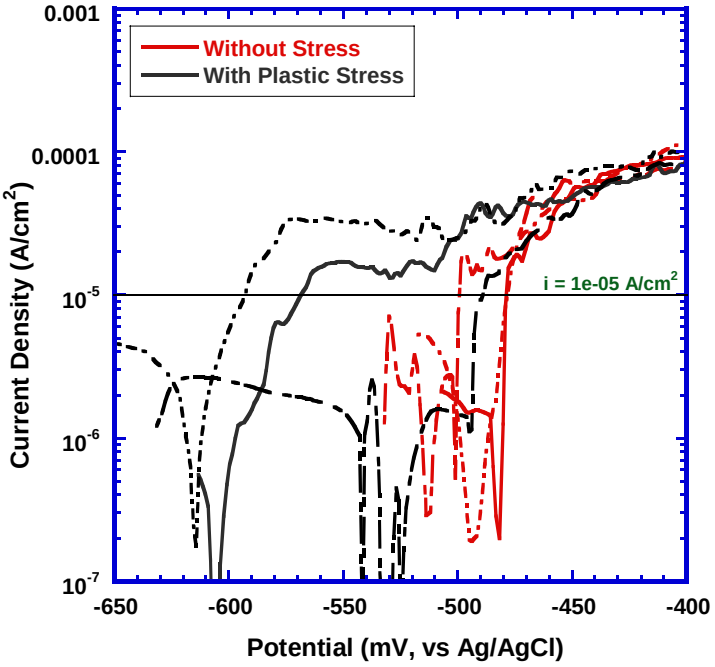


Figure 6.4 Selected anodic polarization scans of AA2024-T351 from capillary cell experiments performed in naturally aerated 0.01 M (10 mM) NaCl (scan rate = 1 mV/s). Application of plastic stress decreases corrosion potential as well as breakdown potential (potential at a current density of 1e-05 A/cm^2 is referred as breakdown potential). While most of the scans show differences after application of plastic stress (strain level > 5%), in few occasions no changes in breakdown potentials have been observed after application of plastic stress.

It can easily be seen from Figure 6.4 that application of plastic stress decreases both corrosion potential as well as the breakdown potential of the alloy. The average value of the corrosion potential is decreased from -525 mV to -600 mV vs. Ag/AgCl with the application of plastic stress. None of the samples show any definite passive region during the potentiodynamic scans. It should be noted that all these samples were tested immediately after polishing. Leaving the polished sample in lab air for a long time (for example samples left overnight after polishing, i.e., more than 12 hrs) could result in stable passive film on the sample surface. So, potentiodynamic tests in those samples may show a short passive region prior to the breakdown, but should not significantly affect the

breakdown potential. It should also be noted that testing on freshly polished samples or samples left overnight after polishing did not affect the conclusions derived from the study (i.e., the effect of stress on corrosion properties of the alloy did not change). However, to maintain the consistency of the tests, freshly polished samples were used for all experiments in this current section.

As these potentiodynamic tests do not show any definite passive region, it is difficult to determine the breakdown potential. Hence, an arbitrary current density of 1×10^{-5} A/cm^2 was chosen to represent the breakdown current and the potential at that current referred as the breakdown potential. It can be seen from the Figure 6.4 that the average breakdown potential decreased from -495 mV to -550 mV vs. Ag/AgCl when a plastic stress was applied. After pitting the current in the potentiodynamic scans become ohmically limited and no IR correction was performed during the electrochemical testing. In some cases multiple cathodic and anodic segments are observed during the potentiodynamic scans for both unstressed and stressed samples. This could be explained by the unstable passivity during the polarization scans [318]. This type of instability could be noticed in certain potential range and mainly depends upon the predominant cathodic process. There are three usual cathodic processes, hydrogen evolution, oxygen reduction and metal cation reduction (though the predominant cathodic process in aluminium corrosion is oxygen reduction). As the experimental polarization is always the sum of all anodic and cathodic currents, multiple segments of cathodic and anodic branches could be observed in some occasions.

Summary of the breakdown and corrosion potentials before and after application of plastic stress is shown in Figure 6.5 and Figure 6.6, respectively. In most cases application of plastic stress decreased both the corrosion and the breakdown potentials. Out of 16 potentiodynamic tests performed on the stressed samples, in three cases

application of plastic stress did not significantly change the breakdown potential (circled area in Figure 6.5) and only in one case applied plastic stress did not change the corrosion potential (see circled area in Figure 6.6). This possibly emphasizes the importance of the presence of defects as initiation point in the exposed area. With the exposed area of one mm diameter, it is possible that in some cases deformation induced features (i.e., delamination etc) were not present inside the capillary droplet (i.e., corrosion test area) and hence the plastically stressed sample behaved similar to the unstressed samples.



Figure 6.5 Summary of the breakdown potentials of AA2024-T351 from different potentiodynamic scans showing the effect of plastic stress (strain level > 5%). The experiments were performed in naturally aerated 0.01 M NaCl (scan rate = 1 mV/s). Few scans (indicated within the circle) do not show significant differences in breakdown potentials after application of plastic stress.

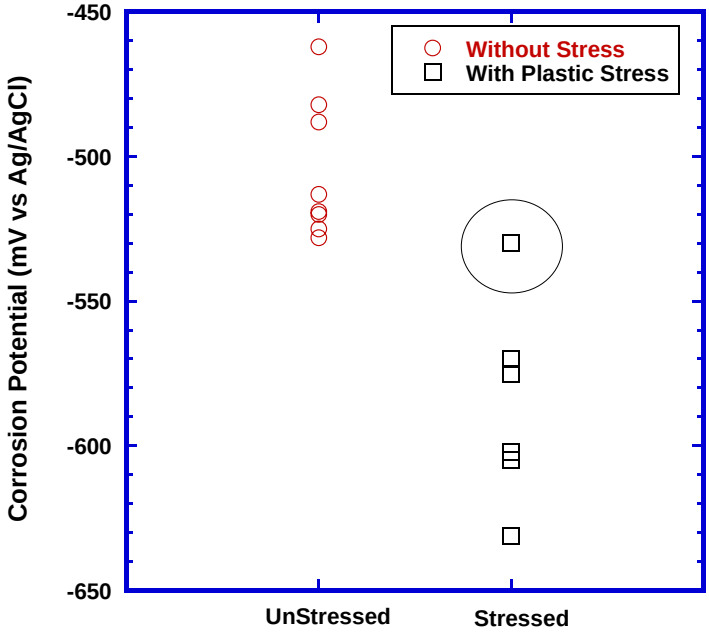


Figure 6.6 Summary of the corrosion potentials of AA2024-T351 from different potentiodynamic scans showing the effect of plastic stress (strain level > 5%). The experiments were performed in naturally aerated 0.01 M NaCl (scan rate = 1 mV/s). A scan (indicated within the circle) does not show significant differences in corrosion potentials after application of plastic stress.

Potentiodynamic polarization scans were also performed at higher chloride concentration (0.1 M NaCl) to check if the aggressiveness of the solution plays any role in determining the effect of plastic stress. Figure 6.7 shows the anodic polarization scans before and after application of plastic stress in naturally aerated 0.1 M NaCl. Breakdown and corrosion potentials of all of the potentiodynamic experiments (for both stressed and unstressed samples) are summarized in Figure 6.8 and Figure 6.9, respectively. Similar to the experiments with naturally aerated 10 mM NaCl, the same arbitrary current density of 1×10^{-5} A/cm^2 is chosen as a breakdown current density. It can be seen from Figure 6.8 and Figure 6.9 that the application of stress has similar effect on the corrosion properties as it was seen with 0.01 M NaCl.

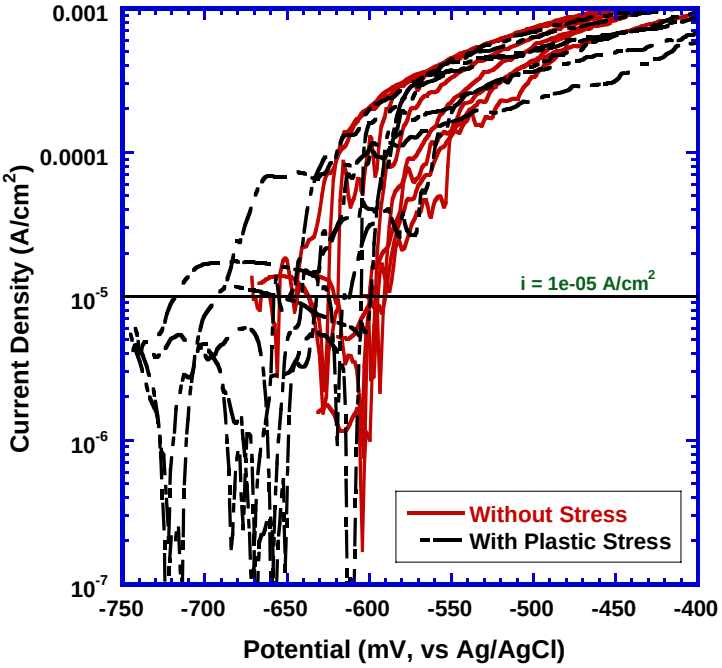


Figure 6.7 Anodic polarization scans of AA2024-T351 from capillary cell experiments in naturally aerated 0.1 M NaCl (scan rate = 1 mV/s) showing the effect of applied stress beyond yield strength (strain level > 5%). Potential at a current density of 1e-05 A/cm^2 is referred as breakdown potential.



Figure 6.8 Summary of the breakdown potentials of AA2024-T351 from different potentiodynamic scans before and after application of plastic stress (strain > 5%) in naturally aerated 0.1 M NaCl. In few cases application of plastic stress decreases both corrosion and breakdown potentials where as in other occasions they remain unchanged even after application of plastic stress.



Figure 6.9 Summary of the corrosion potentials of AA2024-T351 from different potentiodynamic scans before and after application of plastic stress (strain > 5%) in naturally aerated 0.1 M NaCl. In few cases application of plastic stress does not seem to change the corrosion potential.

However, the effect of stress is not always prominent which could be due to the fact that the concentration of 0.1 M NaCl is relatively aggressive and localized corrosion initiation is easier to achieve. By comparison, in 0.01 M NaCl solution microstructural features (developed by applied stress) are necessary to develop the local environments that will ease in the initiation of localized corrosion. So, these results indicate that even the effect of plastic stress could be masked, if any overaggressive electrolyte is chosen for experiments.

6.1.2 Capillary Cell Electrochemical Studies on AA2024-T351 After Surface Treatment[21]

In this part of the study, experiments were carried out after surface treatment for 'S' phase removal from AA2024-T351 samples (as described in Chapter 3) to investigate the specific contribution from 'S' phase particles to localized corrosion initiation during the stressing condition. Results of these experiments are shown in Figure 6.10. After the removal of 'S' phases, prominent passive regions are observed in each of the scans for the unstressed sample.

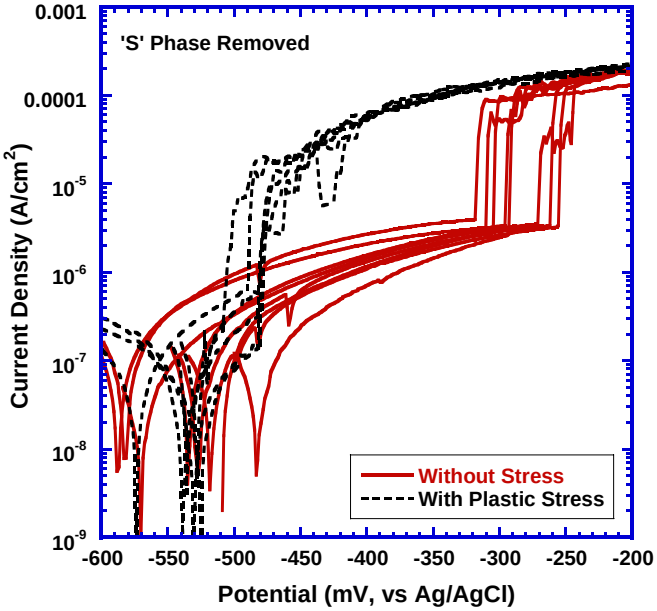


Figure 6.10 Anodic polarization scans of the surface treated AA2024-T351 sample (without 'S' phases) showing the effect of plastic stress (strain level > 5%) when tested in naturally aerated 10 mM NaCl using capillary cell (scan rate = 1 mV/s). Application of plastic stress does not change the corrosion potential, but decreases the breakdown potential. Removal of 'S' phases also brings a smooth passive region in the potentiodynamic scans.

[21] Details of the surface treatment technique are described in Chapter 3 and beneficial effects of 'S' phase removal in Chapter 4. It should be noted that surface treatment not only removes 'S' phases but also partially attacks the 'Fe-Mn' particles on the surface of AA2024-T351.

Application of stress minimizes the span of the passive region by decreasing the breakdown potential from ~ -275 mV vs. Ag/AgCl to -480 mV vs. Ag/AgCl. However, the corrosion potentials of samples do not change even after the application of plastic stress. These results indicate that the complete removal of 'S' phases does not completely remove the effect of stress. It has to be remembered that the surface treatment not only removes the 'S' phases but also partially attacks the 'Fe-Mn' particles present on the surface of AA2024-T351. Morphological changes of the 'Fe-Mn' particles during the surface treatment have already been discussed in Chapter 4. So, deformation induced microstructural changes as well as the morphological changes of Fe-Mn particles under stress could be playing an important role in determining the localized corrosion behaviour of the exposed areas.

Further comparisons of the electrochemical behaviour of stress vs. unstressed samples with and without the presence of 'S' phases is shown in Figure 6.11 and Figure 6.12. It is interesting to note that, the breakdown potentials of unstressed samples with 'S' phases are very close to the breakdown potentials of stressed samples without 'S' phases. Comparison of all the above represented data indicate that 'S' phase may not be the only responsible phase for corrosion initiation in stressing condition. Though the removal of 'S' phases improve the corrosion performance of AA2024-T3, but is unable to eliminate the effect of stress totally.

So, to have a better understanding of the contribution from the deformation induced microstructural changes in determining the localized corrosion phenomena, SEM microscopic analysis of a plastically deformed sample was performed without exposing the specimen to the electrolyte as shown in Figure 6.13. The Stress level of this sample was same as the samples electrochemically tested with the 3-point bend test set up (in all cases the midspan deflection was maintained at ~1.6 mm).

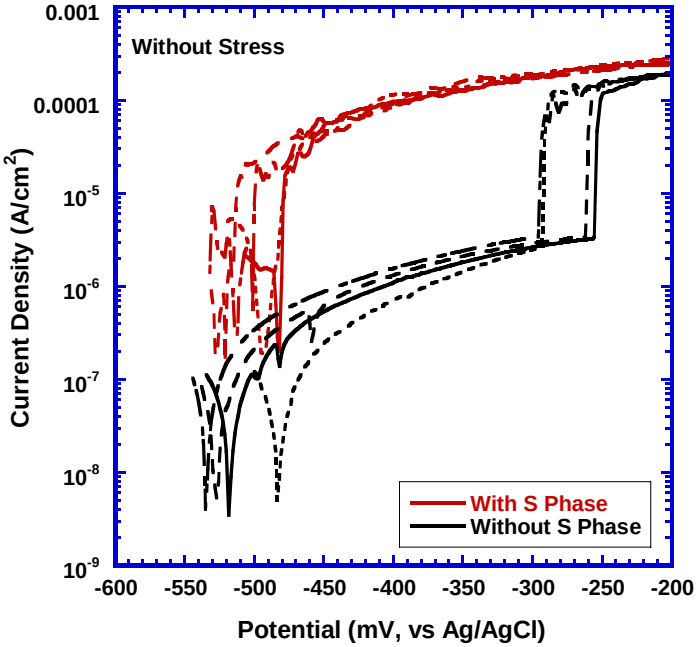


Figure 6.11 Comparison of the potentiodynamic scans of AA2024-T351 in unstressed condition showing the effect of surface treatment. Capillary cell (1 mm diameter) experiments were performed in naturally aerated 10 mM NaCl (scan rate = 1 mV/s). Removal of 'S' phases does not influence the corrosion potential, but increases the breakdown potential.

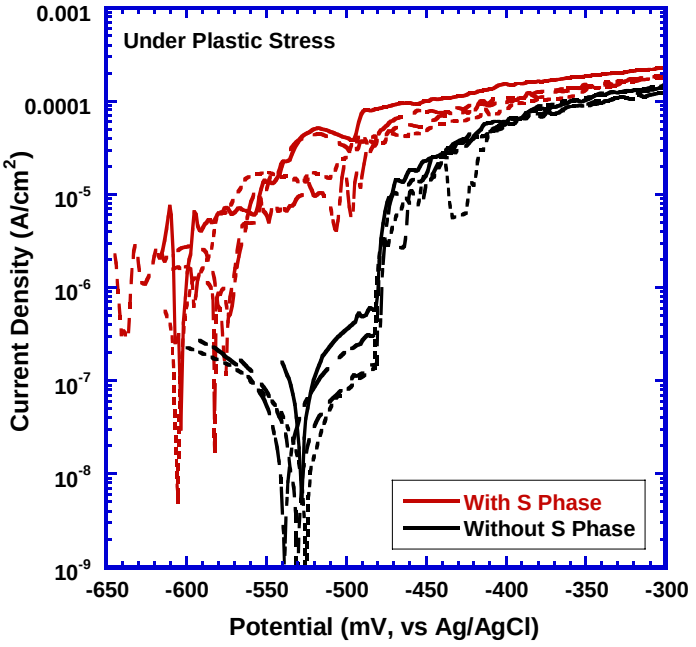


Figure 6.12 Comparison of the potentiodynamic scans of plastically deformed AA2024-T351 sample (strain level > 5%) showing the effect of surface treatment. Capillary cell experiments were performed in naturally aerated 10 mM NaCl (scan rate = 1 mV/s). Application of plastic stress decreases the corrosion and breakdown potential even after the removal of 'S' phases from the samples.

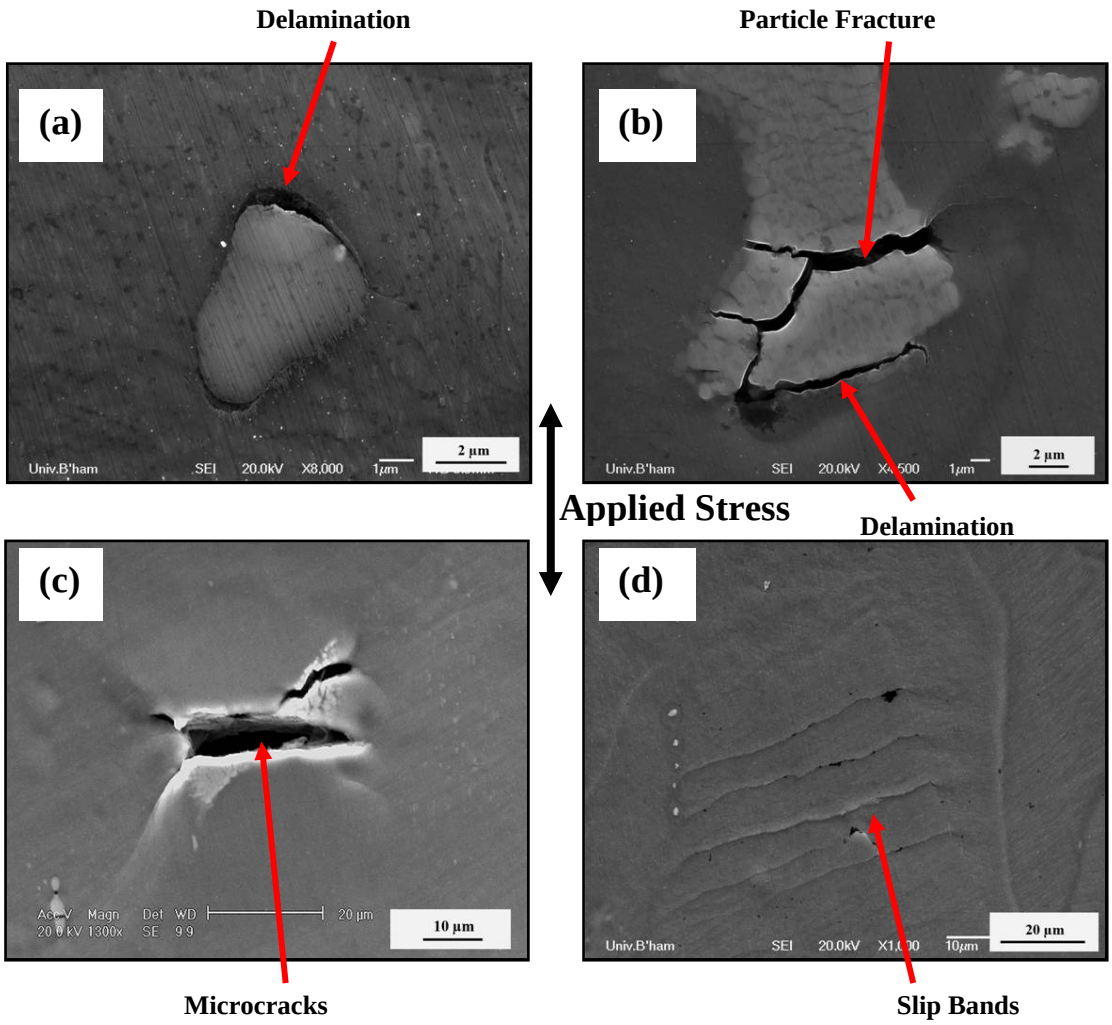


Figure 6.13 Morphological observations of a plastically stressed (strain level > 5%) AA2024-T351 sample using SEM. Applied stress is parallel to the rolling direction. (a)-(b) Shows the delaminations that are frequently observed at this high stress level along with few microcracks in the matrix as shown in (c). (d) Shows the visible slip bands in the deformed matrix. It should be noted that strain level in this case (3-point bend) is much higher than 4-point bend tests under in situ SEM.

Application of stress made the surface rougher as clearly visible under the microscope (Figure 6.13d). Most of the irregular shaped Fe-Mn particles shows fracture which is perpendicular to the applied stressing direction. A typical example of such fracture in a Fe-Mn particle is shown in Figure 6.13b. A few rounded ‘S’ phase particles

show delamination at the edge (Figure 6.13a), but this number seems to be statistically insignificant compared to fractured particles.

In many cases cracks open up perpendicular to the stressing direction (Figure 6.13c). Deformation bands are obvious features as it creates wavy pattern in the matrix (Figure 6.13d). So, the variation in the corrosion behaviour of the exposed area under the droplet during different polarization scans could actually be due to the variation of types and number of defects (particles as well as in the matrix) exposed in that particular area.

So far, the experimental results on the plastically deformed AA2024-T351 prove that stress adversely affects the corrosion performance of the alloy. However, the reason behind such change in the corrosion properties is not fully understood as yet. A few researchers attributed it to the deformation induced changes in both particles and well as in the matrix [29, 35]. Ambiguities still remain in explaining whether the intermetallic particle delamination (e.g., Figure 6.13a-b) or the stress induced deformation of the alloy matrix (e.g., Figure 6.13c-d) play the dominant role in controlling the localized corrosion initiation in the alloy.

Hence, in this current study an experimental approach is taken to separate out the effect of stress on intermetallic particles and on the particle free matrix. A particle free cast Al-0.099Cu binary alloy is selected for further investigation in unstressed and stressed condition. This approach is thought to provide some insights about the contribution from particle delamination vs. the deformation induced changes of the alloy matrix in changing the corrosion behaviour of the alloy under stressing condition.

6.1.3 Capillary Cell Electrochemical Studies of Al-0.099Cu Binary Alloy

In order to resolve the issues associated with the initiation of corrosion from the intermetallic particles, a cast binary alloy Al-0.099Cu is chosen for further investigation under stressing condition.[22]

Because of the low copper content in the alloy, the matrix is supposed to be free of any intermetallic particles and due to its cast structure it is supposed to have large elongated grain structure. Metallographic analysis was performed in details using scanning electron microscopy and EDS. Microstructural analysis proves that the matrix is almost free of intermetallic particles (Figure 6.14a-b). Very few rounded particles in the size range of 1-2 μm were observed in the microstructure (with an occurrence frequency of around 10-15 particles per square mm) [see Figure 6.14c-d]. Most of these particles are identified to consist of aluminium and copper by EDS analysis, with a composition of about 65 wt% of Al and 35 wt% of Cu. A few particles contained approximately 5 wt% of Fe.

The sample was etched with 2% HF + 10% HNO_3 for 90s in order to reveal the cast grain structure. It can be seen from Figure 6.15 that most of the grains are in the size range of 1.5-2 mm.

[22] Details of the alloy compositions can be found in Chapter 3.

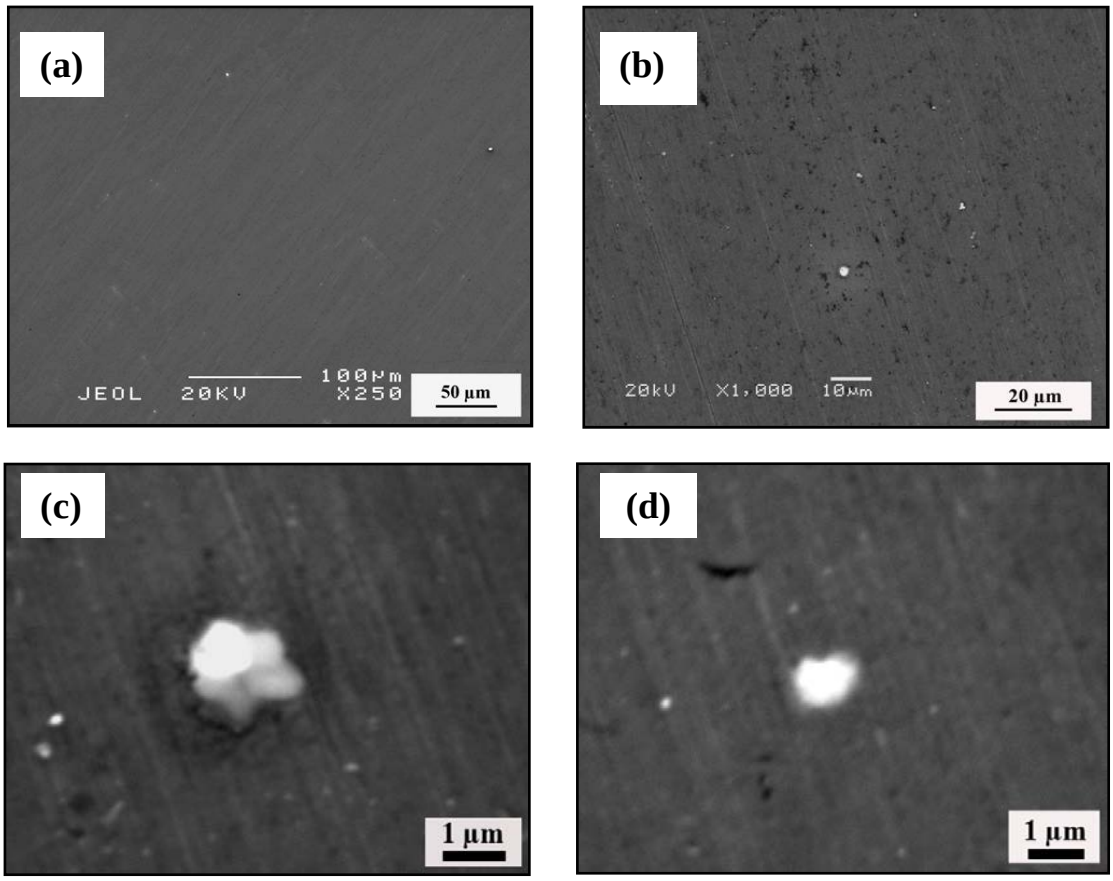


Figure 6.14 (a) SEM micrographs of Al-0.099 Cu alloy showing almost particle free matrix. (b) Showing very few small particles that are present in the microstructure. (c)-(d) Rounded Al-Cu particles with typical composition of 65 wt% Al and 35 wt% Cu. About 10-15 such particles are found per square mm of the alloy surface.

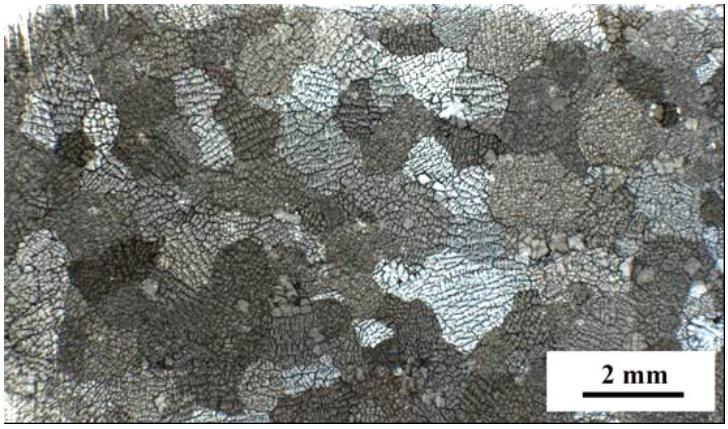


Figure 6.15 Microstructure of the as cast Al-0.099Cu binary alloy as revealed after etching with 2% HF + 10% HNO_3. Each grain is characterized by the presence of many subgrains within it.

Figure 6.16 compares of the potentiodynamic scans performed on Al-0.099Cu binary alloy in unstressed and plastically stressed conditions in naturally aerated 10 mM NaCl. 3-point bend test set up was used to plastically stress the Al-0.099Cu sample as it was performed for AA2024-T351 samples. A strain gauge was used in this case also for measuring the strain on the sample surface. The strain gauge failed at a strain value of 3.5 % which corresponds to 0.7 mm of the midspan deflection. For the consistency of the tests, stress was being applied until the midspan deflection reached ~1.6 mm. Hence, in this case also, the strain value is represented as > 5%. As the matrix of the binary alloy is free of intermetallic particles, change in the state of the passive film after application of plastic stress is thought to play an important role. So, time between stressing the samples and potentiodynamic tests has been controlled. In all cases, the time between the final polishing and stressing is kept constant to five minutes.

If stress plays a role in breaking the passive film and thereby affecting the localized corrosion initiation phenomena, the time required to repair the passive could be crucial. So, a series of tests have been performed as a function of time after stressing the sample to check if any differences can be seen in terms of breakdown potential, corrosion potential or passive current density. The summary of these tests are represented in Figure 6.17 - Figure 6.19. As mentioned earlier, for stressed samples the time referred in those plots is time between plastically stressing the sample and performing the potentiodynamic scan whereas for unstressed samples it was the time between polishing and experiments.

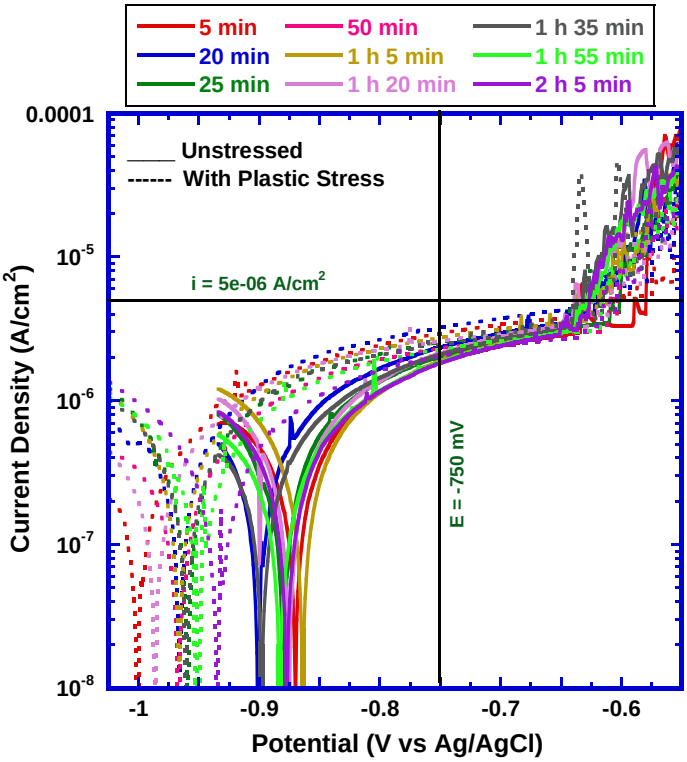


Figure 6.16 Potentiodynamic polarization scans of Al-0.099Cu alloy in naturally aerated 10 mM NaCl (scan rate = 1 mV/s). Time between the application of plastic stress (strain > 5%) and actual measurement is indicated at the top of the curve. Application of plastic stress decreases the corrosion potential of the alloy, but do not influence the breakdown potential.

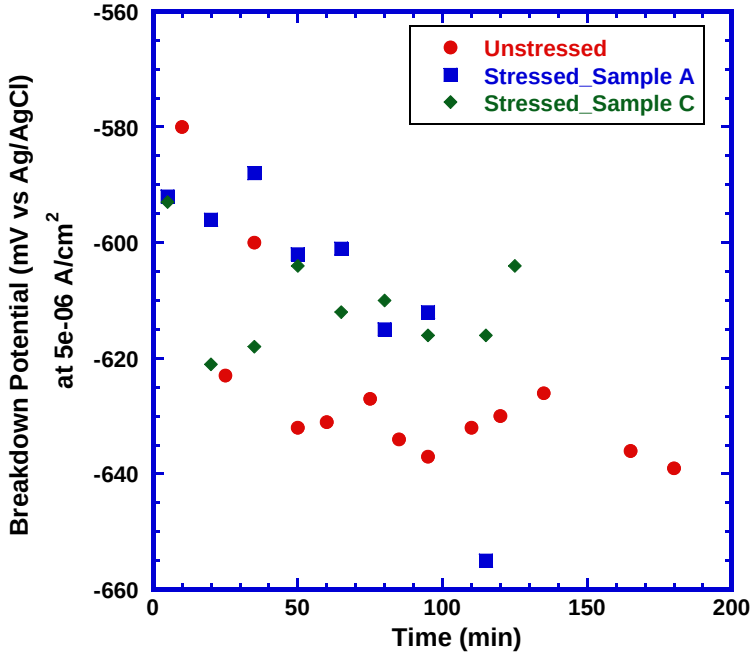


Figure 6.17 Comparison of the breakdown potentials (potential at a current density of 5e-06 A/cm^2) of unstressed and plastically stressed (strain > 5%) Al-0.099Cu binary alloy tested in naturally aerated 10 mM NaCl using capillary cell.

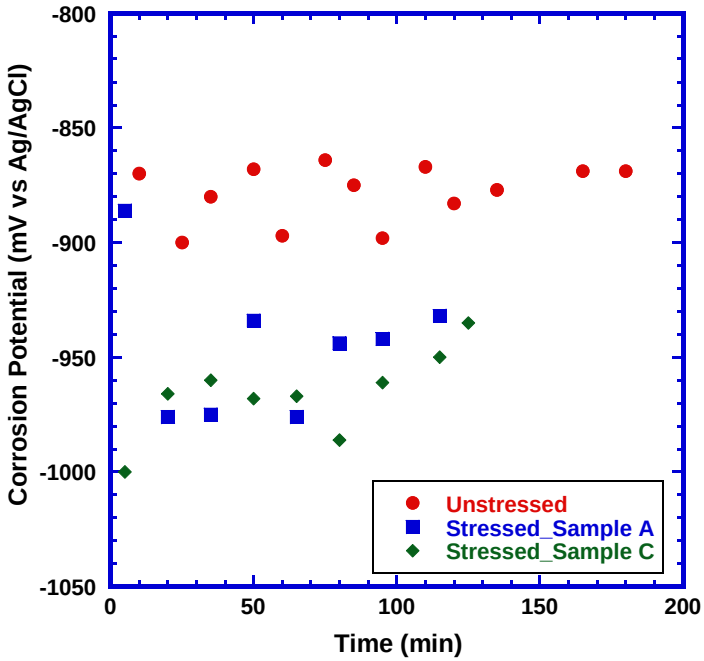


Figure 6.18 Comparison of the corrosion potentials of unstressed and plastically stressed (strain > 5%) Al-0.099Cu binary alloy tested in naturally aerated 10 mM NaCl using capillary cell. In all cases plastically stressed samples show lower corrosion potential than the unstressed samples.

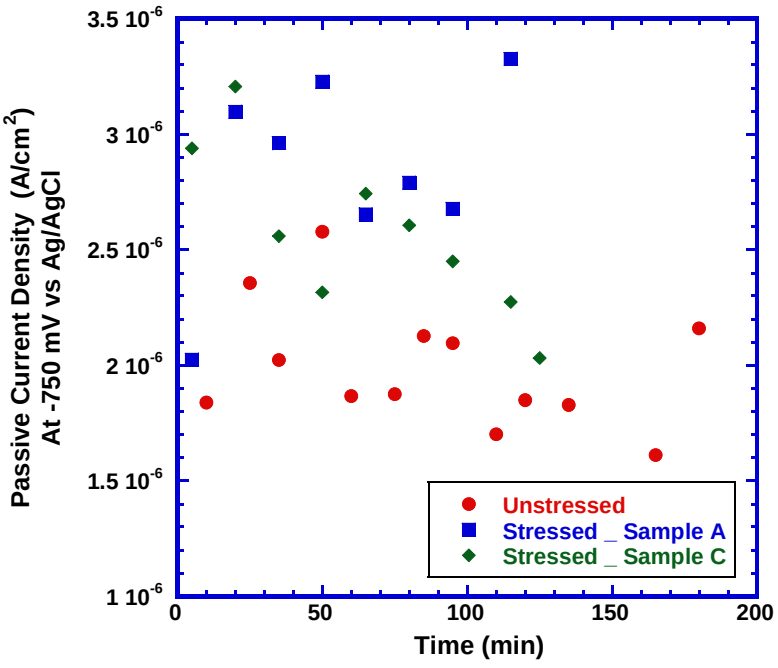


Figure 6.19 Comparison of the passive current densities of unstressed and plastically stressed (strain > 5%) Al-0.099Cu binary alloy tested in naturally aerated 10 mM NaCl using capillary cell. Passive current densities are measured at the middle of the passive region. In most cases plastically stressed samples show slightly higher passive current densities than the unstressed samples.

It can be seen from the Figure 6.16 that the potentiodynamic scans are very repeatable in the unstressed condition, though there is some slight variability in the scans after the sample is plastically stressed. In all the cases scans are stopped right after the breakdown and before reaching the limiting current, so that the initiated pit could not have grown further.

No definite trend has been observed between the breakdown potentials and the time as can be seen from Figure 6.17. For the unstressed samples, breakdown potentials stay between -620 mV to -640 mV vs. Ag/AgCl over the entire time span. In both unstressed and stressed samples, several metastable activities are observed prior to the breakdown. It is surprising to note that (Figure 6.17) stressed samples showed slight increase in the breakdown potential (~ 10 mV) as compared to the unstressed sample. The reason behind this phenomenon is not fully understood yet, though it can well be dealt with statistical analysis of variability. As aluminium alloys shows lot of variation in their breakdown potentials, these values could be within the scatter range. However, application of stress decreases the corrosion potential (Figure 6.18) and increases the passive current density (Figure 6.19) of the Al-0.099Cu binary alloy. These differences in the observations between unstressed and stressed samples could possibly be attributed to the change in the surface oxide film structure/state with the application of stress. Presence of slip bands in the stressed samples will locally change the passive film structure. If the stress is high enough to break the passive film, freshly exposed sample surface will come in contact with the electrolyte and thereby will affect the localized corrosion behaviour of the alloy.

Macroscopic and SEM observations were performed to have a better understanding about the droplet (under the capillary)/matrix interaction. Since the grains are very big, a particular droplet could have interacted with only one or several deformed

grains. The idea of the experiments was to determine whether there were any obvious differences in the corrosion behaviour depending on the location of the capillary droplet. Figure 6.20 shows one such macroscopic image showing capillary-droplet interaction with a stressed microstructure of the plastically deformed Al-0.099Cu alloy.

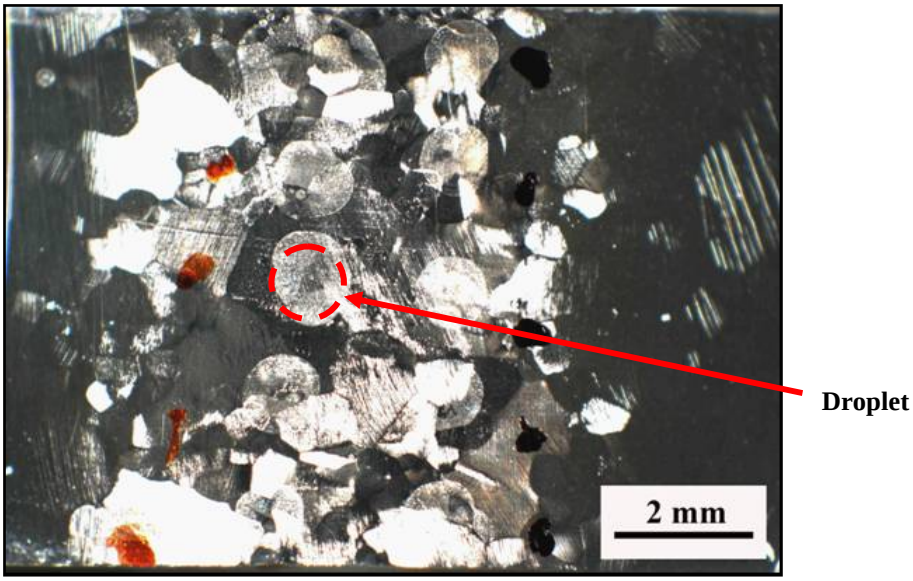


Figure 6.20 Macroscopic image of a plastically stressed Al-0.09Cu sample (strain > 5%) showing the interaction of the droplet (under the capillary) with the deformed grains. Orange and black dots are drawn next to the exposed droplets to identify them clearly in the image.

SEM analysis of the stressed samples were performed after the potentiodynamic tests in 10 mM NaCl solution using a capillary cell and most of the typical microscopic features are shown in Figure 6.21. Figure 6.21(a) shows the interaction between the droplet under the capillary and the matrix. It can be seen that, the droplet could be inside only a single grain or it could interact with several grains. It is interesting to note that different grains have shown the presence of slip/deformation bands in different orientations. Two adjacent grains often show different slip band orientations which could be perpendicular or parallel to the applied stress.

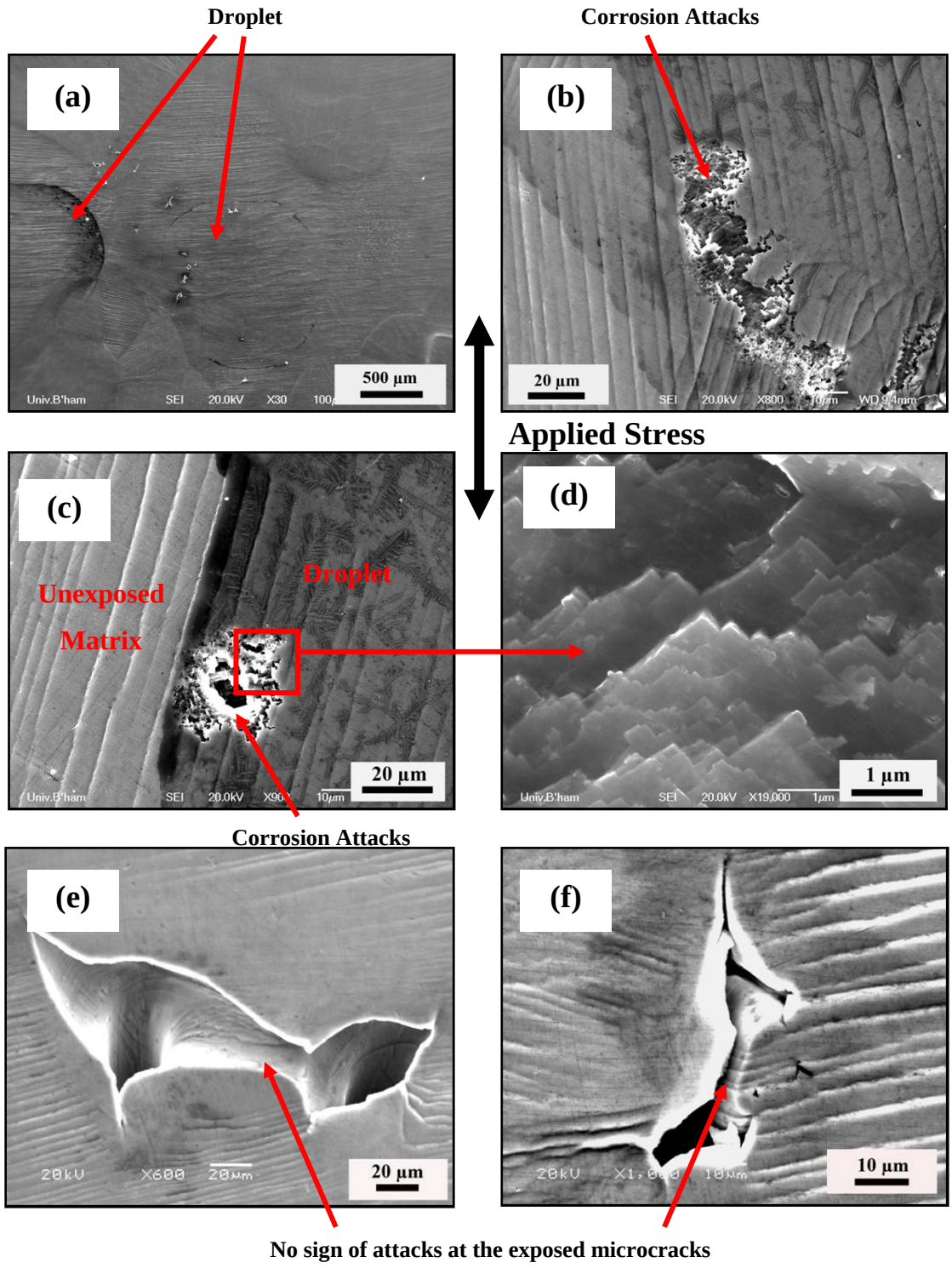


Figure 6.21 SEM images of the plastically stressed Al-0.099Cu binary alloy (strain > 5%) after the potentiodynamic test in aerated 10 mM NaCl using capillary cell. (a) Shows the interaction of droplets with stressed grains, (b)-(c) Corrosion attacks in the exposed areas, (d) Shows the presence of crystallographic corrosion facets at the inner surface of the corrosion attacks, (e)-(f) No sign of corrosion in the microcracks.

Figure 6.21(b)-(c) shows localized corrosion attack inside the exposed area. The inner surfaces of the corrosion attack show the presence of crystallographic corrosion facets. These attacks are not deep as the scans were terminated after the breakdown potential. The presence of such crystallographic corrosion tunnels at the inner surface of a pit in the aluminium alloys has also been reported by Pride [134]. Figure 6.21(e)-(f) shows some of the typical microcracks present in the exposed droplet. Figure 6.21 (e) shows the unfolding of the matrix due to the application of stress. No pitting/localized attacks on or adjacent to these deformation features are observed.

So, the presence of these features may not affect the electrochemical behaviour of the alloy. This is consistent with the electrochemical results as application of stress does not change the breakdown potential of the binary alloy.

6.1.4 Summary of the Stress Assisted Electrochemical Studies in the Plastic Domain

Application of stress in the plastic domain decrease both corrosion potential and breakdown potential of AA2024-T351 (see Figure 6.5 and Figure 6.6). In the surface treated AA2024-T351 samples without ‘S’ phases, stress does not change the corrosion potential but decrease the breakdown potential (Figure 6.10). Surface treated AA2024-T351 samples show a short passive region even in the stressed condition. However, though corrosion performance of the alloy is improved after removal of ‘S’ phases in the stressed condition, the surface treatment does not eliminate the effect of stress completely. These experiments possibly indicate the significance of other intermetallic particles (especially Fe-Mn particles) present in the microstructure. Delaminations at the

interface of those particles with the matrix possibly act as the potential sites of localized corrosion by creating microcrevices although specifics of this phenomenon have not been fully investigated in this study.

Capillary cell electrochemical experiments with the Al-0.099 Cu binary alloy without any intermetallic phases do not show any significant effect of stress on the localized corrosion properties of the alloy. Corrosion potentials of the stressed samples are slightly lower and there were no major changes in the breakdown potentials of the alloy (see Figure 6.17 and Figure 6.18). The decrease in the corrosion potential in the stressed sample could possibly be attributed to the exposure of the fresh active surface to the electrolyte in the slip band regions [25]. If the anodic current increases due to the freshly exposed surface, then it can cause the lowering of OCP (or corrosion potential) as could be found from the Evan's diagram (Figure 6.22). It can be seen from the figure that, if anodic reaction rate increases (from the initial black line to the red line), corrosion potential of the system decrease from initial equilibrium value of E_0 to a lower value of E_1.

Comparing all conditions mentioned above, it can possibly be concluded that without the presence of intermetallic particles, stress induced matrix deformation does not contribute much in changing the breakdown potential. Surface treatment for 'S' phase removal does not eliminate the effect of stress on the breakdown potential for AA2024-T351. Therefore the presence Fe-Mn particle and their morphological changes (i.e., delamination at the particle/matrix interface) under stressing condition could possibly be identified as the key controlling feature for the observed changes in the electrochemical behaviour of AA2024-T351.

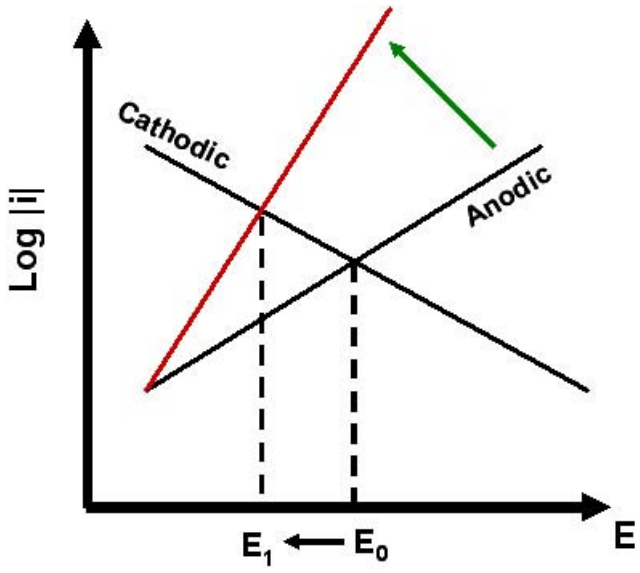


Figure 6.22 Evans diagram illustrating the effects of changes in the anodic reaction rates on the corrosion potential of the alloy. If the anodic reaction rate increases, potential decreases from E_0 to E_1.

6.2 Capillary Cell Electrochemical Studies of AA2024-T351 Under Elastic Stress

6.2.1 Potentiodynamic Polarization Experiments

Effects of applied elastic stress on the electrochemical behaviour of AA2024-T351 alloy was investigated using the capillary cell of 1 mm diameter exposure area. Details of the experimental set up using a 10 kN tensile stressing stage and the sample configuration can be found in Chapter 3. Applied stress is represented as a percentage of the yield stress of AA2024-T351 (Y.S. of AA2024-T351 was determined to be about ~ 375 MPa, Figure 6.1). Aerated 10 mM NaCl solution was used in all experiments as it was found to give good result in the plastic domain. The scan rate for all the potentiodynamic tests were 1 mV/s. Potentiodynamic polarization scans were performed on the specimens stressed to 45%, 70% and 90% of yield stress in the elastic domain. Experiments performed using

the synchrotron technique have shown that applied stress of 70% yield strength (Y.S.) or above affects the localized corrosion behaviour of AA2024-T351 (details of which will be described in Chapter 7). So, AA2024-T351 samples were subjected to 70% Y.S. as well as below and above this stress level (i.e., 45% and 90% Y.S. respectively) to find out if the potentiodynamic technique can be used to distinguish the effect of stress using capillary cell technique of one mm diameter exposed area. Throughout the following study stress was applied parallel to the rolling direction.

Figure 6.23 compares the potentiodynamic scans of unstressed and 45% stressed sample in naturally aerated 10 mM NaCl. Experiments were carried out on the samples which were stored overnight in lab air after polishing to have less variation in the open circuit potential of the alloy as a result of a possible uniform passive film. However, it should be noted that there are no significant differences between the scans performed 3-4 hours of polishing and one day after polishing. It can easily be seen from Figure 6.23 that the applied stress equivalent to 45% of the specimen's yield stress does not have any significant effect on the corrosion properties of the alloy. Corrosion potentials of the samples remain between -575 mV and -650 mV vs. Ag/AgCl in both unstressed and elastically stressed condition. An arbitrary current density of 1e-05 A/cm^2 is chosen to represent the breakdown current and the potential at that current is designated as breakdown potential. Most of the samples show a short pseudo-passive region between the corrosion potential and the breakdown. Breakdown potentials and passive current densities (measured roughly at the middle of the pseudo-passive region) of the specimen also remain same before and after application of stress.

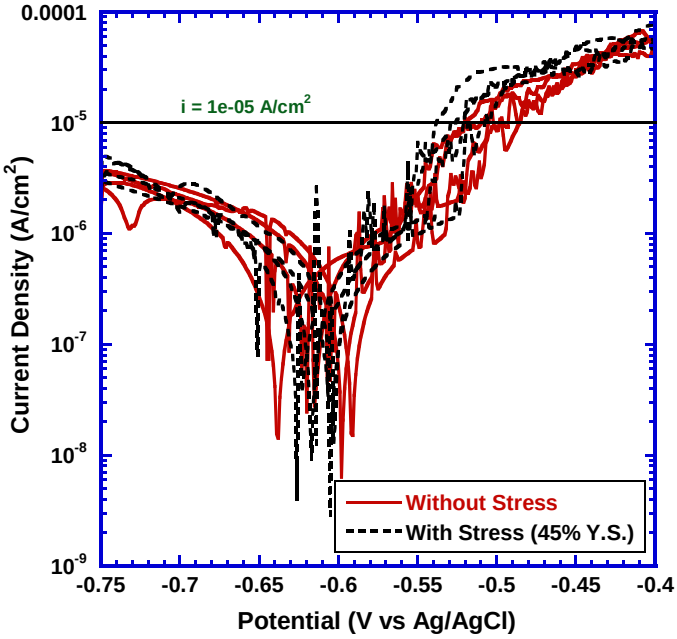


Figure 6.23 Anodic polarization scans of AA2024-T351 showing the effect of applied stress in the elastic domain (45% Y.S.). Experiments were performed in naturally aerated 0.01 M (10 mM) NaCl (scan rate = 1 mV/s) using capillary cell. Application of elastic stress (45% Y.S.) does not seem to change the corrosion potential or breakdown potential of AA2024-T351.

Figure 6.24 compares the potentiodynamic scans of unstressed and 70% stressed sample in naturally aerated 10 mM NaCl. It can be seen from the Figure 6.24 that corrosion potentials of the samples are between -600 mV and -700mV vs. Ag/AgCl for both stressed and unstressed conditions. Application of 70% Y.S. does not change the corrosion potential or breakdown potential of the alloy. In this case also, most of these scans (like 45% Y.S) show a short pseudo-passive region. Passive current densities (measured roughly at the middle of the pseudo-passive region) also remain same in both conditions. Most of the unstressed scans show a small passive region prior to breakdown. Breakdown potential of the stressed sample varies from -575 mV to -500 mV vs. Ag/AgCl. Both the unstressed and stressed samples show metastable activities as observed from the current fluctuations in the passive region. So, comparing corrosion

potential, breakdown potential, and passive current densities between the stressed (70% YS) and unstressed samples it is difficult draw any definite conclusion about the effect of elastic stress on the corrosion properties of the alloy. The potentiodynamic polarization scans with the exposed area of one mm diameter under the microcell are not able to distinguish the difference between the unstressed and elastically stressed (70% YS) AA2024-T351.

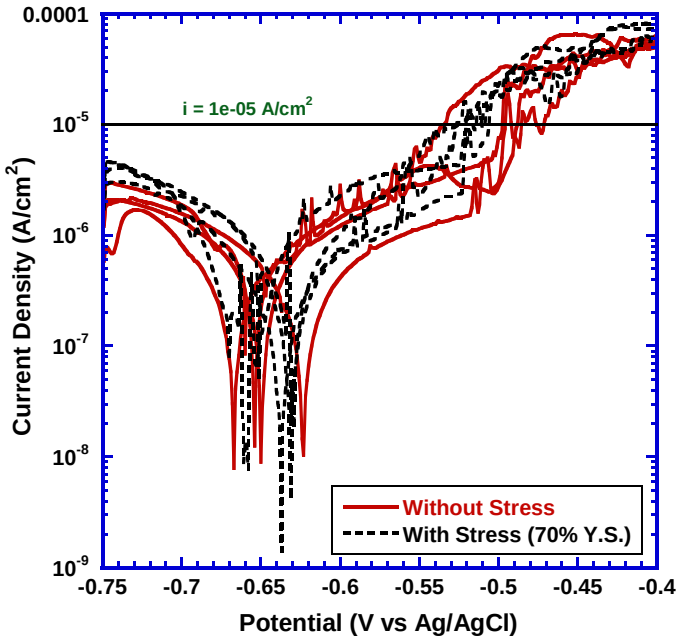


Figure 6.24 Anodic polarization scans of AA2024-T351 showing the effect of applied stress in elastic domain (70% Y.S.). Experiments were performed in naturally aerated 0.01 M (10 mM) NaCl (scan rate = 1 mV/s) using capillary cell. Application of elastic stress (70% Y.S.) does not seem to change the corrosion potential or breakdown potential of AA2024-T351.

So, further anodic polarization experiments were carried out after stressing the sample to 90% Y.S. to check if the increase in stress level can change the corrosion behaviour of the alloy (Figure 6.25).

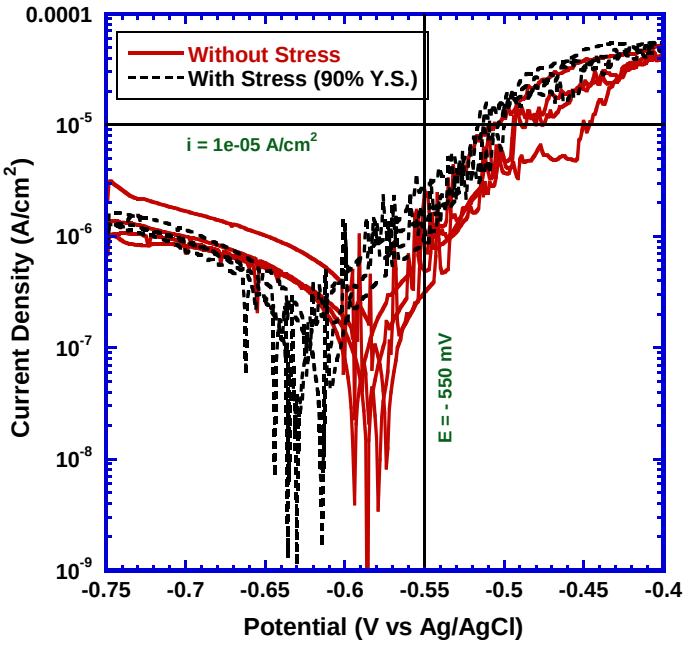


Figure 6.25 Anodic polarization scans of AA2024-T351 showing the effect of applied stress in elastic domain (90% Y.S.). Experiments were performed in naturally aerated 0.01 M (10 mM) NaCl (scan rate = 1 mV/s) using capillary cell. Application of 90% Y.S. does not change the breakdown potential, but slightly lowers the corrosion potential of AA2024-T351.

Comparison between the breakdown potentials, corrosion potentials and passive current densities [measured at a particular potential (i.e., -550 mV vs. Ag/AgCl in this case) in the pseudo-passive region] of unstressed and elastically stressed (90%Y.S.) samples are shown in Figure 6.26, Figure 6.27, and Figure 6.28, respectively. Comparing all the figures it can be confirmed that application of 90% Y.S. has some clear effect on the corrosion properties of the alloy. Corrosion potentials of the stressed sample are lower than the unstressed samples (Figure 6.27) whereas the passive current densities increase after the application of stress (Figure 6.28). Both unstressed and stressed samples show metastable activities as observed from the current fluctuations in the pseudo-passive region.

However, it is interesting to note that application of stress as high as 90% of the material's yield strength does not change the breakdown potential significantly (Figure

6.26). This could be due to the combination of lack of changes in the microstructural features below the yield strength and smaller exposure area under the capillary cell of one mm diameter. Some researchers [319] have shown that even below the yield strength, applied stress has some effect on the corrosion properties. But in all those reported cases, the exposed area was much higher (more than an order of magnitude) than the capillary cell exposure area. Liu *et al.* [319] reported lower breakdown potential with applied stress of 50% Y.S. It has also been reported that with increasing potential, the current increased at a much lower rate for the stressed sample. Liu found metastable pitting in the passive region and speculated that elastic stress could enhance the stability of the initial breakdown events.

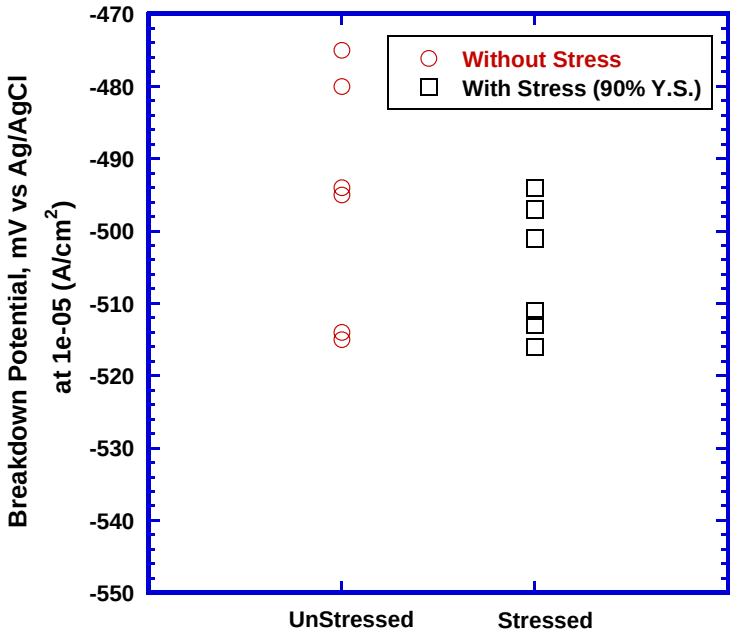


Figure 6.26 Comparison of the breakdown potentials of unstressed and elastically stressed (90% Y.S.) AA2024-T351 samples tested in naturally aerated 10 mM NaCl using capillary cell. Variations in the breakdown potentials of the unstressed samples are higher than the elastically stressed samples. However, no significant change of breakdown potential is observed in the elastically stressed samples.

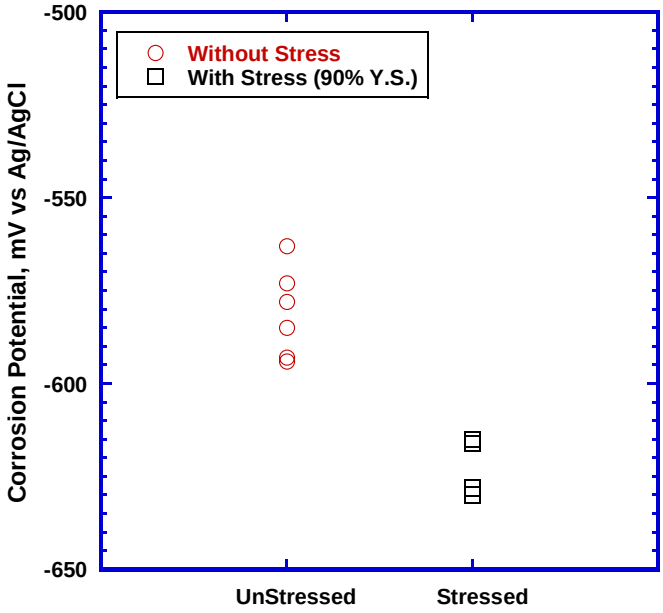


Figure 6.27 Comparison of the corrosion potentials of unstressed and elastically stressed (90% Y.S.) AA2024-T351 samples tested in naturally aerated 10 mM NaCl using capillary cell. Application of elastic stress equivalent to 90% Y.S. decreases the corrosion potential of AA2024-T351.

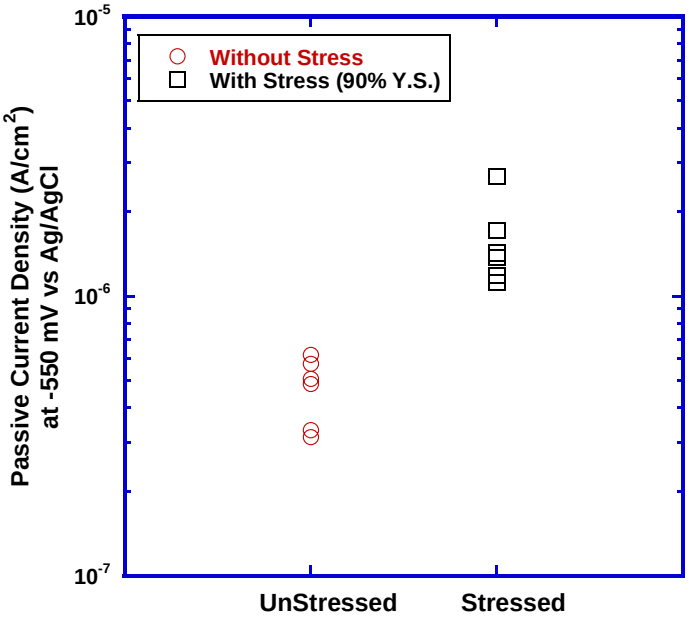


Figure 6.28 Comparison of the passive current densities of unstressed and elastically stressed (90% Y.S.) AA2024-T351 samples tested in naturally aerated 10 mM NaCl by capillary cell. Passive current densities of AA2024-T351 increases after application of elastic stress of 90% Y.S. (It has to be noted that most of the scans actually show a short pseudo-passive region between corrosion potential and breakdown, and the passive current densities are actually measured at a particular potential within those pseudo-passive regions).

6.2.2 Potentiostatic Polarization Experiments

Though application of 90%Y.S. show some definite effects on the corrosion properties of the alloy by lowering the corrosion potential and increasing the passive current density of the stressed sample, applied stresses of 70% Y.S. do not show any detectable difference using potentiodynamic scans.

So, the effect of applied stress was further investigated using a potentiostatic polarization technique and calculating the charge passed within a definite time span. The higher the dissolution of the exposed material, the higher the amount of charge passed. Applied stresses of 45%, 70% and 90% of Y.S. were chosen for the study. All samples were polished a day before the test to avoid variation in the scans as much as possible. Three different potentials were selected for the potentiostatic tests based on the representative potentiodynamic scans of an unstressed AA2024-T351 in naturally aerated 10 mM NaCl at a scan rate of 1 mV/s (see Figure 6.29). One polarization potential was chosen in the passive region (-550 mV vs. Ag/AgCl), the second one was chosen just below the breakdown (-525 mV vs. Ag/AgCl) and the third potential was chosen just above or at the breakdown region (Figure 6.29). Current vs. time plots were obtained from the potentiostatic tests. Then the KaleidaGraph software[23] was then used to run a macro for calculating the indefinite integral, yielding a new curve. This macro found the incremental area under the curve, given the X-Y data points [in this case time (s) and current (A)] describing the curve. This curve was then normalized by the area exposed and charge density (C/cm^2) vs. time (s) was plotted. A point on that curve at any particular time indicates the total charge passed to that time during the experiment.

[23] More details can be found in Chapter 3.

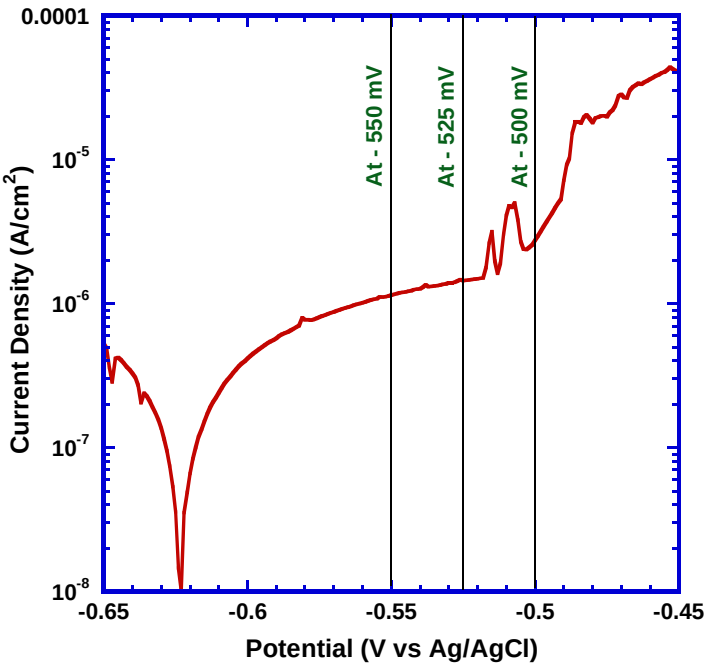


Figure 6.29 Anodic polarization scan of unstressed AA2024-T351 sample in naturally aerated 0.01 M (10 mM) NaCl with a scan rate of 1 mV/s using capillary cell. Test is performed one day after polishing. Three different potentials have been selected from this scan for further potentiostatic polarization. One polarization potential is selected in the passive region (-550 mV), second one is just below the breakdown (-525 mV) and the third potential is just above or in the breakdown region.

6.2.2.1 Effect of Applied Stress Equivalent to 45% Y.S. of AA2024-T351

Comparison of the potentiodynamic scans between the unstressed and 45% Y.S. stressed sample in the capillary electrochemical cell using naturally aerated 10 mM NaCl has been shown in Figure 6.23. An applied stress of 45%Y.S. does not show any clear effect on the corrosion behaviour of the sample. Corrosion and the breakdown potentials remain the same before and after the application of stress.

Metastable pitting is observed in the passive region for both stressed and unstressed samples. However, it has to be noted that different samples and even different

scans in the same sample may vary (as seen earlier from the scatter in the potentiodynamic data for AA2024-T351). So a particular potential which is in the passive region of one scan, could be close to the pitting potential for another scans as the passive region is very short.

Figure 6.30 shows current density vs. time (i.e., i-t curve) for stressed and unstressed samples in naturally aerated 10 mM NaCl. Potentiostatic polarizations at higher potentials show higher current densities in both unstressed and stressed conditions. Fluctuation in the current densities can be seen during the potentiostatic polarization; however absence of any rapid increase in the current densities during the tests indicate that stable pits are not growing in these potential regions.

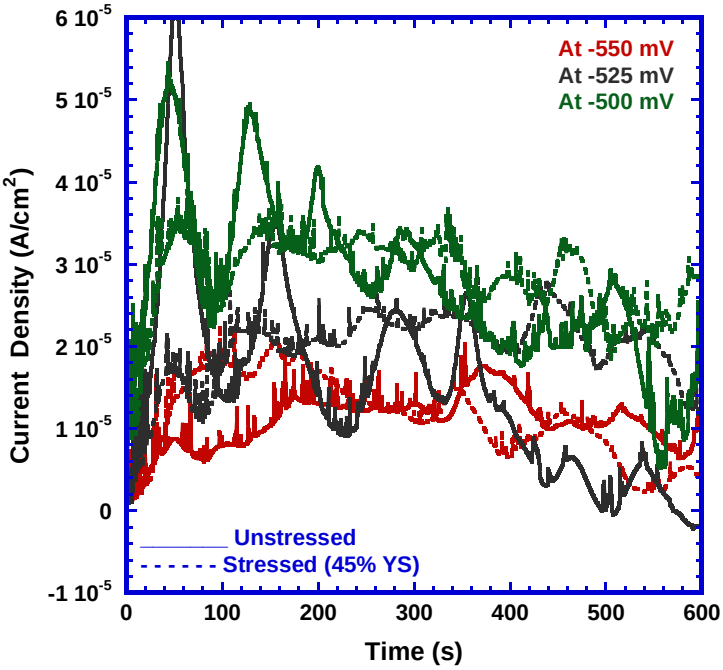


Figure 6.30 Potentiostatic polarization of unstressed and stressed (45% Y.S.) AA2024-T351 samples at different potentials. Experiments were performed in naturally aerated 10 mM NaCl. All potentials were measured vs. Ag/AgCl. Higher fluctuation in the current is seen at higher potential. Stable pit might not be growing under these potentials as no rapid increases in the densities have been observed.

Charge passed as a function of time for both stressed and unstressed AA2024-T351 samples are shown in Figure 6.31. A few potentiostatic polarizations (results not shown) were attempted at a potential of -575 mV vs. Ag/AgCl which is very close to the open circuit potential of the alloy. After some time, the current drifted to the negative direction because total cathodic current (due to oxygen reduction) was more than the total anodic current (metal dissolution). In some occasions, current gradually starts to decrease after 300-400 seconds when the polarization potential was at -525 mV vs. Ag/AgCl (Figure 6.31). During exposure in the electrolyte, the surface of AA2024 could enrich with copper which is a better surface for oxygen reduction, and hence net current becomes negative. As the current densities do not increase rapidly during the exposure period (rather it decreased as a function of time), it could be assumed that stable pitting is not predominant in this potential region.

It should be noted that, Figure 6.31(a) and (b) represents the scans from two different samples prepared by identical polishing method. These representative figures are shown to emphasize on the possible variability in two separate samples even though they are in identical test conditions and prepared identically. It is quite clear from Figure 6.31 that application of 45% Y.S. does not have any significant effect on the charge passed during the tests at three different polarization potentials. However, both Figure 6.31(a) and Figure 6.31(b) shows slightly higher charge passed in stressed sample at -550 mV vs. Ag/AgCl.

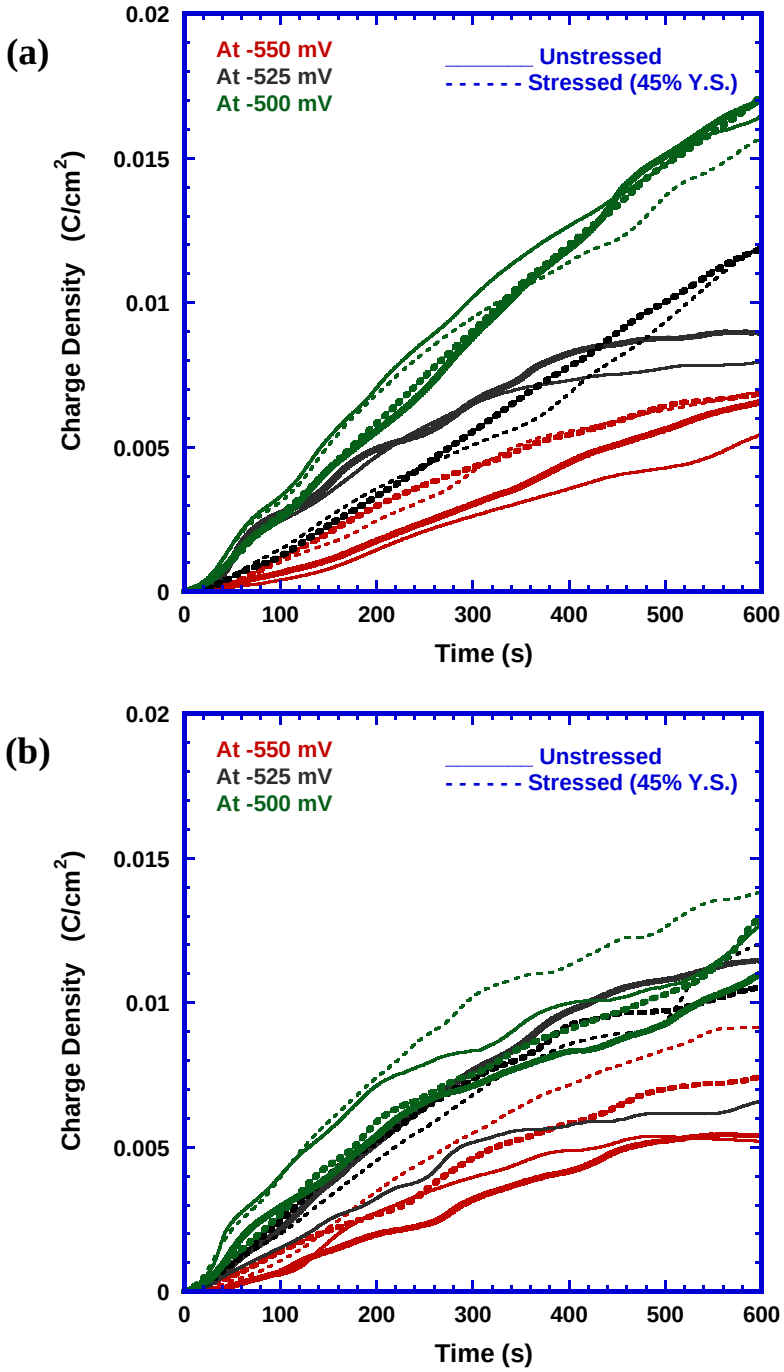


Figure 6.31 Charge passed as a function of time for unstressed and 45% Y.S. AA2024-T351 samples at different polarization potentials. All potentials were measured vs. Ag/AgCl. Experiments were performed in naturally aerated 10 mM NaCl solution using capillary cell. (a) and (b) are showing representative tests from two different AA2024-T351 samples in identical stressing condition.

Stressed and unstressed exposed areas after the potentiostatic tests were analysed using SEM (Figure 6.32). Type and morphology of attacks are same in both stressed and unstressed samples. Most of the 'S' phases are attacked and selective dissolution of Mg from those particles have been confirmed using EDS analysis. In a few occasions shallow pitting are observed in the matrix. Fe-Mn particles do not show any obvious attack on or around them, however in a few cases pitting has been observed adjacent to the particles. However, these could easily be confused with the pre-existing defects adjacent to the Fe-Mn particles.

6.2.2.2 Effect of Applied Stress Equivalent to 70% Y.S. of AA2024-T351

It has already been seen from the Figure 6.24 that results from potentiodynamic scans (performed in naturally aerated 10 mM NaCl using a capillary cell of 1mm diameter with a scan rate of 1 mV/s) can not be used to differentiate between the corrosion behaviour of unstressed and 70% Y.S. AA2024-T351 samples. Scans after application of 70% Y.S. do not show any prominent differences; moreover, aluminium alloys always show a fairly broad scatter range. So, potentiostatic tests were done at three different potentials as described in case of 45% Y.S. samples in the previous section.

Current densities as a function of exposed time at different potentials for both stressed and unstressed samples are compared in Figure 6.33. Current starts to decrease after initial high values as seen from Figure 6.33. As described earlier, this could be due to the enrichment of copper on the surface, especially on the 'S' phase particles as dealloying of Mg (and Al) occurred from the 'S' phase particles. Current densities of all tests at three different potentials are same after 400 seconds of polarization. So, the

difference in the charge passed at the end of 10 minutes period could be attributed to the initial differences of the current at different potentials.

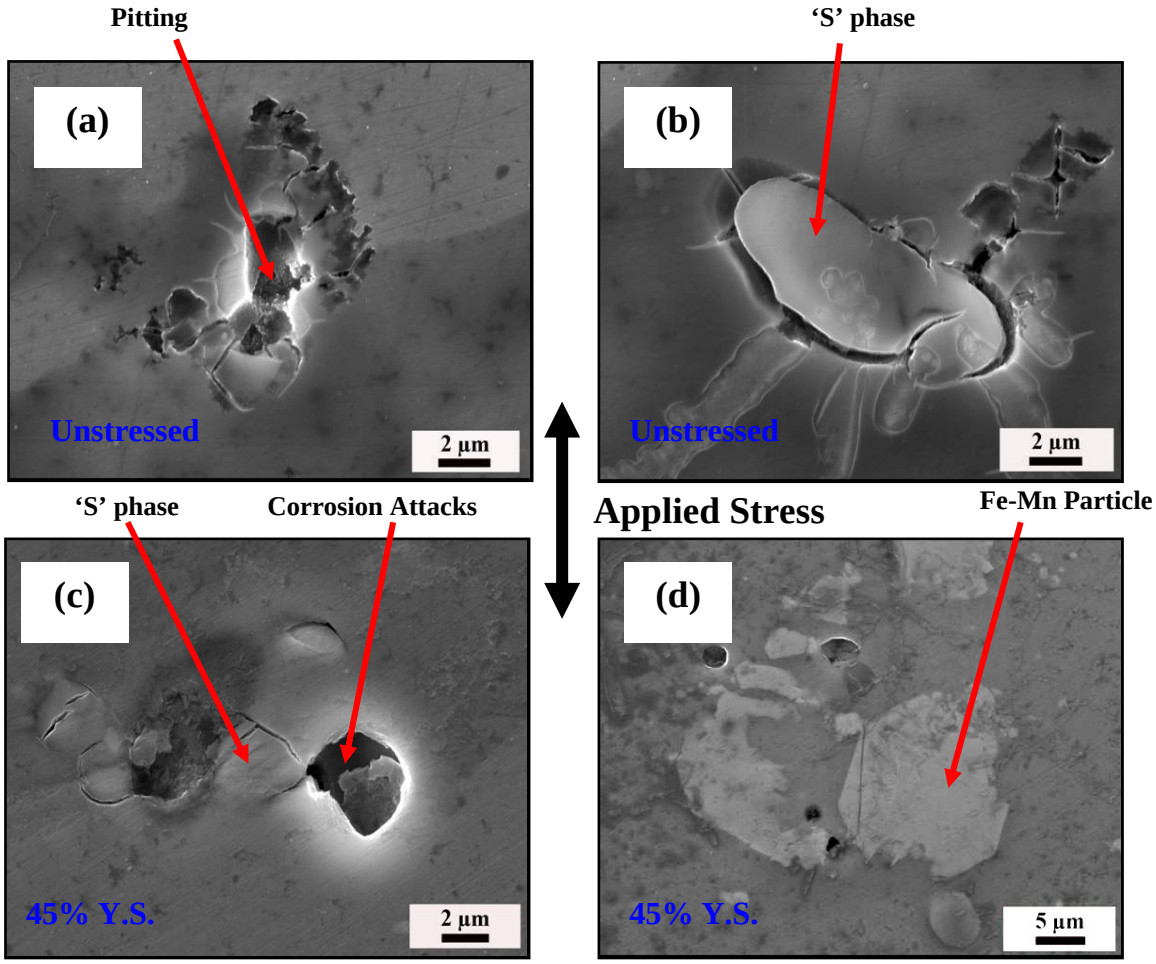


Figure 6.32 SEM micrographs of AA2024-T351 showing the morphology of attacks after the potentiostatic polarization at -500 mV vs. Ag/AgCl for 10 min in naturally aerated 10 mM NaCl. (a) Unstressed, showing very shallow pitting attack in the matrix, (b) Unstressed, showing attack on and around the 'S' phase particles, attacks in the matrix adjacent to the 'S' phase particles, (c) 45% Y.S., 'S' phase particles are attacked as well as attack in the adjacent matrix, (d) 45% Y.S., Fe-Mn particles remain unattacked.

Figure 6.34 shows the comparison of charge passed between unstressed and 70%Y.S. stressed samples as a function of time at different potentials. Figure 6.34a reveals that the amount of charge passed after the application of stress in both potentials

are higher than the unstressed samples. Effect of stress could also be observed from the higher amount of charge passed at -550 and -525 mV vs. Ag/AgCl in Figure 6.34b. These results confirm the fact that application of elastic stress not only affects the dissolution in the passive range but also influence the dissolution rate near or right after the breakdown.

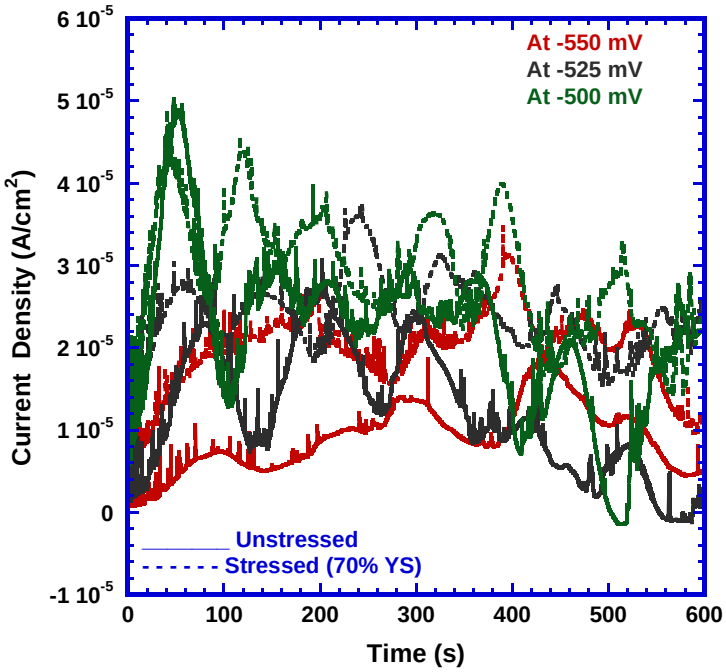


Figure 6.33 Potentiostatic polarization of unstressed and elastically stressed (70% Y.S.) AA2024-T351 samples at different potentials. Experiments were performed in naturally aerated 10 mM NaCl. All potentials were measured vs. Ag/AgCl. Stable pit might not be growing under these potentials as no rapid increases in the densities have been observed. In few cases gradual decrease in the current density can be seen after 400s of exposure.

Comparing Figure 6.31 and Figure 6.34, it could be concluded that effect of stress is more prominent when the elastic is 70% of the yield strength of the AA204-T351 sample than the 45% Y.S. samples. However, it should also be mentioned that in few experiments, 70% Y.S. did not show any distinctive difference than the unstressed samples at -525 and -500 mV vs. Ag/AgCl.

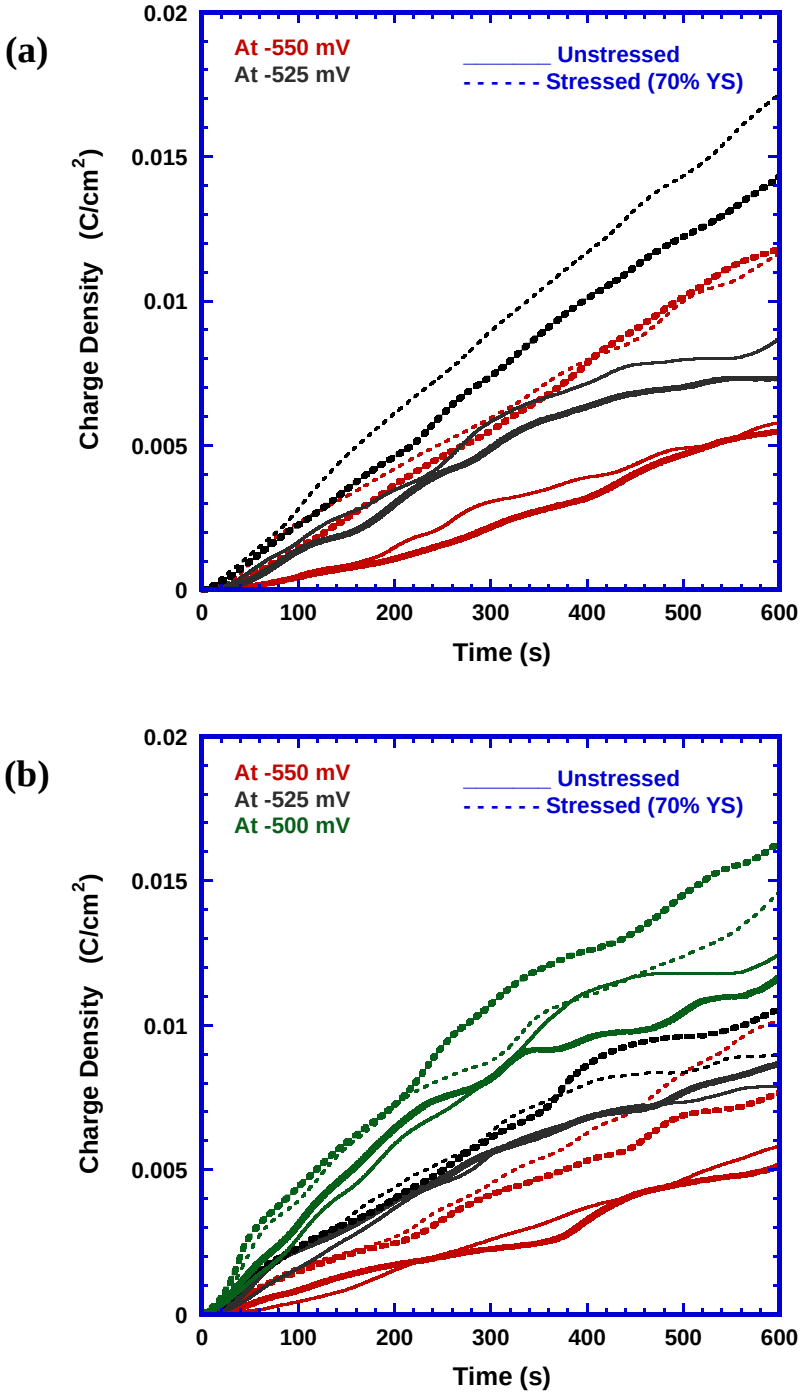


Figure 6.34 Charge passed as a function of time for unstressed and 70% Y.S. AA2024-T351 samples at different polarization potentials. All potentials were measured vs. Ag/AgCl. Experiments were performed in naturally aerated 10 mM NaCl solution using capillary cell. (a) and (b) are showing representative tests from two different sets AA2024-T351 samples in identical stressing condition.

Figure 6.35 shows the analysis of the exposed area after the potentiostatic tests at different potentials. This figure represents the SEM micrographs of the 70% Y.S. samples. However, no detectable differences have been observed between the corrosion morphologies of the stressed and unstressed samples. It was also difficult to determine any differences in the attack morphologies between the samples held at -550 mV and at -500 mV vs. Ag/AgCl, i.e., even at different potentials type/morphology of attacks look same.

SEM analysis confirms the attack on 'S' phases. Most of the 'S' phases show grooving in the adjacent matrix around them (Figure 6.35a-b). Other researchers [211] have also found this type grooving which is mainly caused by the increase local alkalinity due to the oxygen reduction as described in the earlier sections. EDS analysis in this current study show that all the 'S' phase particles showing grooving around them are actually dealloyed of Mg and Al. Mg concentration came down to 0.9-1.2 wt% after the test whereas unexposed normally contain 14-17 wt% Mg. Copper enrichment on the surface of 'S' phase particles have also been confirmed.

Figure 6.35(c) shows unattacked Fe-Mn particle and dealloyed 'S' phase with grooving around it. Since the number of exposed 'S' phase particles are much higher than the Fe-Mn particles, 'S' phase act as the potential site for corrosion initiation and dissolution rather than attack in the interface between Fe-Mn particle and matrix (due to possible delamination). Figure 6.35(d) confirms such observation where potentiostatic polarization even at -500 mV vs. Ag/AgCl does not initiate pitting or grooving around the Fe-Mn particle. This possibly indicate that the copper rich 'S' phase particles become better cathode than the Fe-Mn particles. Figure 6.35(e) shows another dealloyed 'S' phase and possible redistributed fine copper particles adjacent to it.

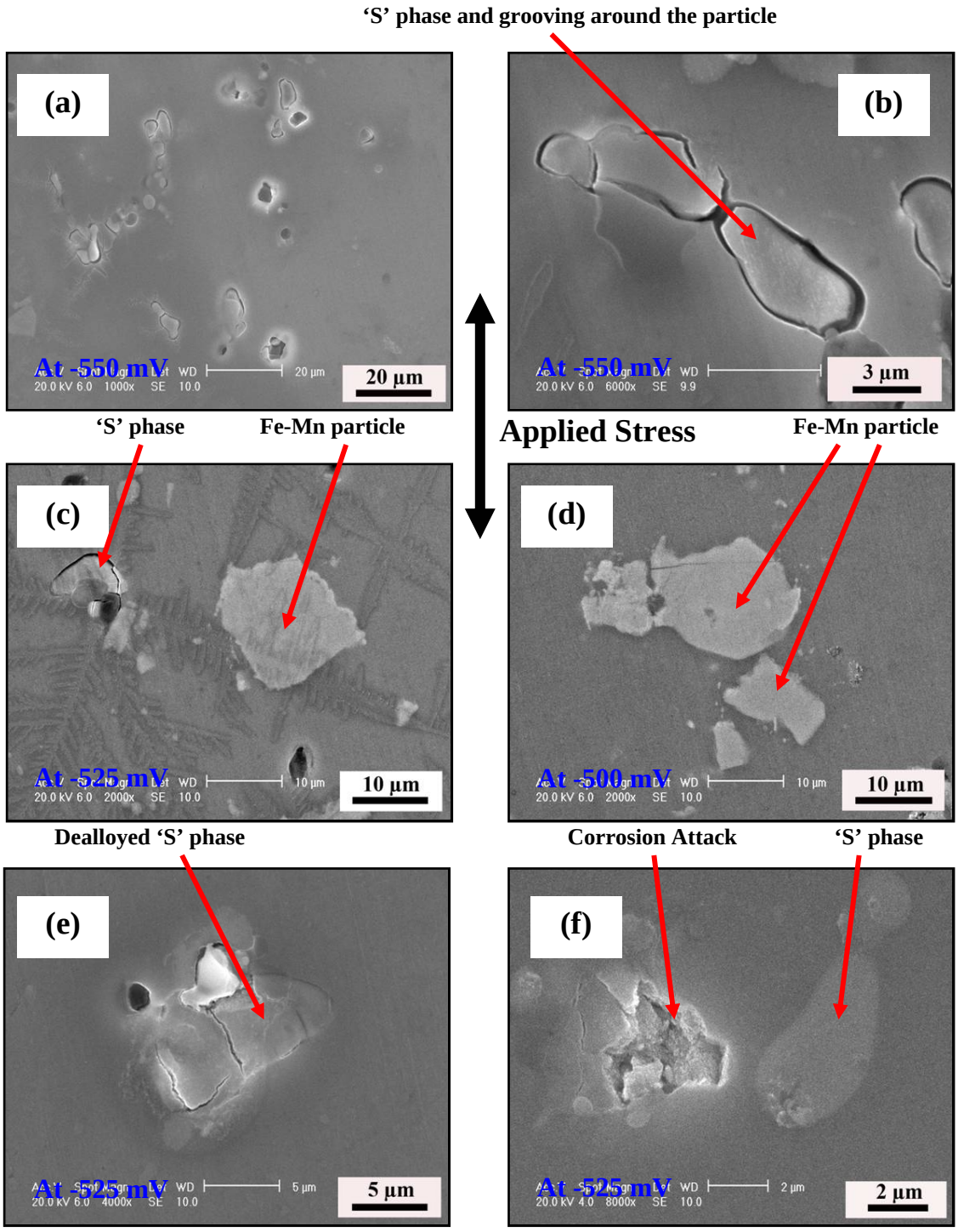


Figure 6.35 SEM micrographs showing the morphology of attacks in the 70% Y.S. AA2024-T351 sample after the potentiostatic polarization in naturally aerated 10 mM NaCl for 10 min. All potentials were measured vs. Ag/AgCl (a) At -550 mV, dealloying of 'S' phases and grooving around them, (b) At -550 mV, dissolution around the edges of 'S' phase, (c) At -525 mV, unattacked Fe-Mn particles, (d) At -500 mV, unattacked Fe-Mn particle, (e) At -525, dealloyed 'S' phase and possible redistributed fine Cu particles adjacent to the particle, (f) At -525 mV, pitting attack next to a 'S' phase could have been initiated in the presence of another 'S' phase.

Pitting next to an 'S' phase particles is shown in Figure 6.35(f). Pitting attack in that particular position could have been initiated by the presence of another 'S' phase particle.

6.2.2.3 Effect of Applied Stress Equivalent to 90% Y.S. of AA2024-T351

Potentiodynamic polarization scans of unstressed and 90% Y.S. AA2024-T351 samples in naturally aerated 10 mM NaCl using capillary cell of 1mm diameter have already been shown in Figure 6.25. It has been seen that corrosion potential decreases after application of 90% Y.S., however no apparent changes in the breakdown potentials have been observed. Current densities in the pseudo-passive region seem to increase after application 90% of its yield stress. Metastable activities increase after the application of 90% Y.S. compared to unstressed samples. Effects of 90% Y.S. on the corrosion properties of AA2024-T351 specimens are further investigated using potentiostatic polarization technique.

Figure 6.36 shows the current density-time curves for the potentiostatic tests of unstressed and 90% Y.S. samples in naturally aerated 10 mM NaCl. The current evolution behaviour of 90% Y.S. sample at -500 mV vs. Ag/AgCl is different than it is observed for 45 % Y.S. samples (Figure 6.30) and 70% Y.S. (Figure 6.33) at same polarization potential. In both 45% Y.S. and 70% Y.S. sample, current decreases after 400s second of exposure. But with applied stress of 90%, current remain constant at the potential of -500 mV vs. Ag/AgCl for first 600 seconds and it even starts rising if the experiments continued further. This behaviour is repeatable and it emphasizes the change in corrosion behaviour with the applied stress of 90% Y.S. when the potential is very close to breakdown potential.

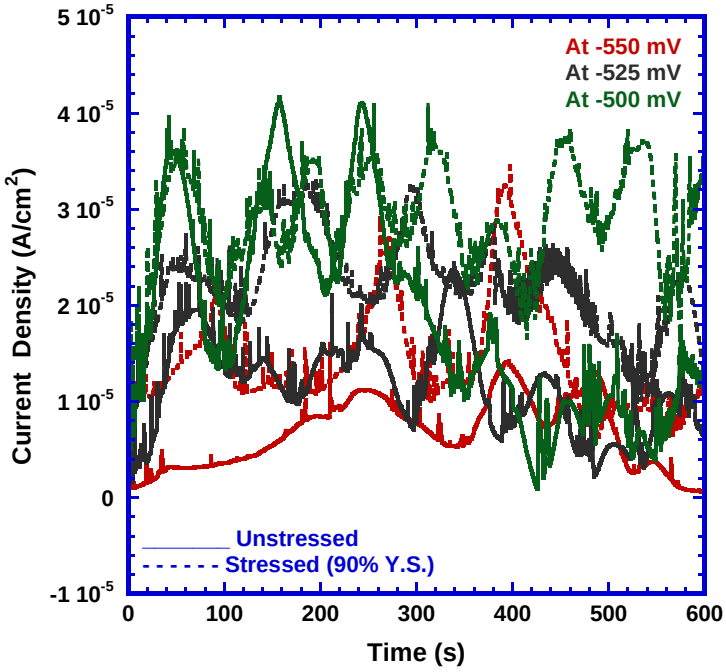


Figure 6.36 Potentiostatic polarization of unstressed and stressed (90% Y.S.) AA2024-T351 samples at different potentials performed in naturally aerated 10 mM NaCl. All potentials were measured vs. Ag/AgCl. Current densities for the stressed samples are higher than the unstressed samples over the entire test span.

Figure 6.37 shows the comparison of charge passed between unstressed and 90%Y.S. AA2024-T351 samples. Figure 6.37 (a) shows clear effect of stress at all applied potentials (i.e., at -550, -525, and -500 mV vs. Ag/AgCl) where as Figure 6.37 (b) does not show that clear effect at -550 mV vs. Ag/AgCl. However, the charge passed at -500 mV vs. Ag/AgCl with application of 90% Y.S. is strikingly different than the other curves. This phenomenon is very repeatable and thus it ensures the adverse effect of stress on the corrosion properties while the potentiostatic polarization potential is very close to the breakdown potential (or just after the breakdown potential). Application of stress close to the yield strength of AA2024-T351 might shorten the passive region by destabilizing the passive film. Overall, the effect of 90% Y.S. is always prominent on the corrosion behaviour of the alloy compared to the unstressed samples over a fairly wide potential range (~50 mV).

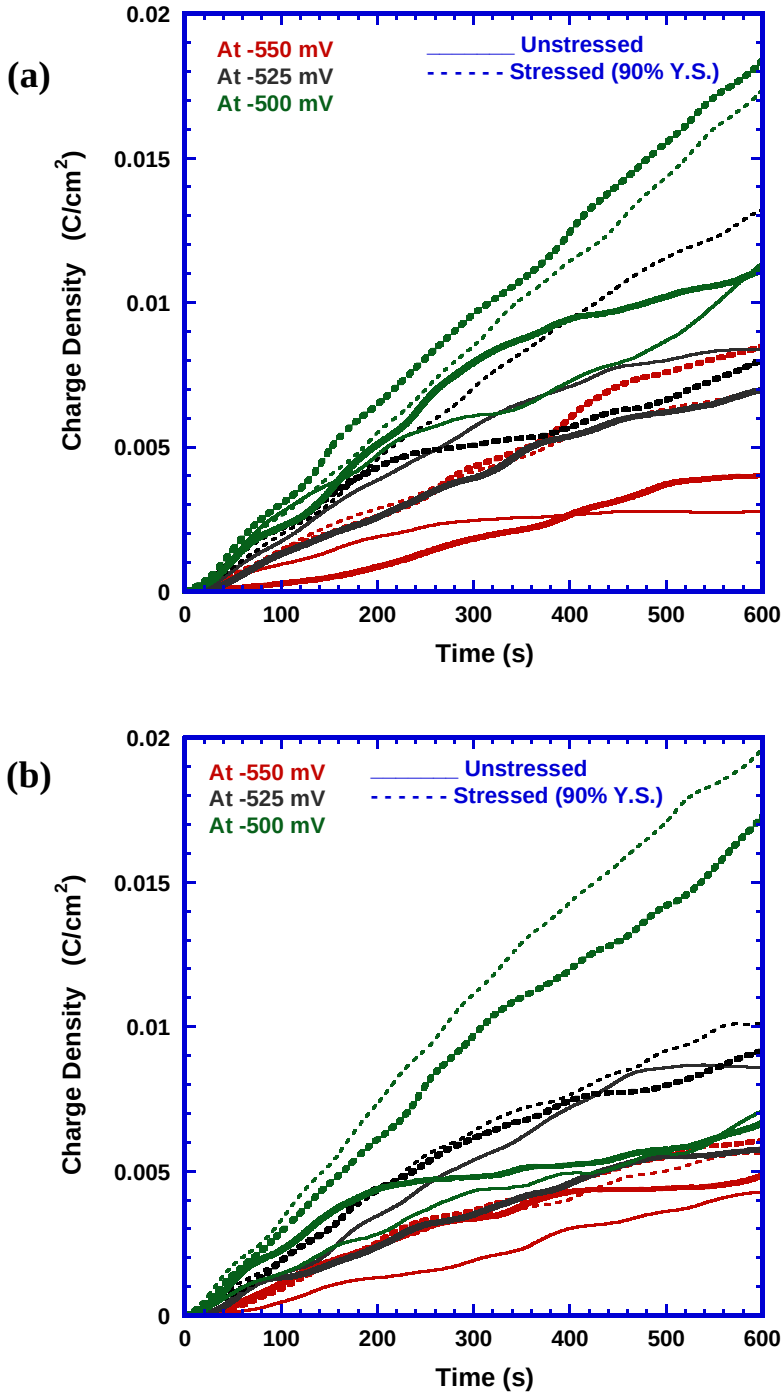


Figure 6.37 Charge passed as a function of time for unstressed and 90% Y.S. AA2024-T351 samples at different polarization potentials. All potentials were measured vs. Ag/AgCl. Experiments were performed in naturally aerated 10 mM NaCl solution using capillary cell. (a) and (b) are showing representative tests from two different sets AA2024-T351 samples in identical stressing condition.

SEM micrographs of the unstressed and 90% Y.S. samples after the potentiostatic tests are shown in Figure 6.38. SEM analysis of the corrosion morphologies does not show any differences between the unstressed and stressed samples. Attacks have been found mostly around 'S' phases in all cases. However, very shallow attacks in the matrix have been observed in unstressed sample at -500 mV vs. Ag/AgCl (Figure 6.38b).

Grooving around the 'S' phase particles can be clearly seen in the stressed sample after polarizing at -525 mV vs. Ag/AgCl (Figure 6.38c), but at the same time many 'S' phase particles remain unattacked at this particular potential. Figure 6.38(d)-(e) show the attack on the 'S' phase particles where partial dissolution of the particle can be seen. Figure 6.38(f) shows a typical example of unattacked Fe-Mn particle after the potentiostatic polarization at -500 vs. Ag/AgCl in the stressed sample. Cathodic grooving around the particle is not observed either.

6.2.3 Summary of the Stress Assisted Electrochemical Studies in the Elastic Domain

Charge passed as a function of time for samples without and with various levels of applied elastic stress is summarized in Figure 6.39. This graph should be carefully analysed before any conclusion can be drawn on the effect of elastic stress on the corrosion properties of AA2024-T351. Since this study deals with small differences in charged passed, scatter of the represented data should be considered to avoid any misleading conclusion.

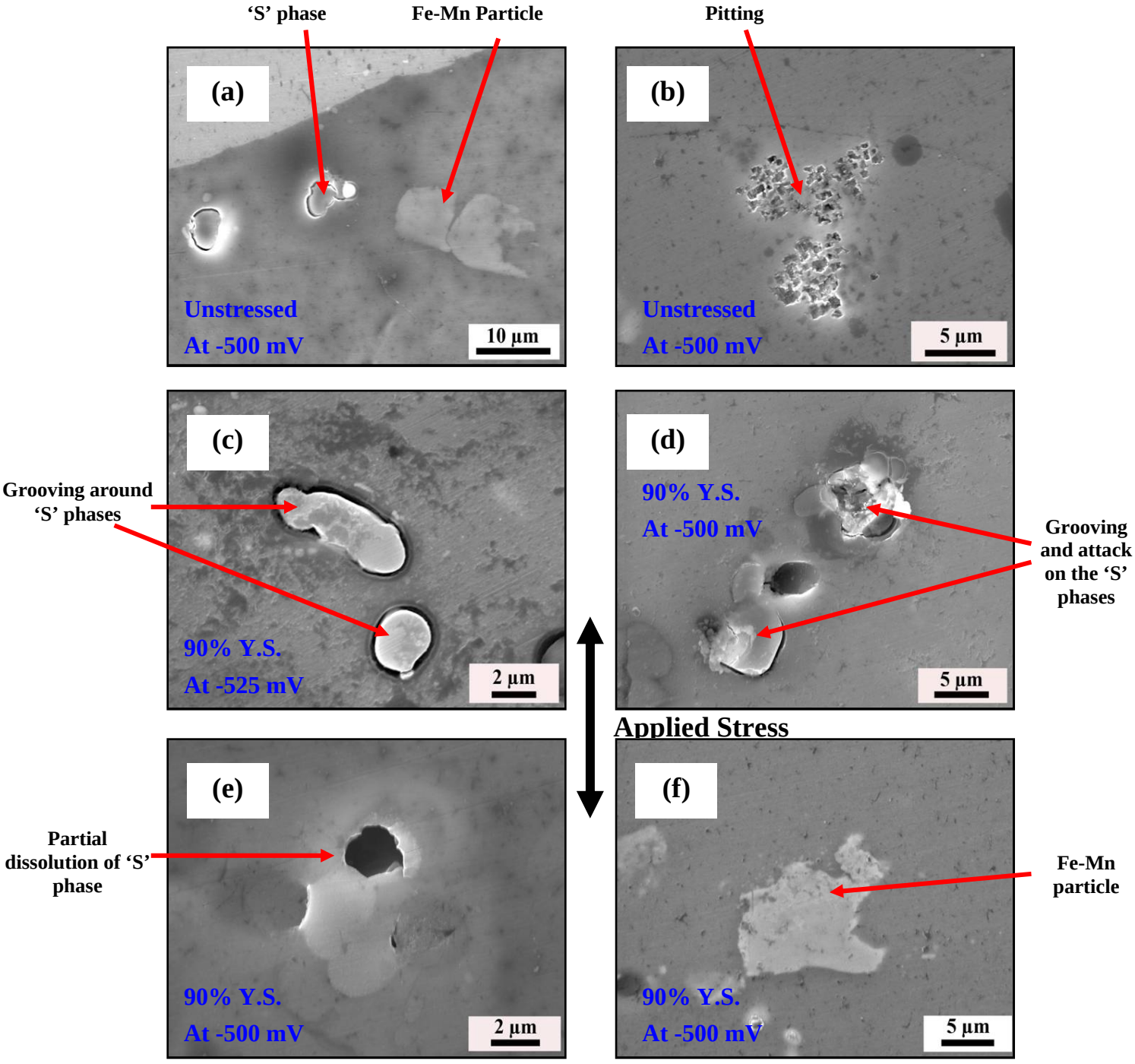


Figure 6.38 SEM micrographs showing the morphology of attacks in the unstressed and 90% Y.S. AA2024-T351 sample after the potentiostatic polarization in naturally aerated 10 mM NaCl for 10 min. All potentials were measured vs. Ag/AgCl. (a) Unstressed at -500 mV, grooving around the 'S' phases and adjacent unattacked Fe-Mn phase, (b) Unstressed at -500 mV, shallow attacks in the matrix, (c) 90% Y.S. at -525 mV, grooving around 'S' phases, (d) 90% Y.S. at -500 mV, attack and grooving around 'S' phase particle, (e) 90% Y.S. at -500, partial dissolution of 'S' phase particle, (f) 90% Y.S. at -500 mV, no grooving or attack around the Fe-Mn particle.

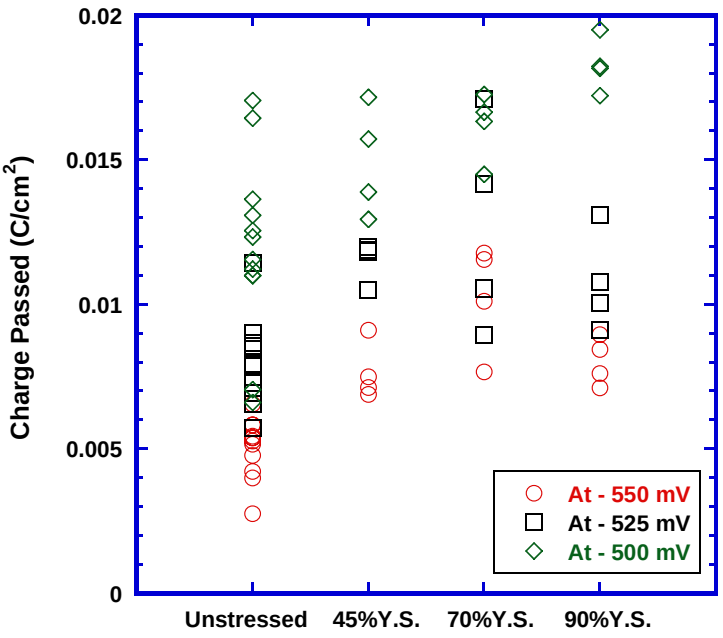


Figure 6.39 Charge passed during the potentiostatic polarization of AA2024-T351 in naturally aerated 10 mM NaCl solution at different potentials in samples without and with various applied stress levels. All potentials were measured vs. Ag/AgCl.

It seems from Figure 6.39 that charge passed for all stressed samples (even at 45% Y.S.) are higher than the unstressed sample at -550 mV vs. Ag/AgCl. This could be correlated with the observations of Liu *et al.* [319] who reported lower breakdown potential with the application of 50% Y.S. However, it should be noted that in this current study, application of 70% Y.S. does not show any significant difference in the breakdown potential (see Figure 6.24). As described earlier, this could be partly due to the small exposure area (with less chance of interaction of defects with the electrolyte) and partly due to the fact that solution is not deaerated in this current study. Deaeration generally gives a longer passive region by decreasing the corrosion potential (due to the decrease in the cathodic reactivity in the absence of oxygen which supports the oxygen reduction as the predominant cathodic reaction), so chances of picking up the metastable activity and any small differences in the breakdown potentials are greater.

Due to the inherent variability in the aluminium alloy, it is difficult to compare the charge passed between two different samples and draw any conclusion. This could be re-emphasised from the charge passed data at -550 mV vs. Ag/AgCl for the unstressed sample (Figure 6.39). It can be seen that in a few cases charge passed at -500 mV is very close to the charge passed at -550 mV. But it should be noted that these data at two different potentials are from two different specimens. So, it is always better (or rather essential) to compare the same sample before and after application of stress to find out the true/actual effect of stress. For this specific reason, the same sample is compared before and application of stress as represented in, Figure 6.31, Figure 6.34, and Figure 6.37.

However, to compromise with the variability in the AA2024-T351 samples, charged passed ratio of the same sample between the elastically stressed and unstressed condition is calculated (Figure 6.40).

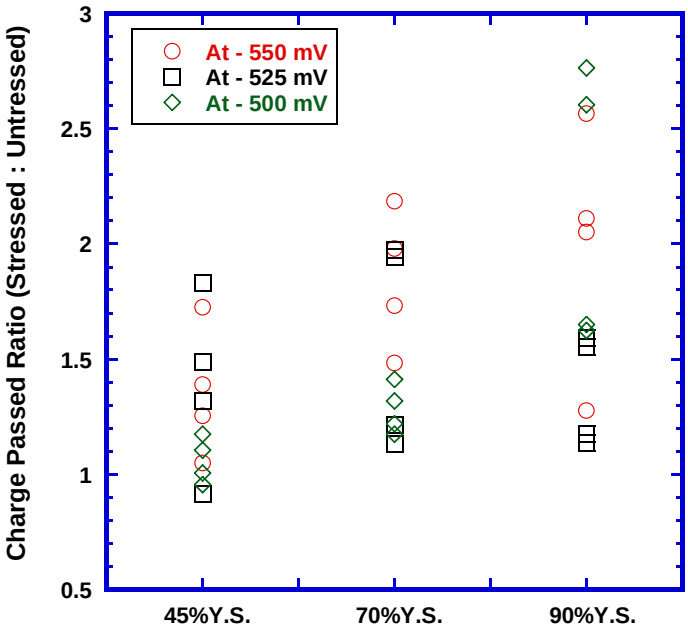


Figure 6.40 Comparison of the charge passed ratio between the elastically stressed and unstressed AA2024-T351 samples. Ratio close to value one signifies minimum effect. Increase in the elastic stress level increases the charge passed ratio at all potentials. All potentials were measured vs. Ag/AgCl.

Comparing the ratios at different potentials from this graph it can be concluded that, 45% Y.S. has shown a slight increase in the charge passed at -550 mV and at -525 mV vs. Ag/AgCl. However, the stress effect is not always prominent at higher polarization potential (i.e., at potentials close to breakdown). Samples stressed to 70% Y.S. had also shown slight increase in charge passed at -550 mV vs. Ag/AgCl. A few of the 70% Y.S. samples show increase in the charge passed at all polarization potentials and in a few cases the samples do not show charge difference while polarizing at higher potential (i.e., at -525 and -500 mV vs. Ag/AgCl). In contrast, the samples stressed to 90% Y.S. always show an increase in charge passed compared to unstressed samples at all polarization potentials. The effect is most prominent at the highest potential (-500 mV vs. Ag/AgCl) as can be confirmed from Figure 6.37.

Comparing all three stressing condition (Figure 6.40) it can be concluded that application of 45% Y.S. shows little effect of stress, whereas 70% Y.S. shows increase in the charge passed at all potentials in most of the cases but there exists few cases where stress does not play any role at higher potential. On the other hand, at applied stress of 90% Y.S., stress effect is always prominent at all potentiostatic polarization potential. As described earlier, higher amounts of charge passed in the sample stressed to 90% Y.S. signifies the higher dissolution of the material during the potentiostatic polarization.

The higher dissolution of the stressed AA2024-T351 samples in the elastic domain could possibly be attributed to either of the following reasons: a) application of stress makes the passive film on the alloy surface more unstable and hence dissolution of the material occur more rapidly/easily; b) application of stress close to yield strength starts forming the micro/nano crevices at the particle/matrix interface where dissolution of the material can occur rapidly. Longer duration of the potentiostatic scans seems to provide the time required for generating the aggressive chemistry in those micro/nano

crevices and thereby contributing to the higher dissolution of the material. However, it should be emphasized that in a few cases unstressed and stressed samples do not show any difference in the charge passed. So, it can be argued that, if only the difference in the passive film results in the higher dissolution, then the effect should be prominent in all the tests on a stressed sample. This is possibly an indication of the decisive role of certain features in the microstructure (in this case the particle/matrix delamination) in determining the corrosion properties. If the exposed area under the capillary does not contain any delaminated features between the particle and the matrix, then the potentiostatic scan does not result into the higher dissolution of the material.

SEM analysis of the both stressed and unstressed samples after tests do not show any particular correlation between corrosion morphology, stressing condition and the polarization potential. In most of the cases attacks have been seen in the form of pitting on the 'S' phases and grooving in the adjacent matrix around the 'S' phases. Dissolution and partial attacks of the 'S' phases are also found. In some cases it was difficult to find any pitting attacks on the matrix due to the corrosion products/marks. Corrosion products are mainly consisting of aluminium and oxygen along with some chlorine. However, no deep pits have been found in the areas where analysis was possible to be performed. In few cases at highest polarization potential (i.e., at -500 mV vs. Ag/AgCl) a few shallow attacks on the matrix have been detected. Fe-Mn particles do not show any grooving around them. When 'S' phase particles and Fe-Mn particles are found together, attacks always occur on the 'S' phase. So, it can be summarized that, in aerated conditions, below applied stress of 70% Y.S., potentiodynamic scans do not seem to reveal the effect of stress on the corrosion properties as the applied stress do not change the pitting or breakdown potential. However, application of 90% Y.S. lowers the corrosion potential and increase the passive current density. Charge passed technique measured from the

potentiostatic polarization is a useful tool to determine the small difference due to the effect of stress. Using this technique, definite adverse effect of applied stress of 70% Y.S. or above on the corrosion properties of AA2024-T351 can be observed.

6.3 Micro-Capillary Electrochemical Cell Studies of AA2024-T351 Under Elastic and Plastic Stress Using a 40 µm Diameter Capillary

The effect of elastic and plastic stress on the corrosion properties of AA2024-T351 under a small exposure area of 40 µm diameter will be discussed in this section. The experiments in this section are different to that of the earlier sections in this chapter mainly in terms of exposed area. In all experiments in the earlier sections of this chapter a capillary cell with one mm diameter exposure was used to find out the effect of plastic and elastic stress. As AA2024-T351 is characterized by the presence of numerous intermetallic particles, even a one mm diameter exposed area would contain several thousands intermetallic particles. Hence, the studies on the AA2024-T351 samples under stressing conditions using a capillary cell would reflect the global behaviour of the samples. It was not possible to distinguish the contribution from the particle free alloy matrix and from different particles in influencing the corrosion properties under stressing conditions. So, to overcome those limitations of the capillary cell, micro-capillary electrochemical techniques with a small exposure area (40 µm diameter) is used for further studies.[24]

[24] Details of micro-capillary electrochemical cell (or micro cell) technique is described in Chapter 3. Studies on specific intermetallics using this technique are further elaborated in Chapter 5.

This technique helps in the selection of any specific type of features in AA2024-T351 samples (i.e., particle free matrix or individual intermetallic particles) under stressing condition and thereby allowing the opportunity to investigate the effect of stress on the corrosion behaviour of that specific feature. In other words, the micro-capillary electrochemical cell is a powerful and effective tool to distinguish the contribution from different features towards the corrosion properties of an alloy in both unstressed and stressed condition. Small exposure area of this technique also allows the possibility of using a notched specimen with a stress distribution to perform a series of tests and thereby investigating the electrochemical behaviour as a function of applied stress, both elastic and plastic, in a single specimen.

Stress distribution in the notched AA2024-T351 specimens are calculated using finite element analysis. Stress distribution around the circular notch in the middle of the specimen varies depending on the applied global stress.[25] It was seen that applied global stress of 200 MPa gives a good distribution of stresses over a fairly spread area and thereby providing opportunity to perform the desired experiments. Stress distribution in the sample with an applied global load of 200 MPa is shown in Figure 6.41. As it can be seen from the figure, with a capillary diameter of 40 μm, multiple experiments can be done in the elastic, near plastic and plastically stressed areas. Surface morphology of a plastically stressed area in AA2024-T351 sample is shown in Figure 6.42. Deformation features on the surface of the stressed sample can easily be observed with the help of optical microscope. The micro-capillary then can be placed in such a way that it can interact with the deformation bands/features (e.g., intermetallic particles).

[25] Details of the finite element analysis for stress distribution can be found in Chapter 3.

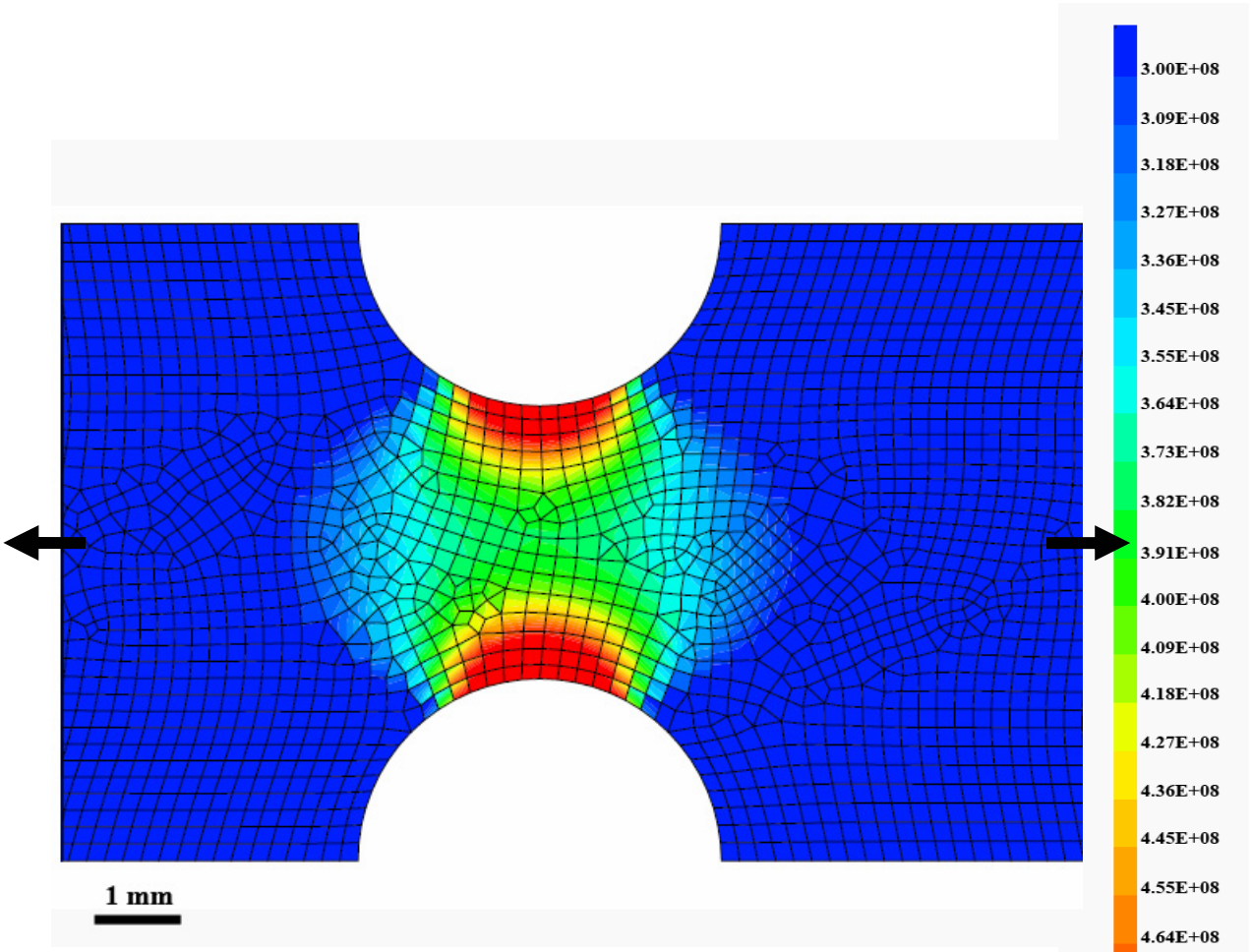


Figure 6.41 Stress distribution in the notched AA2024-T351 specimen when the applied global stress is 200 MPa. The colour marking is indicated in the stress unit of Pa.

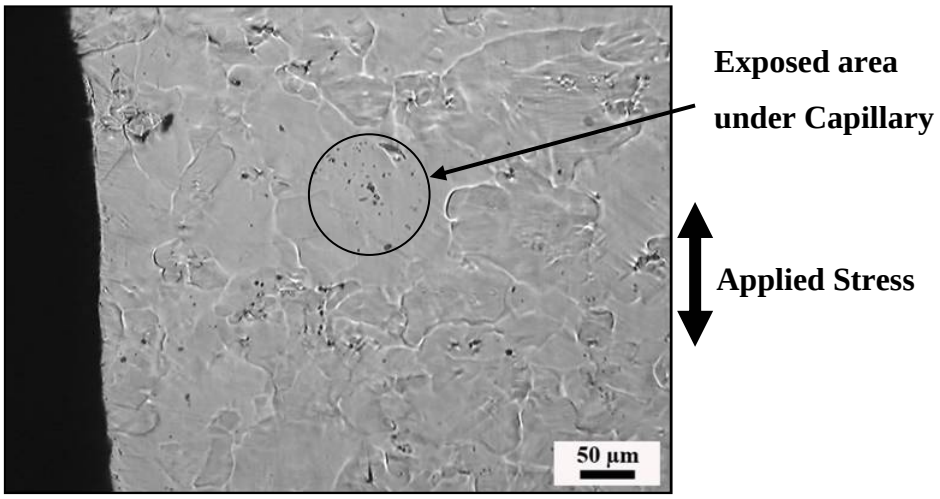


Figure 6.42 Optical micrograph of the plastically deformed area in an AA2024-T351 sample showing the deformation features on the surface. Microcapillary was positioned on deformed places using these images.

AFM studies have also been performed on these deformation bands to have an idea about the surface roughness and depth of the deformation features (e.g. slip band etc.) [see Figure 6.43]. AFM analysis reveals that the depths of the deformation features are in the range of the 225-250 nm.

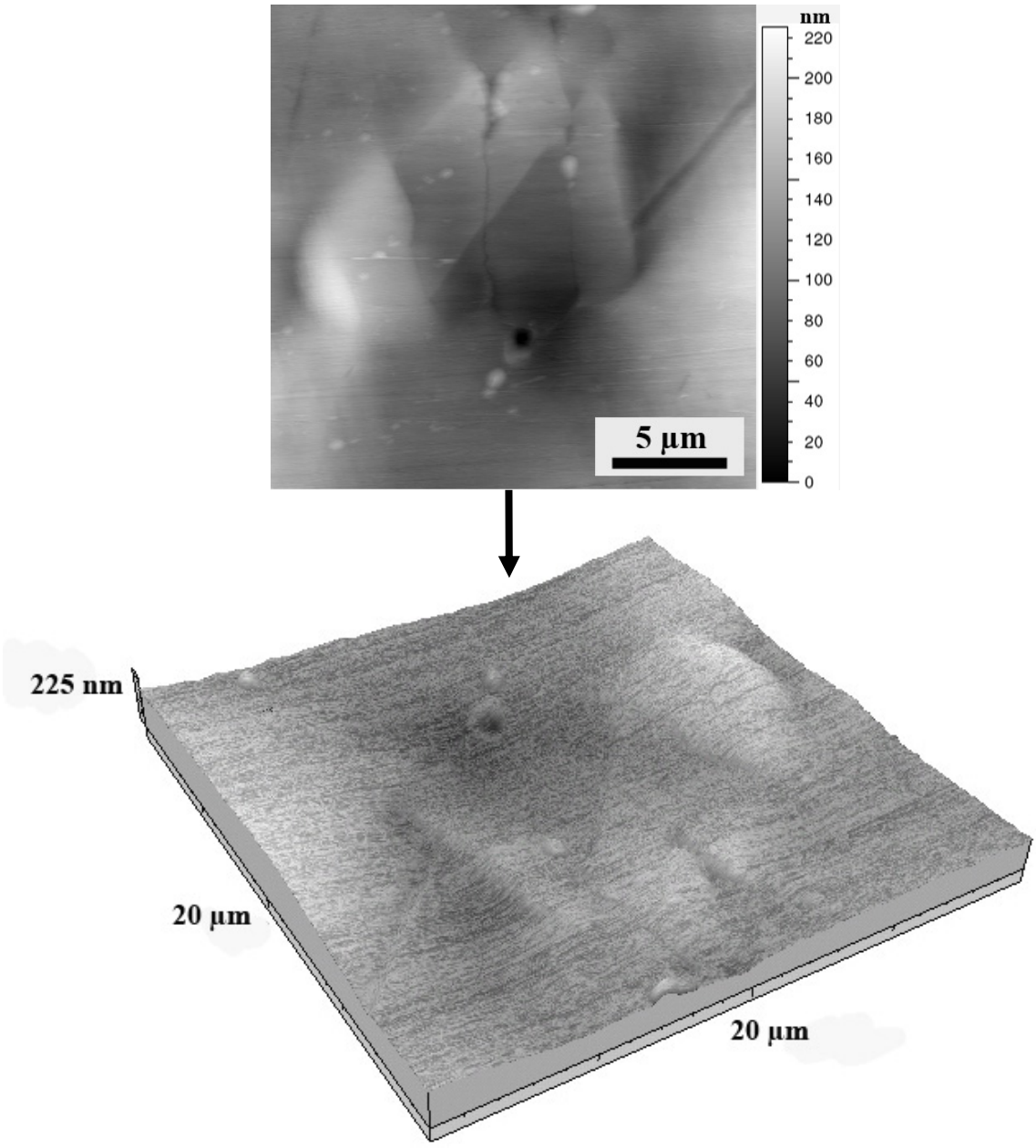


Figure 6.43 Two and three dimensional AFM images of the plastically deformed area in the AA2024-T351 sample. Plastic deformation induced roughness on the specimen surface can be observed. Pre-existing defect in the matrix can also be seen.

6.3.1 Effect of Applied Stress on the Matrix[26] of AA2024-T351

A micro-capillary electrochemical cell with 40 micron capillary diameter was used to investigate the effect of elastic and plastic stress on AA2024-T351 in naturally aerated 0.1 M NaCl solution. It should be noted that throughout the microcell studies naturally aerated 0.1 M NaCl solution was used as an electrolyte (as opposed to 0.01M NaCl in capillary cell) as the configuration of the test cell did not allow the use of less conductive solution than 0.1 M NaCl. However, as described in Chapter 5, use of 0.1 M NaCl solution showed a passive range for both matrix and Fe-Mn particles. Hence, it might be possible to identify any change in the corrosion properties with the application of stress using 0.1 M NaCl. All samples were polished to one micron diamond and after final polishing, samples were kept 1.5 – 2 hours in lab air before starting the tests.

6.3.1.1 Anodic Potentiodynamic Polarization Experiments

Potentiodynamic scans from the starting potential of -700 mV vs. Ag/AgCl at a scan rate of 1mV/s as a function of stress state of a particular sample are compared in Figure 6.44. Applied global stress in this particular case is 200 MPa. It can be seen from the figure that application of plastic stress might have slightly decreased the corrosion potential. But no detectable differences are found in the breakdown potential and in passive current densities between the elastically and plastically stressed samples. The change in the corrosion potentials can be compared with the results obtained using Al-0.099Cu binary alloy as described in Section 6.1.3 (Figure 6.16). Intermetallic particle

[26] In this study 'Matrix' refers to the particle-free area on the surface of AA2024-T351.

free Al-0.099Cu showed decrease in the corrosion potential when stressed plastically, but did not show any change in the breakdown potentials or passive current densities. Comparison of these results in the plastic state between the matrix of AA2024-T351 and particle free Al-0.099Cu binary alloy emphasize the importance of intermetallic particles in determining the corrosion properties of AA2024-T351 in the stressing conditions.

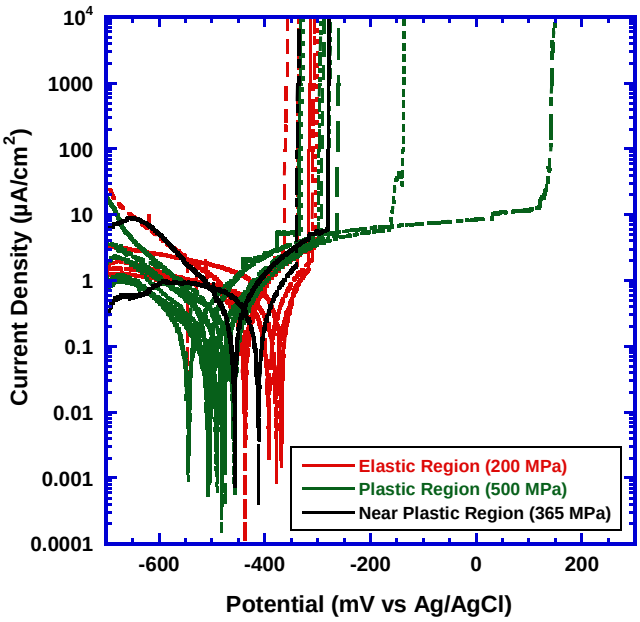


Figure 6.44 Comparison of the potentiodynamic scans in the matrix of AA2024-T351 as a function of stress state when tested in naturally aerated 0.1M NaCl (scan rate = 1 mV/s) using 40 micron diameter capillary. Applied global stress is 200 MPa. Corrosion potentials in the plastic region are slightly lower than the corrosion potential in the elastic region.

Breakdown potentials, corrosion potentials, and passive current densities as a function of stress state are compared in Figure 6.45, Figure 6.46, and Figure 6.47, respectively.

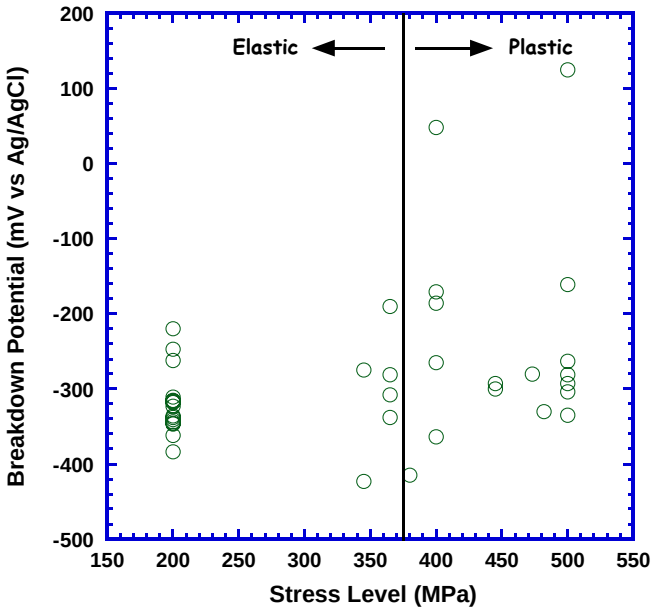


Figure 6.45 Comparison of the breakdown potentials of the matrix of AA2024-T351 as a function of stress state when tested in naturally aerated 0.1M NaCl (40 µm diameter capillary, scan rate = 1 mV/s). Surprisingly in two occasions breakdown potentials are very high (48 mV at 400 MPa and 125 mV at 500 MPa) compared to the other scans.

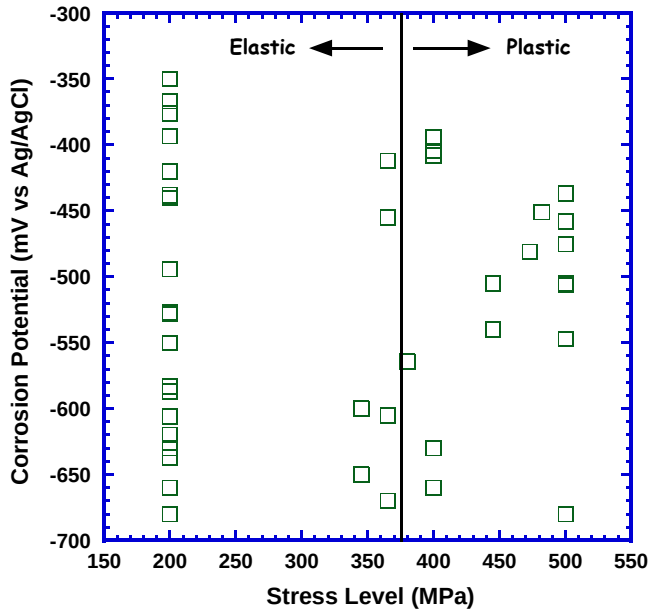


Figure 6.46 Comparison of the corrosion potentials of the AA2024-T351 matrix as a function of stress state when tested in naturally aerated 0.1M NaCl (scan rate = 1 mV/s) with 40 micron capillary. Corrosion potentials are measured from the potentiodynamic scans starting from -700 mV vs. Ag/AgCl. In almost every stress state wide scatter in the corrosion potentials have been observed.

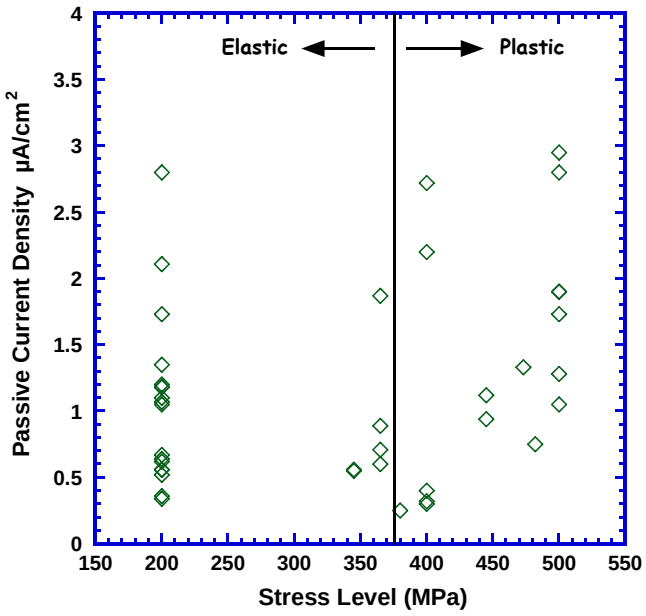


Figure 6.47 Comparison of the passive current densities of the AA2024-T351 matrix as a function of stress state when tested in naturally aerated 0.1M NaCl (40 µm diameter capillary, scan rate = 1 mV/s). Passive currents are measured at approximately middle of the passive region (i.e., between corrosion potential and the breakdown) of each potentiodynamic scans. For consistency of comparison, passive current densities of the scans with higher breakdown potentials (48 mV at 400 MPa and 125 mV at 500 MPa) are measured at ~ -350 mV which is approximately in the middle of short passive region.

Passive current densities (as shown in Figure 6.47) are measured at approximately midpoint of the passive region (i.e., region between the corrosion potential and breakdown potential of the scan). However, it has to be remembered that in many cases the scans do not show any definite passive region, rather they show a very short pseudo-passive region and then breakdown. The scans with higher breakdown potentials show a long passive region. So, to bring the consistency in the comparison, the passive current densities for the scans with longer passive region are also measured at similar potential (i.e., ~-350 mV vs. Ag/AgCl which is approximately in the middle of the pseudo-passive region). It is interesting to note that the initial behaviour of the anodic branches of the scans with higher breakdown potentials is similar to that of the scans with short passive

region. At an elastic stress level of ~200 MPa, breakdown potentials of the matrix stay between -400 mV and -200 mV vs. Ag/AgCl. However more scatter in the breakdown potentials have been observed when the stress level is increased to near plastic and in the plastic level. There are no definite trends in the breakdown potentials as a function of applied stress apart from the increase in the scatter in the data in the plastic state. In a few cases higher breakdown potentials have been observed in the plastic domain. For example, at 400 MPa and at 500 MPa breakdown potentials as high as 48 mV and 125 mV vs. Ag/AgCl have been observed, respectively. Figure 6.46 compares the corrosion potentials of different scans from different samples as a function of applied stress. The most striking feature of this figure is the variability/scatter in the corrosion potential data at an applied stress of 200 MPa. Corrosion potentials vary from -700 mV to -350 mV vs. Ag/AgCl. It should be noted that these corrosion potentials are obtained from different samples. Though all the samples are polished with the same procedure, variation in the data is still observed as the exposed area is very small and as there are some associated variability in the aluminium alloy itself.

So, as described in the Section 6.2, it is always better to compare the same sample as a function of stress state to have a better idea about the effect of stress. Because of the large scatter in the data as presented in Figure 6.46, it is difficult to draw any definite conclusion about the change of corrosion potential as a function of stress state. However when the potentiodynamic scans from a particular sample at different stress state are compared (Figure 6.44), application of plastic stress seems to decrease the corrosion potential. Any definite changes in the passive current densities are not observed as a function of applied stress (Figure 6.47). No definite correlations have been found between the measured corrosion potentials and the breakdown potentials. For example, at a stress level of 400 MPa (Figure 6.46), one sample shows corrosion potential of -660 mV vs.

Ag/AgCl and the other sample at the same stress level shows corrosion potential of -408 mV vs. Ag/AgCl. But, the breakdown potentials for both scans are almost the same (breakdown potentials are -171 mV and -182 mV vs. Ag/AgCl respectively for corrosion potentials -660 mV and -408 mV vs. Ag/AgCl). Any particular effect of stress on the breakdown potentials of the AA2024-T351 matrix have not been found even when a particular sample at different stress state is compared. It is also not clear why a few scans under plastic stress shows higher breakdown potentials than the other scans at the same stress state.

Figure 6.48 shows optical micrographs of AA2024-T351 matrix before and after potentiodynamic tests in naturally aerated 0.1M NaCl. These are examples of some typical scans in the plastic domain showing different breakdown potentials. Figure 6.48 (a) and (b) show the areas of the scans with high breakdown potential of 48 mV and 125 mV vs. Ag/AgCl at stress state of 400 MPa and 500 MPa, respectively. Figure 6.48 shows the micrographs of the scans with a breakdown potential of -293 mV vs. Ag/AgCl at a stress state of 500 MPa. These optical micrographs do not show any obvious differences between the scans with high and low breakdown potentials. In all cases the capillary was positioned in the deformed grains of the sample matrix.

Corrosion morphologies of the exposed samples were analyzed using SEM and are shown in Figure 6.49. As the scans were terminated right after the pit initiation, the pit sizes are very small and not always easy to locate under the microscope. In most of the cases attacks have been observed in the areas which appear to include attacked grain boundaries (Figure 6.49a-b). In some cases pitting attacks have been observed in the matrix adjacent to the grain boundaries (Figure 6.49c). A thick silicone coating at the glass capillary tip avoided the formation of any crevices at the capillary edge.

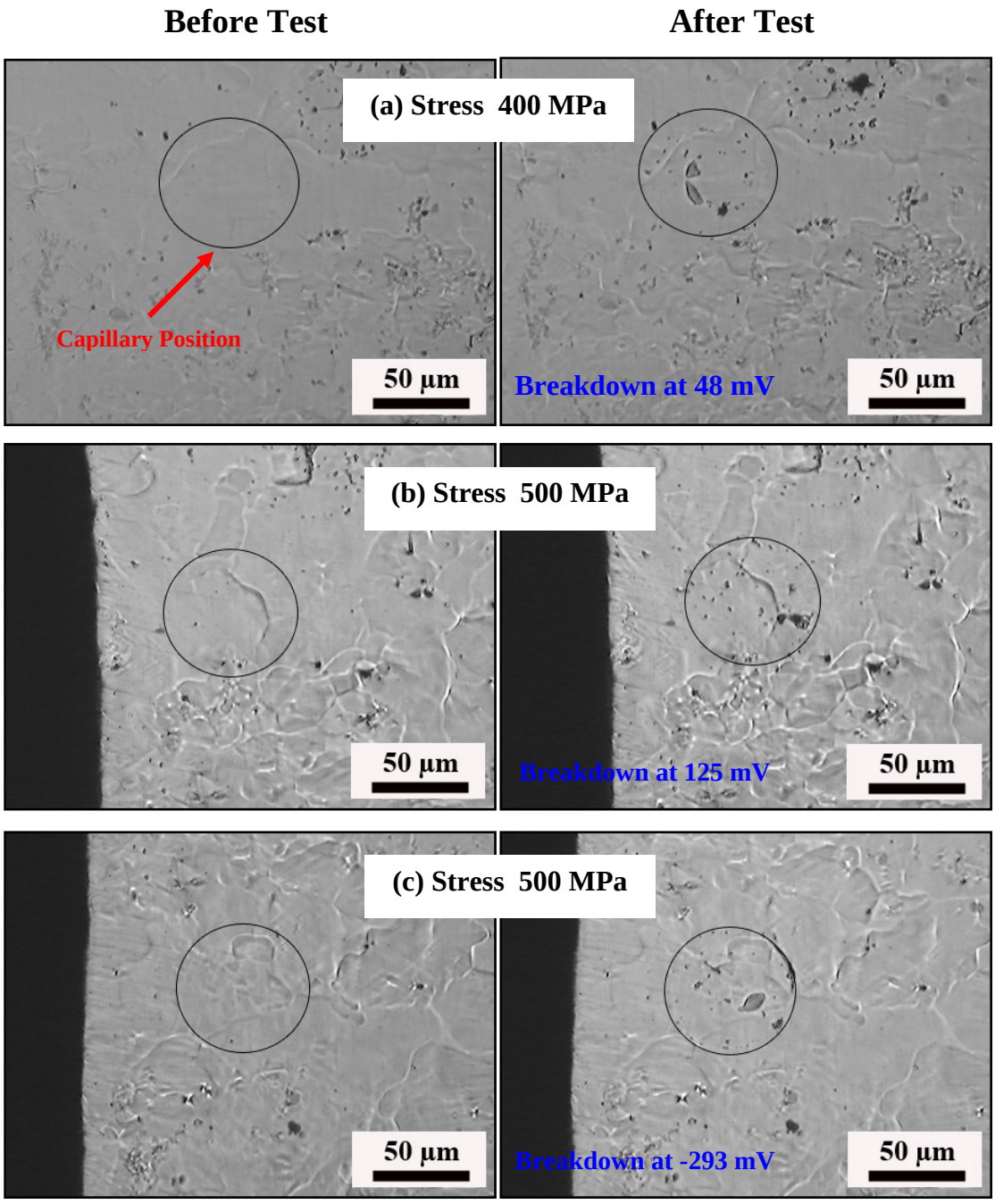


Figure 6.48 Optical micrographs of the plastically stressed areas in the AA2024-T351 matrix before and after the potentiodynamic tests in naturally aerated 0.1 M NaCl using 40 micron diameter capillary. All potentials were measured vs. Ag/AgCl. Surface roughness is easily visible in all the images. (a) Stress level is 400 MPa; E_b ~ 48 mV, E_{corr} ~ -404 mV; (b) Stress level is 500 MPa; E_b ~ 125 mV, E_{corr} ~ -547 mV; (c) Stress level is 500 MPa; E_b ~ -293 mV, E_{corr} ~ -505 mV. In all cases exposed area under the capillary interacted with the deformed grains. However, no visible differences have been found between the micrographs of the areas showing high and low breakdown potentials.

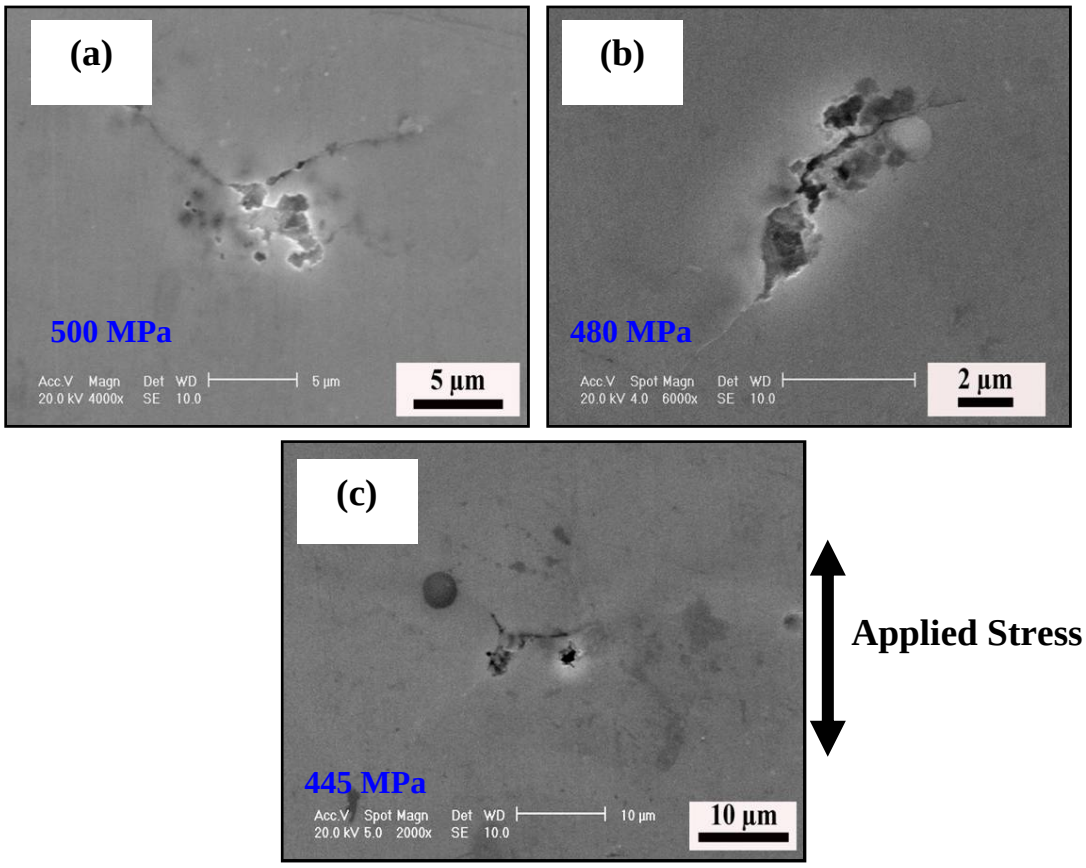


Figure 6.49 SEM micrographs showing the morphology of attacks in the matrix after the potentiodynamic scans in naturally aerated 0.1 M NaCl using 40 micron diameter capillary. All potentials were measured vs. Ag/AgCl. (a) Stress state is plastic (~500 MPa), E_b ~ -161 mV, E_{corr} ~ -458 mV, attack seems to follow adjacent deformed grain boundaries, (b) Stress state is plastic (~480 MPa), E_b ~ -330 mV, E_{corr} ~ -451 mV, attack in the deformed grain boundaries, (c) Stress state is in the plastic region (~445 MPa), E_b ~ -293 mV, E_{corr} ~ -540 mV, pitting attack can be seen in the matrix as well as slight attack in the adjacent grain boundaries. Pits are not always hemispherical in nature, rather the internal surfaces of the attacks seem to be composed of crystallographic corrosion tunnels.

6.3.1.2 Potentiostatic Polarization Experiments

Potentiostatic polarization tests of AA2024-T351 matrix were performed at -400 mV vs. Ag/AgCl for ten minutes using a 40 µm diameter micro-capillary in naturally aerated 0.1 M NaCl as function of stress level. All samples were surface finished to one

micron with diamond suspension and after final polishing, samples were stored 1.5 – 2 hours in lab air before starting the tests. Due to the large scatter in the corrosion potential as well as in the breakdown potentials of the AA2024-T351 it was difficult to select the polarization potential at the passive state. First a polarization potential of -375 mV vs. Ag/AgCl was tried, but it resulted in stable pitting after a few minutes. So, -400 mV vs. Ag/AgCl was selected which is in the passive region for most of the scans and just below the scatter range in the breakdown potential. The charge passed technique as described in Section 6.2 is used to determine the effect of stress on the corrosion behaviour of the alloy.

A comparison of some selected potentiostatic polarization of the matrix at elastic and plastic stress level is shown in Figure 6.50. Because of the small exposed area, the current remains very flat/stable throughout the test with some signs of metastable activities as opposed to the potentiostatic scans with large exposed areas that show numerous fluctuations in the current (Section 6.2). In a few cases current decreases after some initial exposure, which could due more to an increase in the net cathodic current than the net anodic current.

Charge passed during the exposures is calculated and compared in Figure 6.51. In few cases, the charge passed in the plastically stressed sample is higher than the elastically stressed sample. However there are several other cases where no specific differences have been observed between the elastically and plastically stressed samples. It was seen earlier that with larger exposed area (i.e., one mm diameter droplet), stress levels higher than 70% of the yield strength of AA2024-T351 had some definite effect on the corrosion properties. Applied stress of 90% Y.S. showed higher amount of charge passed than the unstressed sample and the plastically deformed sample showed decrease both in breakdown and corrosion potential for AA2024-T3.

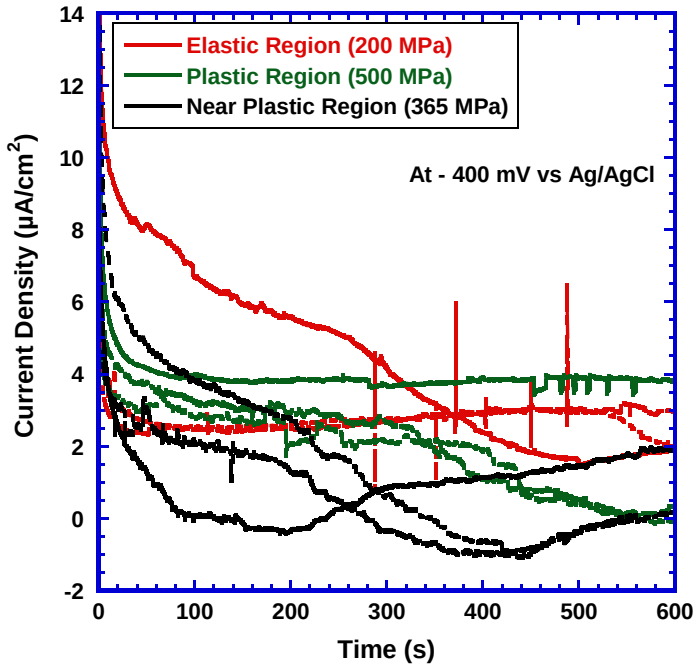


Figure 6.50 Comparison of the potentiostatic polarization of the AA2024-T351 matrix at -400mV vs. Ag/AgCl in naturally aerated 0.1 M NaCl at different applied stress level. As the polarization potential is in the passive region, the resulting current density stays almost flat throughout the test.

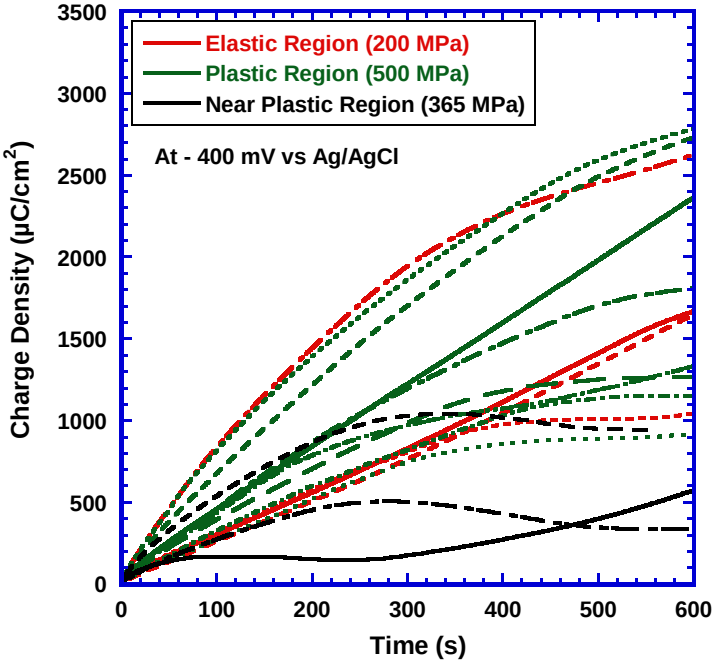


Figure 6.51 Comparison of the charge passed in the AA2024-T351 matrix during the potentiostatic polarization at -400 mV vs. Ag/AgCl in naturally aerated 0.1 M NaCl at different stress level. In few cases, scans in the plastically stressed areas show higher charge passed. However, it is difficult to draw any conclusion as in many cases charge passed in both elastic and plastic domain is same.

This difference in the observation between the micro-capillary cell exposure (i.e., 40 µm diameter area) and large exposure in capillary cell (i.e., 1 mm diameter area) could possibly be explained by the fact that the higher the exposure area, the higher is the chance of interacting with deformation induced features. Apart from that, a capillary cell exposure contain various intermetallic particles including reactive 'S' phases and the Fe-Mn particles whereas in micro-capillary cell only particle free matrix is exposed. Particle free matrix of AA2024-T351 under micro-capillary cell can be compared with the large area exposure of particle free Al-0.099Cu binary alloy. Application of plastic stress in Al-0.099Cu does not have any significant effect on the corrosion properties as can be seen from the exposure of AA2024-T351 matrix utilizing a micro-capillary cell. These observations re-emphasize the role of intermetallic particles in influencing the corrosion properties of AA2024-T351 under stressing conditions. SEM analysis of the exposed area do not show any pitting attack which is expected as the potentiostatic tests are done in the passive region (Figure 6.52).

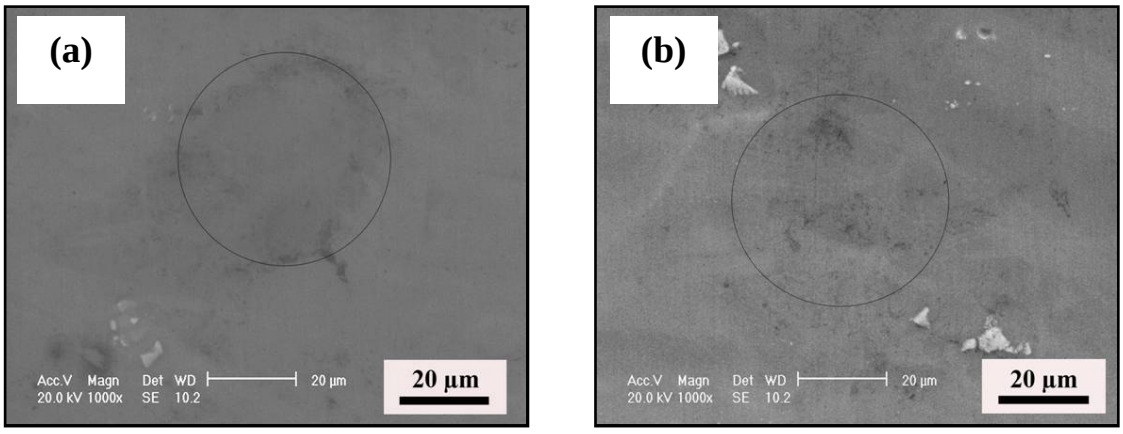


Figure 6.52 SEM micrographs of the AA2024-T351 matrix after the potentiostatic polarization at -400 mV vs. Ag/AgCl for 10 minutes in naturally aerated 0.1 M NaCl. Stress state in the plastic region (~500 MPa). As expected no attacks are seen in the exposed area as the polarization potential was in the passive region.

6.3.2 Effect of Applied Stress on Fe-Mn Particles[27]

Combinations of different experiments with application of stress as described in the previous sections of this chapter emphasize the crucial role of intermetallic particles in determining the corrosion performance of AA2024-T351. Delamination at the interface between the particle and matrix is thought to happen as a function of applied stress. These places of delamination are hypothesized as micro/nano crevices which accumulate aggressive ions and thereby acting as potential sites for corrosion initiation. However, it should be noted that most of the particles do not show any delamination even at very high plastic stress.

But at the same time, each exposure under one mm diameter droplet would contain a large number of intermetallic particles and the presence of only one such crevice would be sufficient to initiate localized corrosion. So it is highly possible that a statistical situation has to be dealt with while performing experiments with a 40 micron diameter micro-capillary on single Fe-Mn particle under stressing conditions. Due to the roughness of the surface in the plastically stressed area (as shown in Figure 6.42) it was difficult to determine if the particle had delaminations at the edge before doing the micro-capillary tests. It has also to be noted that the particles during the micro-capillary tests were identified using optical microscope which was not able to show high resolution images.

[27] Micro-capillary electrochemical cell testing was not attempted on the 'S' phase particles alone mainly because of their small sizes. Surface of the AA2024-T351 samples were rougher in the plastically stressed areas and hence it was difficult to identify the 'S' phase particles under the optical microscope attached with the micro-capillary electrochemical cell.

6.3.2.1 Anodic Potentiodynamic Polarization Experiments

Anodic potentiodynamic polarization scans on the Fe-Mn particles in elastically and plastically stressed areas are summarized in Figure 6.53. Experiments were performed in aerated 0.1 M NaCl solution using a 40 µm diameter capillary at a scan rate of 1 mV/s. All samples were polished to one micron diamond and after final polishing, samples were stored 1.5 – 2 hours in lab air before the starting the tests.

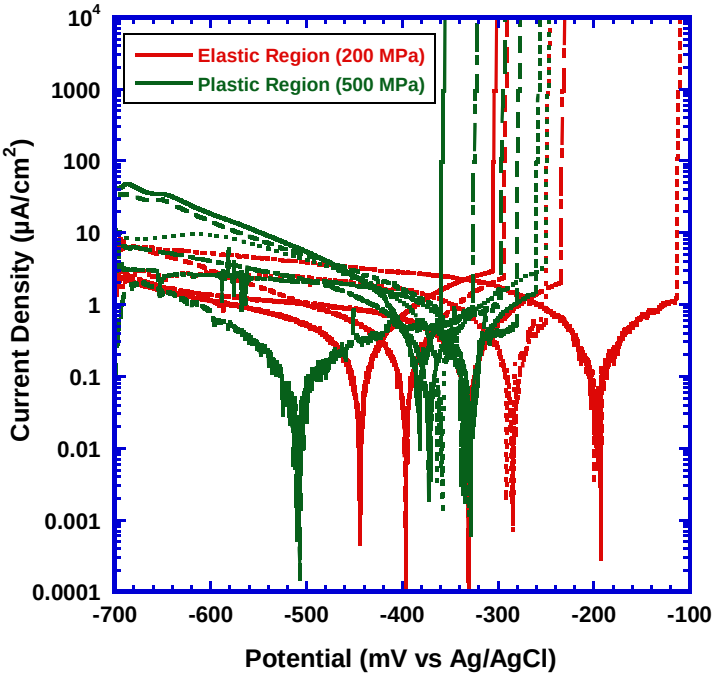


Figure 6.53 Comparison of the potentiodynamic scans on the Fe-Mn particles of AA2024-T351 in naturally aerated 0.1 M NaCl performed using 40 micron diameter capillary (scan rate = 1 mV/s). Wide scatter in the corrosion potentials can be seen in elastic region.

It can be seen from the Figure 6.53 that there are no differences in the potentiodynamic scans between the elastically and plastically stressed Fe-Mn particles. Comparison of the breakdown potentials, corrosion potentials, and passive current densities of Fe-Mn particles at different stress state are shown in Figure 6.54,

Figure 6.55, and Figure 6.56, respectively.

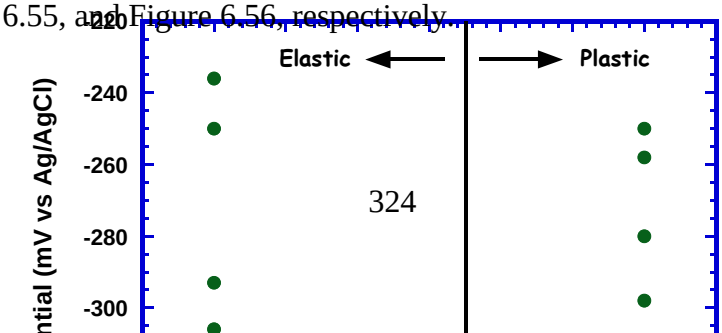


Figure 6.54 Comparison of the breakdown potentials of the Fe-Mn particles of AA2024-T351 as a function of stress state when tested in naturally aerated 0.1 M NaCl (40 µm diameter capillary, scan rate = 1 mV/s). Breakdown potentials of the Fe-Mn particles do not seem to change significantly after the application of plastic stress.

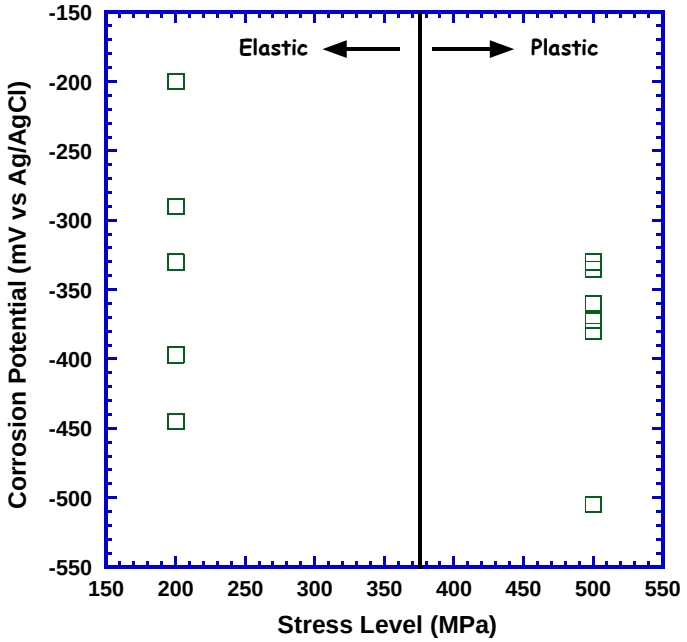


Figure 6.55 Comparison of the corrosion potentials of the Fe-Mn particles as a function of stress state when tested in naturally aerated 0.1 M NaCl (40 µm diameter capillary, scan rate = 1 mV/s). Corrosion potentials are measured from the potentiodynamic scans starting from -700 mV vs. Ag/AgCl. Plastically stressed Fe-Mn particles show less variation in the in the corrosion potentials than the elastically stressed Fe-Mn particles.

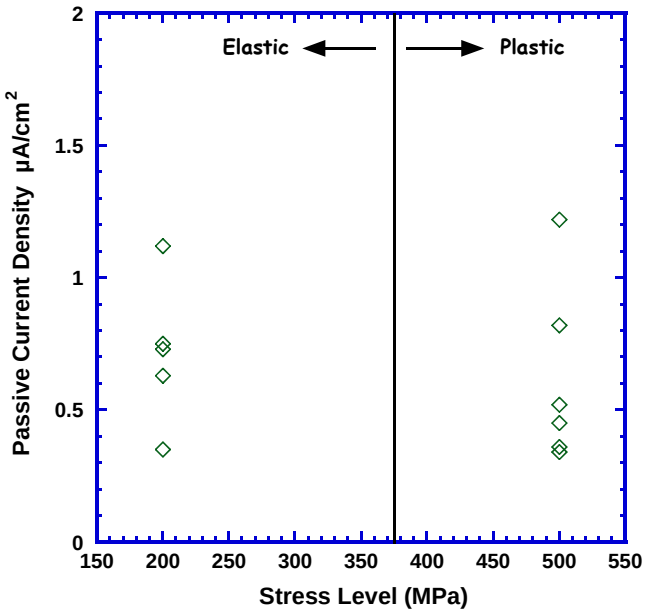


Figure 6.56 Comparison of the passive current densities of the Fe-Mn particles as a function of stress state when tested in naturally aerated 0.1 M NaCl (40 µm diameter capillary, scan rate = 1mV/s). Passive currents are measured approximately at middle of the passive region (i.e., between corrosion potential and the breakdown) of each potentiodynamic scans. Application of plastic stress does not seem to influence the passive current densities of the Fe-Mn particles.

It is difficult to distinguish the effect of stress on the Fe-Mn particles based on data presented in Figure 6.54,

Figure 6.55, and Figure 6.56. Application of plastic stress do not change the breakdown or corrosion potential of the particles. Passive current densities also remain similar after application of plastic stress. Furthermore, breakdown potentials are in the range of -400 to -200 mV vs. Ag/AgCl in both elastic and plastic region.

Analysis of the exposed Fe-Mn particles was performed using SEM to determine the morphologies and location of attacks which is shown in Figure 6.57. In most of the cases [Figure 6.57 (a)-(d)] pitting attacks have been observed in the matrix adjacent to the particle rather than on the particles or at the edge of the particles. Attack morphologies and types in these cases are similar to the findings from the earlier micro-capillary studies of unstressed Fe-Mn particles as described in the earlier sections.

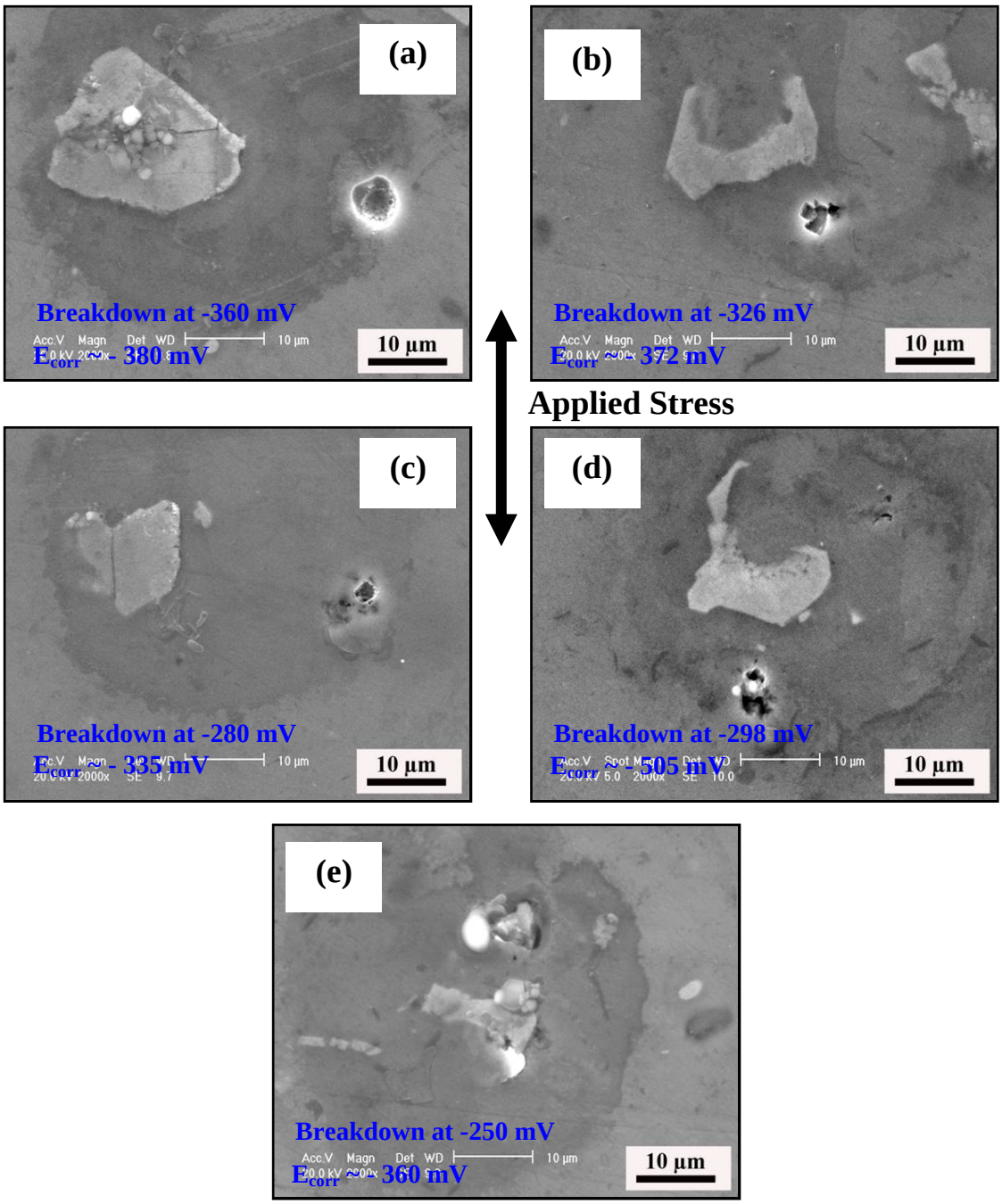


Figure 6.57 Morphology of Fe-Mn particles and the nature of attack after potentiodynamic scan in naturally aerated 0.1 M NaCl in plastically stressed condition (~500 MPa). All potentials were measured vs. Ag/AgCl. Breakdown and corrosion potentials associated with each particle are indicated in the image. (a)-(d) Pitting attack in the adjacent matrix, no delamination have been found at the particle/matrix interface. (e) Pitting is not found in the matrix, particles have been attacked in this case.

As seen from the earlier micro-capillary studies (in Chapter 5), pitting attack can initiate at the adjacent matrix, on the particle or at the edge of the particle. High resolution SEM micrographs do not reveal the presence of any delamination at the particle/matrix interface even at very high plastic load [Figure 6.57 (a)-(d)]. Figure 6.57 (e) do not show any attack in the adjacent matrix, rather it shows attacks on the particle itself.

It is also interesting to note that, the breakdown and corrosion potentials of the potentiodynamic scans for the Fe-Mn particles showing attack on the particle [Figure 6.57 (e)] are not any different than the other Fe-Mn particle scans showing attack on the adjacent matrix [Figure 6.57 (a)-(d)].

6.3.3 Summary of the Micro-capillary Electrochemical Cell Studies as a Function of Applied Stress

Microelectrochemical studies were performed on the matrix and Fe-Mn particles of AA2024-T351 in naturally aerated 0.1 M NaCl using a 40 micron diameter micro-capillary as a function of applied stress. In all cases a global stress of 200 MPa was applied on the double-notched specimen to achieve a wide range of stress distribution in elastic and plastic regions on the sample as shown in Figure 6.41.

Application of tensile plastic stress seems to decrease the corrosion potential of the matrix if the same sample is compared before and after application of stress. No changes in the breakdown potentials and passive current densities were observed after application of stress. However, when corrosion potentials of the matrix of different samples are compared (Figure 6.46), a large scatter were observed (from -700 mV to -350 mV vs. Ag/AgCl). The scatter in the data makes it difficult to determine any particular trend in the corrosion potentials as a function of applied stress. The scatter in the

corrosion potentials of the matrix could be attributed to the inherent variability of the AA2024-T351 samples even if all samples are prepared by same procedure.

Potentiostatic polarizations of the particle free matrix also do not reveal any change in the charge passed during the test after application of plastic stress. Potentiostatic tests were performed at a polarization potential of -400 mV vs. Ag/AgCl which was in the passive region. Application of a tensile stress of 90% Y.S. showed higher amount of charge passed during the capillary cell experiments (1 mm diameter exposure area). But when a 40 micron diameter micro-capillary was used, the matrix did not show any difference in the charge passed even in the plastically deformed area. This difference between the two techniques could possibly occur due to the fact that capillary cell exposes a larger area of the alloy in the electrolyte compared to the micro-capillary technique. The higher the exposed area, the higher the chance of having defects/irregularities that act as preferential localized corrosion initiation sites during the exposure.

Exposed areas under the capillary cell also contain different intermetallic particles which could contribute to the poor corrosion properties of the alloy under the application of stress. Micro-capillary experiments on the matrix can rather be compared with the experiments with Al-0.099Cu binary alloy without any intermetallic particles. Application of plastic stress decreased the corrosion potential of Al-0.099Cu binary alloy (Section 6.1.3) without affecting the breakdown potential and the passive current density. Those observations are similar to the findings of this section using a 40 micron diameter micro-capillary (i.e., in both cases breakdown potentials and passive current densities do not change). Comparisons of these results re-confirm the role of intermetallic particles even under the stressing conditions.

Micro-capillary experiments on the Fe-Mn particles as a function of applied stress did not appear to show any effect of stress on the corrosion properties of Fe-Mn particles. Though the delamination between the intermetallic particles and matrix is thought to play a crucial role in determining the corrosion properties under stressing condition, the results from the micro-capillary technique under stressing condition are not surprising. It is discussed earlier that only a few intermetallic particles show delamination at their interface with the alloy matrix, but as the numbers of intermetallic particles under a droplet (in the capillary cell) are very high, the probability of exposing a delaminated area is also high. Only one delaminated area creating a crevice would be sufficient enough to induce pitting attack. So, when a single Fe-Mn particle is tested under the micro-capillary, the probability of exposing area with delamination decreases significantly.

To observe the difference in the corrosion behaviour of the Fe-Mn particles after application of tensile stress, it is probable that a particle with a delaminated area needs to be exposed under the capillary. SEM analyses of the exposed Fe-Mn particles after the tests do not show any delamination at the edge of the particles. In most of the cases attacks have been found within the adjacent matrix. Only a single delamination could be sufficient enough to cause pitting, but the micro-capillary has to be at the proper place to interact with that particular delamination. Otherwise, potentiodynamic scans may not show any difference between elastically and plastically stressed Fe-Mn particles as seen in this current study.

6.4 Discussion

Earlier studies have shown that applied stress can affect the localized corrosion behaviour of structural metals like steel and aluminium by influencing dissolution rate [20-22], passivity [23-25], and localized corrosion initiation [27, 28, 30-34] and propagation [29, 319]. In aluminium alloys, pre deformation/stressing is thought to produce surface defects such as slip lines, microcracks, decohesion between phases as well as making the surface rougher [35]. It is also speculated that all these surface defects could serve as potential sites for pit initiation by making passive film less stable than a flat surface. Electrochemical tests on a plastically stressed AA2024-T351 specimen show decrease in corrosion potential and breakdown potential (Figure 6.5). Though presence of micro cracks and deformation bands were seen under the exposed area (results not shown), it is difficult to make definitive conclusions about the most responsible features affecting the corrosion properties of the alloy.

Gutman and his co-workers [21, 237, 238] tried to explain the change in the corrosion behaviour of materials under the application of stress using ‘mechanochemistry’ or ‘mechanochemical model’. However, these models are more focused towards the deformation induced changes in the chemical potential of the alloy rather than passive film oriented theories of local breakdown under stressing condition. According to Gutman’s theory, stress induced microstructural changes such as, slip band formation and dislocation pile up play a crucial in determining the corrosion of that particular material. Various features of anodic electrochemical behaviour of materials are due to the different values of chemical potential of the metal sample at different stages of deformation [21]. Gutman [21] also argued that the mechanochemical behaviour of the metal is the same in both passive and transpassive state and independent of the surface

oxide film. However, ambiguity still remains with this theory of 'mechanochemical activation of solid' on whether the theory is strong enough to explain some of the dramatic changes in the localized corrosion behaviour of materials under the application of stress.

On the other hand, Bombara [25] investigated the possible role of oxide films under straining conditions in initiating localized corrosion. It was assumed that the primary effect of stress is to produce fresh metal areas disbanded from the overlaying passive coverage. These freshly exposed areas without passive films may show high dissolution rate as well as becoming active crevices at any film rupture. Effect of stress on the pitting susceptibility is also described by the influence of stress on the mechanical integrity of the protective oxide film [34, 239]. Structural and compositional variations within the oxide film are thought to provide weak points for mechanical fracture and subsequent anodic activity may lead to the formation of pits.

Passive films theories seem to be more convincing than the 'mechano-chemical' model which assumes passive film is not playing any key role in changing the localized corrosion behaviour. However, none of these models considers the presence of intermetallic particles or inclusions in the matrix. One of the main drawbacks of the 'mechano-chemical' model is that it does not consider the presence of inclusions like MnS as a contributing factor towards determining the corrosion properties of the alloy. However, other researchers [28, 30, 240] found out the crucial role of microcracks near inclusions (i.e., MnS or oxide inclusions) in stainless steel as a controlling factor in localized corrosion initiation in steel. These microcracks are normally formed by an applied load.

However, the possible role of the intermetallic particles in determining the corrosion behaviour of the aluminium alloys subjected to an applied load have not been

studied in detail, as yet. The presence of different types of intermetallic particles (with different reactivity and shape) in the aluminium alloy matrix makes it difficult to investigate their role separately. Connolly [36] studied the effect of stress on the intermetallic particle behaviour and its effect on localized corrosion in AA 2024-T351. Connolly found that application of tensile stress above yield stress decreased both the corrosion and breakdown potentials. It is also concluded that the possible reason for the increased electrochemical reactivity could be due to the delamination at the particle/matrix interface. These findings match with the observations in the current study as delamination between the particle and the matrix is observed as a function of applied stress (see Figure 6.2). Decrease in the corrosion and breakdown potentials after application of plastic stress can also be seen in Figure 6.4.

However, it should be noted that most of the particles observed during the in situ SEM work of this study do not show any delamination even at a high plastic load (equivalent to 140% of the yield strength of AA2024-T351). But, due to the presence of a large number of intermetallic particles in the AA2024-T351, the likelihood of exposing such a flaw is high even with very small exposure area. Chen *et al.* [8] found that the average density of particles is approximately ~ 323,000 particles per cm^2. Since the localized corrosion properties of an alloy could be determined even by a single weak point, it is highly probably that the exposed area of one mm diameter would contain such delaminated areas.

Buchheit *et al.* [9] found that different intermetallic particles covered about 4.2% of the total alloy surface. Relatively large and irregular shaped ‘Fe-Mn’ intermetallic particles were revealed to constitute about 12% of all intermetallic particles. So, from these findings it would be logical to assume that statistics might play a role in corrosion initiation at the crevices due to delamination at the particle/matrix interfaces, especially

with smaller exposure area. One delamination between the particle/matrix is found in about eighty particles analysed during the current study. However, a small area of one mm diameter could possible contain more than 3500 intermetallic particles (~ 400 of them could be irregular shaped Fe-Mn particle), and hence it is possible that quite a few of them would be delaminated after application of stress depending on the morphology of the particle.

Liu *et al.* [29, 319] showed the effect of stress on the corrosion behaviour of AA2024-T3. In Liu's work, unstressed AA2024-T3 showed corrosion potential of -850 mV and average breakdown potential of ~ -670 mV vs. SCE when tested in deaerated 1 M NaCl. Application of stress equivalent to 50% of Y.S. of AA2024-T3 decreased the corrosion potential and breakdown potential to -880 mV and -780 mV vs. SCE, respectively. Stress was applied parallel to the transverse direction and corrosion penetration was in 'L' direction. Metastable pitting had been observed in the passive region. These findings are quite similar to the findings of this current study where the applied stress is in the plastic region (Figure 6.5). But application of elastic stress of 70% Y.S. in this current study does not show any change in the breakdown or corrosion potential (Figure 6.24). This could be due to the small exposure area in this current study (0.0113 cm^2) compared to Liu's [29, 319] studies where they used exposure area of around 0.2 cm^2. The higher the exposed area, the higher is the chance of the interaction between the deformation-induced features (such as slip lines, rough surface, microcracks, and especially delamination between phases etc) with the electrolyte. Liu *et al.* [29, 319] reported the change of breakdown potential from -670 mV to -780 mV vs. SCE, which is lower than the corrosion potentials found in this current study (Figure 6.23, Figure 6.24, and Figure 6.25). Higher corrosion potential, very short passive region and smaller

exposure area may have been the reasons for not being able to distinguish the effect of applied stress below 90% Y.S.

Liu *et al.* [29] reported two different breakdown potentials of AA2024-T3 under stressing conditions in S-T and S-L samples. Liu assumed that the lowering of the first breakdown potential of the stressed sample could be due to the enhancement of the transient attack on 'S' phase particles by tensile stress. It was also assumed that stress might have some influence on the 'S' phase surface oxide films or at the particle/matrix interface. Though Liu explained the effect of stress in increasing the propagation rate of localized corrosion in the form of intergranular corrosion, no convincing evidence was presented to support their assumption on the effect of stress in changing the breakdown potential.

Effects of stress on the electrochemical behaviour of AA2024-T351 without 'S' phases is shown in Figure 6.10. Comparison between Figure 6.10, Figure 6.11, and Figure 6.12 indicates that though the removal of 'S' phase can improve the corrosion performance of AA2024-T351, complete removal of 'S' phase can not totally eliminate the effect of stress. It should also be noted, again, that the surface treatment technique not only removes the 'S' phases from the alloy, but it also partially attacks the Fe-Mn particles.[28] Detailed study about the morphology of the Fe-Mn particles after the surface treatment can be found in Chapter 4. Partial attack on the Fe-Mn particles during the surface treatment technique possibly minimizes the chance of having a tight crevice at the particle/matrix interface. These findings indicate the possibility of the importance of some type of deformation induced features in the matrix as well as the change in the particle/matrix interface as a result of the applied stress (Figure 6.13).

[28] Effect of surface treatment on 'S' phases and Fe-Mn particles are discussed in details in Chapter 4.

Effects of stress on the electrochemical behaviour of a near intermetallic particle free matrix was studied using an Al-0.099Cu binary alloy. The role of deformation induced features in the matrix in influencing the corrosion behaviour, specifically changes in the corrosion potential, of aluminium alloys can be emphasized from this study as delamination at particle/matrix interfaces is likely. Gutman [237] reported that impedance measurement did not show any rupture of the electrochemical continuity of the oxide film when stressed below yield strength. However, the state of the passive film on the alloy surface could change with applied plastic stress or even at a stress close to yield strength and thereby affecting the localized corrosion initiation as described by Bombara [25].

Figure 6.16 to Figure 6.19 reveal that the application of plastic stress affects the corrosion potentials of Al-0.099Cu binary alloy, but do not affect the breakdown potentials or the passive current densities. SEM analysis in the exposed area shows the presence of slip bands and deformation induced microcracks. Even in this case no definite changes in the breakdown potentials have been observed. These results indicate that the deformation induced features in the particle free aluminium alloy matrix do not influence the localized corrosion initiation.

Electrochemical studies with a one mm diameter capillary cell have been performed to investigate the effect of applied stress at three different levels (i.e., 45%, 70% and 90% of the yield stress of AA2024-T351). Yield stress of AA2024-T351 in this current study is determined to be approximately 375 MPa. First, potentiodynamic scans were performed on specimens with an applied stress of 45%, 70% and 90% Y.S. Though application of 70% Y.S. did not show any change in the breakdown and corrosion potentials (Figure 6.24), changes have been observed in the corrosion potentials and passive current densities when the applied stress is 90% Y.S. (Figure 6.25). No definite

changes have been observed in the breakdown potentials even at stress level as high as 90% of Y.S.

So, potentiostatic tests were performed on samples stressed to different elastic stress levels and charges passed after ten minutes of exposure were compared utilising the capillary cell test with one mm diameter exposed area. It was observed that, the higher the dissolution of the exposed material, the higher the amount of charge passed. Figure 6.31, Figure 6.34, and Figure 6.37 show the comparison of the charge passed between unstressed and 45%, 70% and 90% Y.S. samples. Summary of all the potentiostatic tests are presented in Figure 6.39. However, as the effect of elastic stress in most cases show very small difference in their corrosion performance, it is better to compare the electrochemical results from the same sample before and after application of stress. Otherwise the variability and scatter in the data even in identically prepared samples can impose difficulties in drawing any definite conclusions of stress effects (Figure 6.39).

To deal with the inherent variability of the AA2024-T351 samples, charged passed ratio of the same sample between the elastically stressed and unstressed condition is calculated (Figure 6.40). By comparing these ratios at different potentials from this graph it can be concluded that the application of 45% Y.S. has shown a slight increase in the charge passed at -550 mV and at -525 mV vs. Ag/AgCl. However the stress effect is not always prominent at higher polarization potential. Samples stressed to 70% Y.S. have also shown slight increase in charge passed at -550 mV. A few of the 70% Y.S. samples showed an increase in the charge passed at all polarization potentials and in a few cases the samples did not show charge difference while polarized at higher potential (i.e., at -525 and -500 mV vs. Ag/AgCl). In contrast, the samples stressed to 90% Y.S. always showed an increase in charge passed compared to unstressed samples at all polarization potentials. The effect is most prominent at the highest potential (-500 mV vs. Ag/AgCl)

as can be confirmed from Figure 6.37. Comparing all three stressing condition (Figure 6.40) it can be concluded that application of 45% Y.S. shows little effect of stress, 70% Y.S. shows an increase in the charge passed at all potentials in most of the cases, whereas at applied stress of 90% Y.S., the stress effect is always prominent at all potentiostatic polarization potential.

No differences in the morphology of attacks have been identified between the unstressed and elastically stressed samples (Figure 6.32, Figure 6.35, and Figure 6.38). Most of the attacks are found on and near the 'S' phases. Grooving around the 'S' phase particles due to the increase in the local alkalinity from oxygen reduction reaction has been seen in most of the cases and this is consistent with the observation of other researchers [29, 174, 198, 211, 317]. At a particular polarization potential during the potentiostatic test some of the 'S' phases remain unattacked whereas most show grooving around them or attack on them.

These type of differences in the behaviour of 'S' phases has been reported by Shao *et al.* [12]. Using the microreference electrode technique they found that some 'S' phases are non-reacting with no attack around the periphery. It was assumed that these particles must have been protected by some kind of film that dissolves very slowly in NaCl solution [43]. After the removal of the film the 'S' phase was found to be dissolved very quickly. Schmutz *et al.* [43, 44] also reported the presence of some kind of surface film on 'S' phases when they used ex situ AFM topographic and Volta potential mapping (Kelvin Probe Technique) to examine the corrosion that occurred at different intermetallics particles in AA2024-T3 during immersion in NaCl solution.

After the potentiostatic tests in this current study utilising a one mm diameter exposure area, Fe-Mn particle do not show any attack or grooving around them. Furthermore, when Fe-Mn particles and 'S' phase cluster together, attacks have always

been observed on the 'S' phases. A few shallow attacks have been detected in the matrix and even in the highest polarization potential deep pitting has not been observed. Absence of any deep pitting indicates that all the potentiostatic polarizations are in the passive region or in the region near breakdown indicating pit initiation rather than propagation. It is interesting to note that potentiodynamic polarization scans on the AA2024-T351 using a capillary cell of one mm diameter exposure area do not create grooving around the particles in the exposed area (results not shown). From Figure 6.25 it can be seen that during the potentiodynamic scans the exposed area stays in the anodic region for about 200 s (as the scan rate is 1 mV/s). Therefore, this short time may not be enough to produce grooving around the particles or completely dissolve the 'S' phases.

Comparing Figure 6.31, Figure 6.34, and Figure 6.37 it can be concluded that applied stress of 70% Y.S. or above has definite adverse effect on the corrosion properties of AA2024-T351. It is difficult to draw any definite conclusion about the reason behind the change in the corrosion properties when the applied elastic stress is close to yield stress. However the electrochemical studies on the Al-Cu binary alloys and the morphological analysis of the attacks in the unstressed and elastically stressed samples after the potentiostatic tests indicate that changes in the corrosion properties could possibly be attributed to any of the following reasons: a) application of stress makes the passive film on the alloy surface more unstable and hence dissolution of the material occur more rapidly/easily; b) application of stress close to yield strength starts forming the micro/nano crevices at the particle/matrix interface where dissolution of the material can occur rapidly.

As the applied stress approaches the yield strength of the alloy, it is possible that delamination at the particle/matrix interface starts occurring along with the local change in the passive film structure. Longer duration of the potentiostatic scans seem to provide

the time required for generating the aggressive chemistry in those micro/nano crevices and thereby contributing to the higher dissolution of the material. However, it should be emphasized that in few cases unstressed and stressed samples did not show any difference in the charge passed. So, it could be argued that, if only the difference in the passive film results in the higher dissolution, then the effect should be prominent in all the tests on a stressed sample. This is possibly an indication of the decisive role of certain features in the microstructure (in this case the particle/matrix delamination) in determining the corrosion properties. If the exposed area under the capillary does not contain any delaminated features between the particle and the matrix, then the potentiostatic scan does not result into the higher localized corrosion reactivity of the material.

Micro-capillary electrochemical studies with very small exposure areas (i.e., 40 μm diameter capillary) emphasize the importance of interaction between the deformation features and electrolyte in determining the corrosion properties of AA2024-T351. Application of plastic stress seems to have a little effect on the corrosion potential of the alloy matrix (Figure 6.44) but it does not seem to affect the breakdown potential (Figure 6.45). The behaviour of the AA2024-T351 particle free matrix (Figure 6.44) under plastic stress is very similar to the behaviour of Al-0.099Cu binary alloy (Figure 6.16) and these similarities indicate the importance the intermetallic particles under stressing conditions (as AA2024-T351 shows decreases in both corrosion and breakdown potentials under plastic stress, Figure 6.4).

In this current study no differences have been found between the elastically and plastically stressed Fe-Mn particles when they are tested individually using the micro-capillary of 40 micron diameter (Figure 6.53). This is not surprising as the SEM analysis (Figure 6.57) after the tests do not show any presence of delamination at the particle/matrix interfaces. Attacks have been found in the adjacent matrix in most of the

cases. As described earlier, most of the particles on the alloy surface do not show delamination even under the application of plastic stress. It should again be noted that it requires only a single micro-crevice at the delaminated interface between the particle and the matrix to initiate pitting/localized corrosion. If the exposed area is high, chances of exposing such micro-crevices in the electrolyte become higher and this could be a possible reason why application of plastic stress using one mm diameter capillary area shows a clear effect of plastic stress while the micro-capillary (40 micron diameter) exposure do not. Effects of applied stress on the Fe-Mn particles can clearly be seen if micro-crevices at the delaminated areas are exposed under the capillary. Since none of the particles in this current study show delamination (Figure 6.57), potentiodynamic scans do not show any significant difference between the unstressed and plastically stressed samples (Figure 6.53).[29]

6.5 Conclusions

Effects of applied elastic and plastic tensile stress in initiating localized corrosion in aluminium alloys were investigated in this chapter. The main focus of this chapter is to compare the corrosion performances between the unstressed and stressed samples of different aluminium alloys. Efforts have also been made to identify the possible features

[29] The number of micro-capillary electrochemical tests needed to be performed in order to find a delamination at the particle/matrix interface would be enormous. For example, approximately 600 tests will be required with a 40 micron diameter capillary to cover an equivalent surface area of a capillary cell exposure (i.e., 1 mm diameter). Even utilising a one mm diameter capillary cell (which may be having approximately 400 Fe-Mn particles), 3 out of 16 potentiodynamic scans did not show any change in the breakdown. These observations possibly emphasize the statistical complexity of finding a delamination at the particle-matrix interface.

responsible for changing the corrosion behaviour of AA2024-T351 under stressing condition. Ambiguities still remain concerning the behaviour of the intermetallic particles present in AA2024-T351 microstructure under stress and their contribution towards changing the corrosion performance of the alloy. Therefore this chapter also focuses on identifying the role of those intermetallic particles in enhancing localized corrosion activities under stress. Findings of this study are summarized as follows:

1. Application of tensile stress above yield stress can cause delamination at the intermetallic particle/matrix interfaces. Delamination could possibly form micro/nano-crevices at the particle-matrix interface and could possibly act as preferential sites for localized corrosion initiation. However, only a very few particles showed delamination after the application of stress. Most of the particle/matrix interfaces remain unaltered even after the application of stress in the plastic region. But, considering the fact that aluminium alloys have thousands of intermetallic particles in every square cm of surface area, delamination in only a few or even just one would be enough to cause pit initiation. Pre-existing flaws next to particles could open up during the application of stress and provide potential sites for corrosion initiation. Application of plastic stress also produces surface defects like slip bands, microcracks, decohesion between phases as well as making the surface rougher. As a consequence, the exposure area during the corrosion process plays a role in determining the corrosion properties of the alloy.
2. Under the capillary cell (with an exposed area of one mm diameter), both the corrosion and breakdown potentials of AA2024-T351 decreased with the application of plastic stress. After ‘S’ phase removal from the AA2024-T351 matrix, application of stress did not change the OCP, but it decreased the

breakdown potential. The exact reason behind this phenomenon is not completely understood as yet.

3. Effects of applied elastic stress (equivalent to 45%, 70% and 90% yield strength of AA2024-T351) on the corrosion properties of AA2024-T351 have also been investigated using a one mm diameter capillary cell. Potentiodynamic scans could not resolve the difference between the stressed and unstressed samples in the elastic domain. Hence, potentiostatic tests at differential potentials and at different elastic stress levels were performed on AA2024-T351 samples. Charge passed during a specific period of time were calculated and compared between different stress levels. It was observed that the higher the dissolution, the higher the amount of charge passed. Application of 45% YS show slight effect of stress at a polarizing potential in the passive region, 70% YS showed effect at different polarization potentials (i.e., in the passive region and also close to breakdown) and 90% YS had clear and definite effect which could be confirmed from the higher amount of charge passed after stressing compared to the unstressed experiments.
4. Capillary cell experiments (with a diameter of one mm) on an intermetallic particle free binary alloy (Al-0.099Cu) showed that the application of stress even in the plastic domain does not have an effect on the breakdown potential. Corrosion potentials were observed to decrease with the application of plastic stress. Plastic stress produced slip bands, surface roughness and microcracks on the alloy surface. These features were exposed under the droplet, but still the breakdown potential did not change. This could possibly emphasize the crucial role of the morphological changes and subsequent electrochemical behaviour of intermetallic particles under stressing condition.

5. Micro-capillary experiments (with an exposure area of 40 micron diameter) were performed on AA2024-T351 as a function of applied stress to investigate the effect of stress on the corrosion properties. The main advantage of this technique was its flexibility of selective exposure of different microstructural features. Application of plastic stress showed a slight decrease in the corrosion potential of the AA2024-T351 matrix as compared to elastically stressed sample matrix. However scatter in the data made it difficult to draw definite conclusions about the effect of stress on the particle free matrix.
6. Micro-capillary experiments did not show any clear differences in the breakdown potentials and in the passive current densities between the elastically and plastically stressed particle free matrixes of AA2024-T351. Fe-Mn particles in the elastic and plastic region behave similarly when corrosion potentials, breakdown potentials, and passive current densities are compared. SEM analysis of the exposed Fe-Mn particles in the plastically deformed region did not reveal any delamination at the particle/matrix interface or any attack associated with them. In most of the cases attacks had been observed in the matrix adjacent to the particle. However, it should be noted that due to the presence of numerous intermetallic particles on the surface of AA2024-T351, statistics might play a crucial role in the possibility of finding a delaminated feature under the micro-capillary.
7. So, it is clear from the above studies that application of 70% YS and above has clear effects on the corrosion properties of AA2024-T351. Exposure area also plays a crucial role in determining the corrosion properties during the tests. Capillary cells with one mm diameter exposure area show adverse effect of stress beyond 70% YS, whereas micro-capillary (with 40 micron diameter) technique do not show any definite effect on corrosion properties even in plastically stressed

samples. Combination of all the tests performed in this study indicates the crucial role of intermetallic particles in the determining the corrosion properties of AA2024-T351 in both stressed and unstressed condition. Presence of only slip bands and rougher surface in a plastically stressed sample do not change the breakdown potential of the alloy (e.g., experiments on Al-0.099Cu binary alloy and micro-capillary experiments on the particle free AA2024-T351 matrix), though it can decrease the corrosion potential. Hence, it can be concluded that the presence of intermetallic particles are possibly very crucial in lowering the breakdown potential of AA2024-T351.